

TERRESTRIAL AND SPACE ENVIRONMENT RESEARCH AT MSFC

September 28, 1967

By

Margaret Alexander
S. Clark Brown
Dennis W. Camp
Charles C. Dalton
Lee W. Falls
George H. Fichtl
Ernst D. Geissler
C. Kelly Hill
J. W. Kaufman
William T. Roberts
O. E. Smith
Robert E. Smith
George S. West, Jr.



CONTENTS . . .

Page

INTRODUCTION TO RESEARCH ACHIEVEMENTS REVIEW ON AEROSPACE
ENVIRONMENT RESEARCH AT MSFC

by Ernst D. Geissler	1
REFERENCE	2

STRUCTURE OF ATMOSPHERIC TURBULENCE

by George H. Fichtl	Page
SUMMARY	3
INTRODUCTION	3
VARIANCE OF TURBULENCE	4
GUST FACTORS	6
WIND SPECTRA	8
CONCLUDING COMMENTS	8
REFERENCES	10

LIST OF TABLES

Table	Title	Page
I.	Values of σ	6

LIST OF ILLUSTRATIONS

Figure	Title	Page
1.	σ/u^* versus z/L'	5
2.	G versus z	7
3.	Experimental Values of Turbulence versus von Karman Values of Turbulence	9

WIND AND GUST CHARACTERISTICS IN THE LOWER 150 m OF THE ATMOSPHERE
AT KSC, FLORIDA

by Margaret Alexander, Dennis W. Camp, C. Kelly Hill, and John W. Kaufman	Page
SUMMARY	11

CONTENTS (Continued) . . .

	Page
INTRODUCTION	11
NASA'S 150-m METEOROLOGICAL TOWER FACILITY	12
CHARACTERISTICS OF WIND VELOCITY PROFILE DATA	13
Variability of Wind Speed and Direction	13
Ratio of Maximum Wind Speeds to Peak Wind Speeds	13
Winds Associated with a Thunderstorm	14
GUST FACTOR ANALYSIS	15
GUST CHARACTERISTICS	19
CONCLUSIONS	19
REFERENCES	19

LIST OF ILLUSTRATIONS

Figure	Title	Page
1.	NASA Launch Complex 39, KSC, Florida	12
2.	Scheme for Placement of Meteorological Sensors on NASA's 150-m Meteorological Tower, KSC, Florida	12
3.	Sigma (S. D.) Curves of Wind Speed and Wind Direction Versus Wind Speed Computed from Wind Velocity Data Recorded at NASA's 150-m Meteorological Tower, KSC, Florida	13
4.	Ratio of Maximum Wind Speeds to Peak Wind Speeds Computed from One 5-min Sample of Data	14
5.	Ratio of Maximum Wind Speeds to Peak Wind Speeds As a Function of Mean Wind Speed Based on 74 5-min Samples of Wind Speed Profile Data	14
6.	Height-time Cross Section of Wind Associated with A Thunderstorm as Observed at 150-m Meteorological Tower, KSC, Florida, on May 9, 1967 (14:13:10.5 - 14:23:10.5 Zulu). Test Number 150094; ws-m/sec	15
7.	Equation for Computing Gust Factor with Two Examples	16

CONTENTS (Continued) . . .

	Page
8. Mean Gust Factor for Six Heights as a Function of Mean Wind Speed and Five Mean Wind Speed Averaging Periods from Data Recorded at NASA's 150-m Meteorological Tower, KSC, Florida	17
9. Maximum Gust Factor for Six Heights as a Function of Mean Wind Speed and Five Mean Wind Speed Averaging Periods from Data Recorded at NASA's 150-m Meteorological Tower, KSC, Florida	18
10. Percentage of Occurrence of Gusts Having Various Durations Based on 1400 Gusts Recorded at the 18-m Level on NASA's 150-m Meteorological Tower, KSC, Florida	19
11. Percentile Gust Shapes Based on 583 Gusts of Time Duration of 4 to 6 sec Occurring at the 18-m Level	19

**A STATISTICAL ANALYSIS OF WINDS FOR AEROSPACE VEHICLE DESIGN,
MISSION PLANNING, AND OPERATIONS**

by O. E. Smith, Lee W. Falls, and S. Clark Brown

	Page
SUMMARY	21
INTRODUCTION	21
EXTREME VALUE THEORY	21
WIND DATA SAMPLES FOR CAPE KENNEDY	24
Hourly Peak Wind Sample	24
Daily Peak Wind Sample	25
Winds Aloft Sample	25
ANALYSIS	25
Peak Wind Speeds at 10-m Reference Height Above Natural Grade	25
Winds Aloft Analysis.	33
CONCLUSIONS	49
REFERENCES	50

LIST OF TABLES

Table	Title	Page
I.	Peak Design Wind Profiles	26
II.	Comparison of the 90th and 95th Percentile Design Wind Speed at 10-14 km Altitude with Maximum Wind Speed for the 10-15 km Layer at Cape Kennedy, Florida	36
III.	Probability (%) That the Maximum Wind Speed, W , in the 10-15 km Layer Will Occur One or More Times Less Than (Equal to or Greater Than) Specified Values, W^* , for k -Consecutive 12-hr Periods at Cape Kennedy, Florida	38

CONTENTS (Continued). . .

Table	Title	Page
IV.	An Example for January in the Computation of Probabilities of Runs and Conditional Probabilities for Maximum Wind in the 10-15 km Layer at Cape Kennedy, Florida	40
V.	Runs and Conditional Probabilities for the Maximum Wind in the 10-15 km Layer Being < 50 m/sec (January, Cape Kennedy, Florida)	42
VI.	Runs and Conditional Probabilities for the Maximum Wind in the 10-15 km Layer Being < 75 m/sec (January, Cape Kennedy, Florida)	43
VII.	Runs and Conditional Probabilities for the Maximum Wind in the 10-15 km Layer Being \geq 50 m/sec (January, Cape Kennedy, Florida)	44
VIII.	Runs and Conditional Probabilities for the Maximum Wind in the 10-15 km Layer Being \geq 75 m/sec (January, Cape Kennedy, Florida)	45
IX.	$P \{I \text{ Successes in } J \text{ Periods}\}$ Maximum Wind Being < 50 m/sec in the 10-15 km Layer (January, Cape Kennedy, Florida)	47
X.	$P \{I \text{ Consecutive Successes in } J \text{ Periods}\}$ Maximum Wind Being < 50 m/sec in the 10-15 km Layer (January, Cape Kennedy, Florida)	48

LIST OF ILLUSTRATIONS

Figure	Title	Page
1.	Probability of Maximum Daily Peak Thunderstorm Winds at Cape Kennedy, Florida	23
2.	Fisher-Tippett Type I Distribution (Gumbel Distribution)	23
3.	Fisher-Tippett Type II Distribution	23
4.	Fisher-Tippett Type III Distribution	24
5.	January Hourly Peak Wind Speed Cumulative Percentage Frequency (10 m Level) at Cape Kennedy, Florida	26
6.	July Hourly Peak Wind Speed Cumulative Percentage Frequency (10 m Level) at Cape Kennedy, Florida	26
7.	January Hourly Peak Wind Speed Percentiles Versus Time of Day (10 m Level) at Cape Kennedy, Florida	27
8.	July Hourly Peak Wind Speed Percentiles Versus time of Day (10 m Level) at Cape Kennedy, Florida	27
9.	Monthly Percentiles (All Hours) Hourly Peak Wind Speed (10 m Level) at Cape Kennedy, Florida	28

CONTENTS (Continued). . .

Figure	Title	Page
10.	Probability (%) of Occurrence of Thunderstorms by Months Versus Time of Day in the Cape Kennedy Area for the Period January 1957 - December 1962	29
11.	Comparison of Daily Peak Winds With Maximum Daily Peak Thunderstorm Winds in July	30
12.	Calculated Risk Versus Exposure Time With Peak Wind Speed Referenced to 10 m (30 ft) Level at Cape Kennedy, Florida in July	31
13.	Calculated Risk Versus Exposure Time With Peak Wind Speed Referenced to 10 m (30 ft) Level at Cape Kennedy, Florida in October	32
14.	Fisher-Tippett Type I Distribution Collated to Peak Wind Speed Samples at Cape Kennedy, Florida in October	33
15.	Hourly Exposure Period Probability for Peak Wind Speed Being > 32 Knots (10 m Level) at Cape Kennedy, Florida in October	34
16.	Frequency of Scalar Wind Speed Exceeding 50 m/sec as a Function of Altitude and Months for the Years 1956-1963 at Cape Kennedy, Florida	35
17.	Frequency of Scalar Wind Speed Exceeding 75 m/sec as a Function of Altitude and Months for the Years 1956-1963 at Cape Kennedy, Florida	35
18.	Twice Daily Maximum Wind Speed in the 10-15 km Layer at Cape Kennedy, Florida	35
19.	Plot of Maximum Wind Speed in the 10-15 km Layer for the Years 1956-1963 During January at Cape Kennedy, Florida	39
20.	Probability of the Maximum Wind Speed in the 10-15 km Layer Being \geq and < Specified Values for k 12-hr Periods During January at Cape Kennedy, Florida	45

DIURNAL VARIATION OF DENSITY AND TEMPERATURE IN THE UPPER ATMOSPHERE

by Robert E. Smith	Page
SUMMARY	51
DIURNAL VARIATION IN ATMOSPHERIC DENSITIES	51
CONCLUSIONS	54
FUTURE ACTIVITIES	55
REFERENCES	55

LIST OF ILLUSTRATIONS

Figure	Title	Page
1.	Thermosphere Probe	52
2.	Diurnal Survey of the Thermosphere	53
3.	Marshall - University of Michigan Probe (MUMP) Diurnal Survey of the Thermosphere	53
4.	Temperature - Height Profiles	54
5.	MUMP Diurnal Survey of the Thermosphere	54

IONOSPHERIC DISTURBANCES CAUSED BY GROUND BASED ACOUSTIC
ENERGY SOURCES

by William T. Roberts	Page
SUMMARY	57
IONOSPHERIC DISTURBANCES	57
FUTURE PLANS	61
REFERENCES	62

LIST OF ILLUSTRATIONS

Figure	Title	Page
1.	Phase-Path Sounder Site Arrangement	58
2.	Pulaski, Tennessee Site Antenna Towers	58
3.	Huntsville Receiver Site	59
4.	Ionospheric Reflection of Transmitted Waves	60
5.	MSFC Swept-Frequency Ionosonde	60
6.	Record of Passage of Acoustic-Gravity Wave	60
7.	The Frequency Range of Acoustic Waves That Can Exist in the Atmosphere (Light Area) Considering the Limitations Imposed by Absorption and Acoustic Cutoff.	61

THE MASSES OF METEORS AND THE SELECTION OF A REPRESENTATIVE DATA SAMPLE Page

by Charles C. Dalton

SUMMARY	63
LIST OF SYMBOLS	63
INTRODUCTION	64
DATA SAMPLES OF METEORS	64
CONCLUSIONS	72
REFERENCES	72

LIST OF ILLUSTRATIONS

Figure	Title	Page
1.	Probability of Not Encountering Larger Meteoroids	64
2.	Mean Puncture Flux from Meteoroid Influx	65
3.	Meteor Velocity versus Absolute Photographic Magnitude	66
4.	Weighted Distribution of Velocity for Harvard-Mass Regimes	66
5.	Relation Between Harvard Meteor Mass and Magnitude-Above-Plate-Limit Extrapolated for 60 Degrees Zenith-to-Radiant and 11 km/sec Presupposing Harvard Luminous Efficiency	67
6.	Extrapolated Relations Between Meteor Absolute Photographic Magnitude and Magnitude-Above-Plate-Limit Presupposing Harvard Luminous Efficiency	67
7.	Mean Relation Between Meteor Velocity, Absolute Photographic Magnitude, and Magnitude-Above-Plate-Limit Extrapolated for 60 Degrees Zenith-to-Radiant and 11 km/sec Presupposing Harvard Luminous Efficiency	68
8.	Luminous Efficiency versus Velocity for Dustball Meteors	69
9.	Model Approximating Öpik's Luminous Efficiency for Dustball Meteoroids Smaller than One Hundred Grams	69
10.	Velocity-Dependence of the Intercept for the Model in Figure 9	70
11.	Velocity-Dependence of the Slope for the Model in Figure 9	70
12.	Criterion for the Right-Hand Discontinuity in Figure 9: Luminous Efficiency Independent of Mass for Smaller Meteoroids	70

MARTIAN ATMOSPHERIC VARIABILITY

by George S. West, Jr.

SUMMARY	75
INTRODUCTION	75
BASIS FOR DEVELOPMENT OF THE MSFC MODELS	75
PLANS FOR OBTAINING FUTURE DATA	78
REFERENCES	80
BIBLIOGRAPHY	80

LIST OF ILLUSTRATIONS

Figure	Title	Page
1.	Previous Models of the Mars Atmosphere	76
2.	Comparison of Martian Temperature Profiles Derived from Mariner IV	77
3.	Idealized Martian Temperature Profiles Assuming F ₂ or F ₁ Ionization Layer	78
4.	Atmospheric Density	79
5.	Microwave Spectroscopy Experiment Configuration	79

INTRODUCTION TO RESEARCH ACHIEVEMENTS REVIEW ON AEROSPACE ENVIRONMENT RESEARCH AT MSFC

By

Ernst D. Geissler

This review is concerned with problems of terrestrial and space environment and is the second of this kind on this subject. The first review was held in September 1965 and covered four topics. The present review covers seven items on terrestrial and space environment research.

The seven papers in this review are only samples of related activities in the Aerospace Environment Division of the Aero-Astrodynamic Laboratory. Several important topics are not included in this review, for example, investigation of fine structure of winds at altitudes around maximum dynamic pressure (jet stream level) and the broad problems of analysis and prediction of the atmosphere at orbital altitudes which are so important for orbital lifetime predictions.

The first topic was discussed in the previously mentioned research review, but many high resolution measurements of wind profiles have been obtained since then and valuable insights have been gained.

The second topic has been given coverage in a recent seminar program under the title "Environment Induced Orbital Dynamics" June 6&7, 1967 at MSFC [1].

Also, environmental research activities are carried out in the Space Sciences Laboratory, in particular in the areas of space radiation and micro-meteoroids. Discussions of these activities will be given in another meeting.

The responsibility within MSFC for formulating aerospace environment criteria is part of the Aero-Astrodynamic Laboratory's function and is directly related to the laboratory's work in the area of systems engineering and mission analysis. The Aerospace Environment Division is the responsible organizational element within the laboratory for conducting studies and research directed toward establishment of design and operational aerospace environment criteria.

The significance of having an integral group within the organization responsible for the study of atmospheric and space environment relations to engineering program requirements was recognized many years ago. Whereas earlier the concern was primarily with the atmosphere, in recent years increasing interest has also been directed towards aeronomy, planetary atmospheres and general space environment.

The development of an adequate set of space vehicle design and operational criteria is a job which requires a close relation between the scientific community and the engineers. The Aero-Astrodynamic Laboratory is striving to do enough research and to monitor enough outside research to provide the necessary input into various vehicle design and operational studies. Development of proper conceptual statistical tools is an important aspect of this endeavor.

While it may appear that there is only one set of terrestrial and space environment data, which would apply to all vehicles and increase in scope only with extension of the sphere of operations, actual experience shows a constant widening of the type of questions asked and data needed.

Even today, after many years of research and several generations of space vehicles, the major portion of the laboratory's effort is still devoted to the area of atmospheric dynamics for that early portion of the flight, where the vehicle is exposed to the largest external forces.

The significance of ground wind effects has increased with increasing size of the vehicles, and the sensitivity of the large Saturn V vehicle to ground wind effects required introducing a mechanical damping system for the vehicle on the ground as a fairly late design modification. In addition to this, a program was initiated to measure and interpret atmospheric turbulence phenomena close to the ground because

the atmospheric turbulence is a vehicle load producing factor during its stand on the launch pad and immediately after take-off. Also, the vulnerability to high ground winds required a thorough knowledge of exposure probabilities and related statistical techniques. The first three papers in this review will be devoted to this subject area.

The remaining papers will be concerned with more exotic items. The discussions of diurnal variation of density and temperature in the upper atmosphere [120 - 330 km] is just one sample of recent experimental results out of a very broad effort directed to gain understanding of high altitude atmospheric properties. They are subject to strong statistical and periodic variations and are of immediate interest for lifetime predictions, altitude control and station keeping studies connected with the AAP program.

The next discussion about ionosphere disturbances represents a modest attempt to make a contribution towards the understanding of the dynamics of the upper atmosphere, the flow fields and interaction of the electrically charged particles with general pressure disturbances of the neutral component of the upper atmosphere.

The presentation about masses of meteors and sample selections is considered a valuable contribution towards the proper interpretation of optical meteor sightings which contains about the most

critical particle size from the designers point of view and where some question exists about interpretation of observational data.

Finally, there will be some discussion of models available for the Martian Atmosphere. These models have been studied recently as a contribution for the planning of a planetary exploration program. The obvious message here is the lack of precise information and the indication of many gaps to be filled.

Much of the Aero-Astroynamics Laboratory's design and operational criteria work is formulated into environmental criteria guideline reports. One report considers the terrestrial atmosphere up to an altitude of 100 km. The other covers altitudes above 100 km, including the space environment, lunar, and planetary environments. These documents have been widely used in MSFC's programs, by other NASA organizations and by the DOD.

REFERENCE

1. Environment Induced Orbital Dynamics, Volumes I and II. Seminar Program, June 6-7, 1967, Marshall Space Flight Center, prepared by the Aero-Astroynamics Laboratory, Volume I 31 July 1967, Volume II 31 October 1967.

STRUCTURE OF ATMOSPHERIC TURBULENCE

By

George H. Fichtl

SUMMARY

The properties of the longitudinal component of turbulence are examined. It is found that the ratio of the variance of turbulence to the surface friction velocity is an increasing function of z/L' for unstable conditions and a constant for stable conditions. For neutral conditions, this ratio is 3.1. Tentative design values for the variance of turbulence are based upon this ratio for neutral conditions and KSC design ground wind envelopes. A theory of the variation of the gust factor with height based upon Rice's theory of exceedance probabilities is presented.

Finally the spectrum of turbulence is analyzed. An examination of the spectra of Dryden, von Kármán, and Lappe revealed that the turbulence data fit the three spectra equally.

INTRODUCTION

Within the atmospheric boundary layer, defined in this paper to be the first 150 m of the atmosphere, a thermally stratified shear flow exists. Energy is transferred from the mean shear flow to the turbulent portion of the total flow field via the gradients of mean velocity and entropy which produce Reynolds stresses and cause heat transfer to occur, respectively. Accordingly, the structure and intensity of turbulence in the atmospheric boundary layer are directly dependent upon the mean flow conditions. In principle, once the boundary conditions and the distributions of mean velocity and temperature are specified, the statistics, such as second and higher order velocity moments, of the turbulent portion of the total flow, can be determined through the hierarchy of the turbulence moment equations. In general, a closure hypothesis is required since the moment of equations constitute an infinite set of equations. The above comments imply that, associated with each mean (steady state) wind profile, i. e., 95.0, 99.0, and 99.9 percentile profiles, there is a unique set of

design statistics that characterize the turbulence structure of steady state design wind profiles. This means that the steady state design wind profiles and turbulence design statistics, in the form of spectral inputs or in the form of discrete gust inputs, should be prescribed so that they consistently reflect the coupling implied by the equations of motion. This may be accomplished experimentally, in part, by relating the longitudinal variance of turbulence to the mean flow since the square of the variance of turbulence is the net energy contained within the longitudinal spectrum. Accordingly, the first purpose of this paper is to relate the variance of the longitudinal component of turbulence and the gust factor to existing steady state design wind profiles for Kennedy Space Center. Based upon experimental observations, the longitudinal spectrum can be prescribed and related to the mean flow by allowing adjustable parameters like the integral scale of turbulence, for example, to appear in the analytical representation of the spectrum. Once the mean flow is related to the variance of turbulence and the scale of turbulence, the turbulence design input associated with a given steady state wind profile may be prescribed consistently.

Therefore, the second purpose of this paper is to test the analytical expressions of the longitudinal spectrum of turbulence derived by Dryden, von Kármán, and Lappe as to the adequacy of these expressions being reasonable representations of turbulence at KSC.

If, on the other hand, a gust factor is desired rather than a spectral wind input to describe turbulence, the variance of turbulence may still be used to couple the steady state wind profile to the turbulent portion of the flow field by introducing a suitable assumption about the statistical process of the turbulence. In particular, the assumption that turbulence is a Gaussian process is employed in this paper, and an expression is obtained that relates the gust factor to the variance of turbulence.

To relate the mean flow properties to the turbulence existing in the atmospheric boundary layer even on an experimental basis, as in this paper, a closure hypothesis must be introduced to effect a dimensional analysis that will imply the universal functions needed. In this paper the closure hypothesis of Monin and Obukhov [1] has been employed to imply relationships between the variance of turbulence and the mean flow.

VARIANCE OF TURBULENCE

The similarity hypothesis of Monin and Obukhov [1] predicts that within the steady mean-flow surface-boundary layer, characterized by constant tangential eddy stress and constant vertical heat flux,

$$\frac{\sigma}{u^*} = f\left(\frac{z}{L'}\right), \quad (1)$$

where σ and u^* denote the variance of the longitudinal wind fluctuations and the surface friction velocity, respectively, and $f(z/L')$ is a universal function of z/L' where z is the height and L' is given by

$$L' = \frac{u^* \frac{d\bar{u}}{dz} T}{kg \frac{d\theta}{dz}}. \quad (2)$$

In eq. (2), \bar{u} is the mean wind speed, T and θ denote the mean Kelvin temperature and potential temperature, respectively, k and g denote the von Kármán constant with numerical value equal to 0.4 and the acceleration of gravity, respectively, and u^* plays the role of a scaling velocity that is related to the surface stress τ through the relationship

$$u^* = \left(\frac{\tau}{\rho}\right)^{1/2},$$

where ρ is the mean density of air. Formally,

$$\tau = -\overline{\rho u' w'}$$

where u' and w' denote the longitudinal and vertical components of the turbulence portion of the velocity vector and the overbar denotes the time-averaging operator. In the absence of w' data, which is the situation at Kennedy Space Center at the present time, it is necessary to estimate u^* through a knowledge of the mean wind and temperature profiles.

Upon employing the Boussinesq approximation as discussed by Dutton and Fichtl [2] and invoking the conditions of Reynolds number similarity [3], steady state and horizontally homogeneous flow with negligible mean horizontal pressure gradient and hypothesizing that the ratio of the eddy heat conduction coefficient to the eddy momentum coefficient is a unique function of the gradient Richardson number, the similarity hypothesis of Monin and Obukhov predicts that

$$\frac{kz}{u^*} \frac{d\bar{u}}{dz} = \phi\left(\frac{z}{L'}\right), \quad (3)$$

where $\phi(z/L')$ is a universal function of z/L' . Upon integrating the above expression, subject to the boundary condition that the mean wind must vanish at z_0 (the mean height of the roughness elements at the surface of the earth), it is easily shown that

$$\bar{u} = \frac{u^*}{k} \left(\ln \frac{z}{z_0} - \psi\left(\frac{z}{L'}\right) \right), \quad (4)$$

where

$$\psi\left(\frac{z}{L'}\right) = \int_0^{-z/L'} \frac{1 - \phi(\xi)}{\xi} d\xi. \quad (5)$$

The definitions of L' and ϕ permit one to write

$$\frac{z}{L'} = \phi\left(\frac{z}{L'}\right) Ri, \quad (6)$$

where Ri is the gradient Richardson number defined to be

$$Ri = \frac{g}{\theta} \frac{d\theta}{dz} \frac{1}{\left(\frac{d\bar{u}}{dz}\right)^2}. \quad (7)$$

It follows from eq. (6) that

$$\frac{z}{L'} = h(Ri), \quad (8)$$

where $h(Ri)$ is a universal function of Ri . Ri is a parameter that characterizes the stability in a gravitational stratified shear flow [2] so that eq. (8) implies that z/L' is an equally valid parameter for specifying stability provided that z/L' is a single-valued function of Ri . This requirement is satisfied in general. The functions $h(Ri)$, $\psi(z/L')$ and $\phi(z/L')$ are given by Lumley and Panofsky [4].

For the sake of conciseness, these functions will not be presented in this paper, but they are known and are determined from data that consist of simultaneous measurements of heat flux, surface stress, and the mean wind and temperature profiles. The procedure for determining u^* based upon measurements of the mean wind and temperature profiles, with a known value of the surface roughness length, is as follows: (a) determine Ri and evaluate z/L' with eq.(8), (b) determine $\phi(z/L')$ from eq.(6) and thus $\psi(z/L')$ with eq (5), and (c) calculate u^* with the aid of eq.(4).

The scaling velocity u^* has been determined for seven cases of turbulence at KSC, and the ratio σ/u^* for these cases as a function of z/L' is shown in Figure 1. It appears that, for fixed L' and u^* ,

that σ is a decreasing function of height for unstable conditions ($z/L' < 0$), while σ is invariant with height for stable conditions ($z/L' > 0$). In addition, it appears in the case of neutral conditions ($z/L' = 0$), that σ/u^* has a wide spread of values; however, this spread may be false as a result of trends that existed in the data and which could perhaps cause unusually high values of σ . In the case of neutral stability, the Monin-Obukhov similarity hypothesis predicts σ/u^* to be a constant, $f(0)$. Based upon a mean value of σ/u^* for neutral conditions, $f(0) = 3.1$. Values of $f(0)$ reported by other authors are 2.45 by Davenport [5], 2.3 by Monin [6], 2.9 (O'Neill, Nebraska), 2.5 (Australia), 2.1 (Brookhaven), and 2.2 (pipe flow) by Lumley and Panofsky [4], and 2.7 by Prasad [7]. This wide range of values of $f(0)$ can be attributed to differences in the horizontal

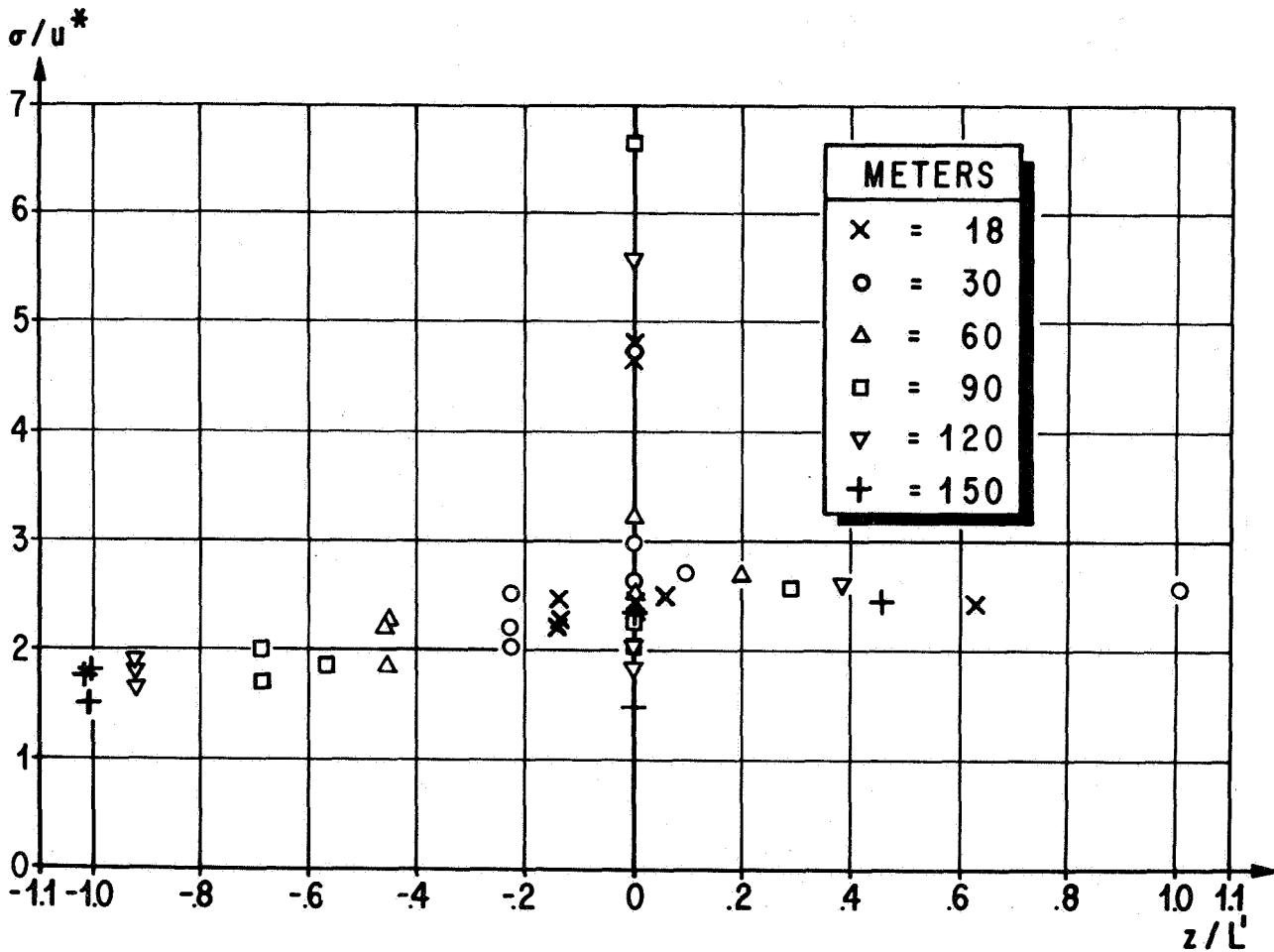


FIGURE 1. σ/u^* VERSUS z/L'

distribution of obstacles (houses, trees, hills, etc.). Gurvitch (Panofsky [8]) has found that σ/u^* is essentially constant for unstable conditions (z/L'). However, in his analysis, he used local values of u^* and L' , while in this study u^* and z/L' were determined with the wind and temperature data at 18 and 60 m. In general, the horizontal tangential eddy stress should decrease with height above the boundary layer so that the results of Gurvitch imply that σ decreases with height in the same proportion as the local friction velocity. The results in this study show that σ/u^* decreases with decreasing z/L' for unstable conditions. This appears to be in agreement with Gurvitch since u^* in this study is the surface friction velocity, thus requiring σ/u^* (surface u^*) to decrease with height.

The relationship between σ and u^* can play a useful role in the development of wind inputs for launch vehicle response calculations. In particular, it could aid in (1) the problem of developing a spectral input since σ^2 is the net energy contained within a given spectrum and (2) the development of a theory for the variation of the gust factor with height. It must be remembered that spectral inputs and gust factors are merely different ways of representing the same thing, namely, the wind fluctuations about a steady state profile.

In most instances strong winds are associated with a neutral ($\frac{z}{L'} = 0$) atmospheric boundary layer. In the cases of the 95.0, 99.0, and 99.9 percentile wind envelopes for Kennedy Space Center [9], the wind speeds are sufficiently strong so that neutral conditions can be assumed to exist if and when they occur, and one may interpret these design wind envelopes as wind profiles. In the case of the neutral boundary layer, $\psi(0)$ vanishes and the neutral wind profile is given by

$$\bar{u} = \frac{u^*}{k} \ln \frac{z}{z_0} \quad (9)$$

Table I shows the values of σ associated with the 95.0, 99.0, and 99.9 percentile levels of occurrence wind profiles for Kennedy Space Center based on values of u^* calculated from eq. (9) with the aid of the 18.3 m design winds and a surface roughness equal to 0.05 m.

It was pointed out previously that according to the similarity hypothesis of Monin and Obukhov, σ/u^* is an invariant with height for neutral conditions. This is strictly true within only the lowest portion of the atmospheric boundary layer where the tangential eddy stress and vertical heat flux are constants. The upper limit of this layer is in the order of 60 m at most. Above the constant stress and vertical heat flux layer, σ decreases so that above 60 m the values of σ in Table I are probably slightly conservative.

Table I. Values of σ

Percentile level of occurrence	Wind speed (m sec ⁻¹)	σ (m sec ⁻¹)
95.0	10.3	2.2
99.0	13.5	2.8
99.9	16.9	3.6

GUST FACTORS

If we assume that low level atmospheric turbulence is a stationary and random Gaussian process, then the theory of Rice [10] and the experimental results presented above provide a means for constructing a meaningful theory of the variation with height of the gust factor. Rice's theory predicts that the expected number of horizontal wind fluctuations per unit time that exceed the horizontal fluctuation velocity u' is given by

$$N(u') = N_0 e^{-u'^2/2\sigma^2} \quad (10)$$

where N_0 is the total number of positive crossings of the turbulence trace about the steady state wind per unit time. Combining eqs. (1), (4), and (10),

$$u' = \left(-2 \ln \frac{N}{N_0} \right)^{1/2} kf \left(\frac{z}{L'} \right) \left(\ln \frac{z}{z_0} - \psi \left(\frac{z}{L'} \right) \right)^{-1} \bar{u} \quad (11)$$

By definition the instantaneous wind u is merely the sum of the mean wind and the departure from that mean, so that upon using eq. (11), the result is

$$u(z) = G\left(z, \frac{N}{N_0}\right) \bar{u}(z), \quad (12)$$

where

$$G\left(z, \frac{N}{N_0}\right) = 1 + \left(-2 \ln \frac{N}{N_0}\right)^{1/2} k f\left(\frac{z}{L'}\right) \left(\ln \frac{z}{z_0} - \psi\left(\frac{z}{L'}\right)\right)^{-1} \quad (13)$$

G may be interpreted as the gust factor. For the case of strong winds (neutral wind conditions, $z/L' = 0$), $f(0) = 3.1$, and $\psi(0) = 0$, so that eq. (13) reduces to

$$G\left(z, \frac{N}{N_0}\right) = 1 + \left(-2 \ln \frac{N}{N_0}\right)^{1/2} \frac{k 3.1}{\ln z/z_0} \quad (14)$$

Figure 2 shows G as a function of z for $1 - N/N_0 = 0.5, 0.95, 0.99, 0.999$, and $z_0 = 0.05$ (tentative value of surface roughness for the NASA 150 m meteorological tower site at KSC). G may be interpreted as that gust factor which, when applied to the mean wind, will yield a peak wind that accounts for an expected fraction of gusts equal to $1 - N/N_0$. The results for $z > 60$ m are probably conservative since

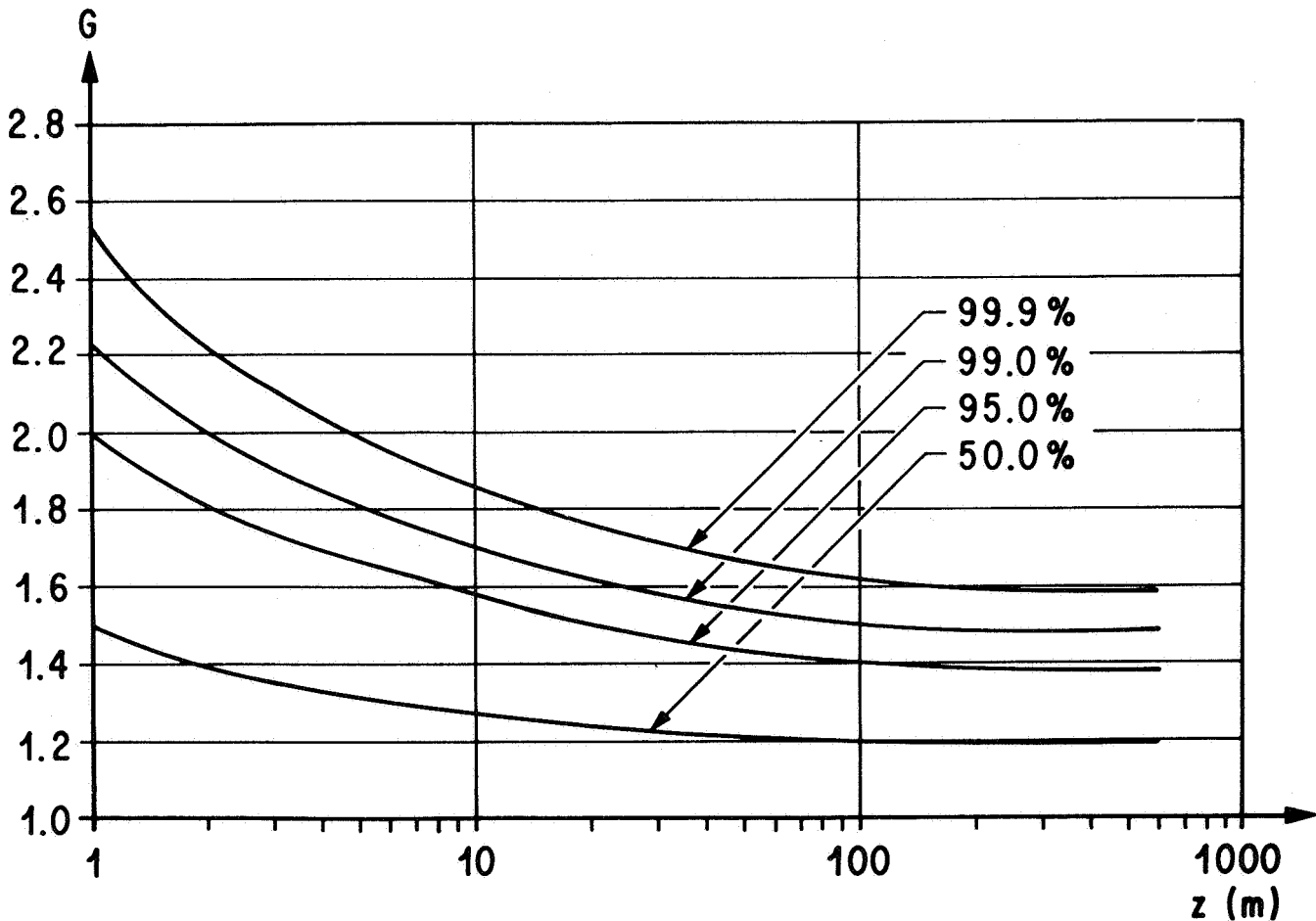


FIGURE 2. G VERSUS z

σ is overestimated as a result of breakdown of the Monin-Obukhov similarity hypothesis above 60 m. The curves for $z < 60$ m appear to be in agreement with the recent experimental results for KSC by Alexander [11].

WIND SPECTRA

In many instances it is useful to provide spectral wind inputs in the form of an analytical expression. For this purpose the analytical expressions of the longitudinal component of turbulence derived by Dryden and von Kármán [12] and Lappe [13] were selected to be tested against data from the NASA 150 m meteorological tower at Kennedy Space Center. These expressions are given by

$$\text{Dryden } \Phi(\nu) = \sigma^2 \frac{4L}{1 + (2\pi L\nu)^2} \quad (15)$$

$$\text{von Kármán } \Phi(\nu) = \sigma^2 \frac{4L}{(1 + 70.78 (L\nu)^2)^{5/6}} \quad (16)$$

$$\text{Lappe } \Phi(\nu) = \sigma^2 \frac{2\pi L}{(1 + 2\pi L\nu)^2}, \quad (17)$$

where $\Phi(\nu)$ is the spectral energy per unit wave number, L is the scale of turbulence, $\nu (= \omega / \bar{u})$ is the wave number in units of cycles per meter, and ω is the frequency in units of cycles per second. The most obvious difference between these spectra is the asymptotic behavior at large values of wave number. The spectra of Dryden and Lappe both behave like ν^{-2} for large wave number, while the von Kármán spectrum behaves like $\nu^{-5/3}$, in accordance with the concept of the inertial subrange by Kolmogorov (MacCready, 1962) [14]. Although the von Kármán spectrum behaves correctly for large wave numbers, both the Dryden and Lappe spectra facilitate analytical computations because of their rational form.

To compare the above mentioned representations with observations, time spectra obtained at 18, 30, 60, 90, 120 and 150 m were averaged in the vertical and converted to space spectra with the aid of Taylor's hypothesis [15] employing the 60 m level mean wind. These spectra were fitted to the analytical expressions given by eqs. (15) through (17) by the method of least squares and yielded a value for the scale of

turbulence for each type of spectrum under consideration. Experimental values of the horizontal integral scales of turbulence were obtained by vertically averaging the associated time correlation functions and then employing Taylor's hypothesis to convert time correlations to space correlations with the aid of the 60 m level wind speed and finally producing the integral

$$L = \int_0^\infty R(\xi) d\xi, \quad (18)$$

where ξ denotes lag distance. To account for trends that produce a constant value for the correlation function, R^* , greater than zero for large ξ , the observed correlation function $R_0(\xi)$ was corrected by the relationship

$$R(\xi) = \frac{R_0(\xi) - R^*}{1 - R^*} \quad (19)$$

derived by Webb [16]. Figure 3 shows a plot of the scale of turbulence obtained from the analytical expressions of von Kármán against the values of L calculated with the aid of eq. (18). Similar results were obtained for the Dryden and Lappe spectra.

The results appear to show a one to one correspondence between the two scales of turbulence in each case, and it appears that each spectrum may fit the data equally well. The results of the von Kármán spectrum appear to be in agreement with recent observations from Project Lo-Locat [17]. However, the results with regard to the Dryden and Lappe spectra appear to disagree in that the project Lo-Locat data revealed a poor fit to these analytical expressions. This may be attributed to the fact that the comparison in Project Lo-Locat was primarily in the inertial subrange, while the comparison in this paper was concerned with a wider range of wavelengths which included the inertial subrange as well as the knee of the spectrum.

CONCLUDING COMMENTS

The variance of turbulence has been shown to be related to the mean wind profile through the surface friction velocity and the Monin-Obukhov similarity hypothesis. This permits a prediction to be made of the energy associated with the horizontal wind fluctuations that would be consistent with a design wind

envelope, assuming that a design wind envelope may be interpreted as a wind profile. The technique presented in this paper is valid up to the 60 m level. However, above this level, an allowance should be made for the effects of the variation with height of the horizontal Reynolds stress, the Coriolis forces, and the pressure gradient forces upon the mean flow. Blackadar's [18] recent theory of the wind profile above the surface layer appears to account for these factors. In addition to these problems, it is necessary to be sufficiently judicious in the selection of parameters so that all the pertinent parameters are included in a dimensional analysis that would predict the dimensionless groupings of these parameters upon which σ/u^* is dependent. The wind profile law could aid in the solution of this problem. For example, the surface Rossby number

$$R_0 = \frac{u_g}{2 \Omega z_0 \sin \phi}$$

appears in the wind law of Blackadar [18], and it is reasonable to assume that σ/u^* also depends upon this parameter since the mean flow drives the turbulent portion of the flow. In defining R_0 , u_g , Ω , and ϕ denote the geostrophic wind at the top of the boundary layer, the angular velocity associated with the rotation of the earth on its axis, and the latitude, respectively. Finally, the variance of turbulence is dependent upon the surface roughness length. This means that a design value for σ derived from the NASA 150 m tower data may not be applicable at a given launch site because this σ was obtained for roughness conditions different from those on the launch pad. However, this effect may be taken into account by assuming that σ/u^* for neutral wind conditions (strong winds) is a true constant and evaluating u^* with the neutral wind profile using the launch site roughness. In this calculation it is implicitly assumed that the turbulence over the launch pad would be in equilibrium; this assumption is open to question.

It was noted earlier that the gust factor prediction in this paper is in agreement with the recent experimental results of Alexander [11] for the case of the neutral boundary layer. This agreement is best in the region below 60 m. The prediction above the 60 m level could be improved by accounting for the variation of the variance with height. In addition, the prediction of the gust factor at all levels could be improved by a better definition of the probability density function of the longitudinal wind fluctuations. Experimental and theoretical evidence now exists suggesting that the wind fluctuations at a point do not constitute a Gaussian process as assumed in this paper. It would perhaps be worthwhile to examine the statistical distribution of wind fluctuations. This information would also be useful in problems related to the diffusion of toxic fuels.

The results concerning the analysis of the horizontal scales of turbulence are most applicable at the 60 m level. The spectra used in this study appear to show a variation with height for both unstable and stable conditions, implying that the scale of turbulence is a function of height. However, for the neutral cases (strong winds), the spectra appeared to have no variation with height, thus implying that the horizontal scale of turbulence is independent of height for the strong wind situation. These results appear to agree with those of Davenport [5].

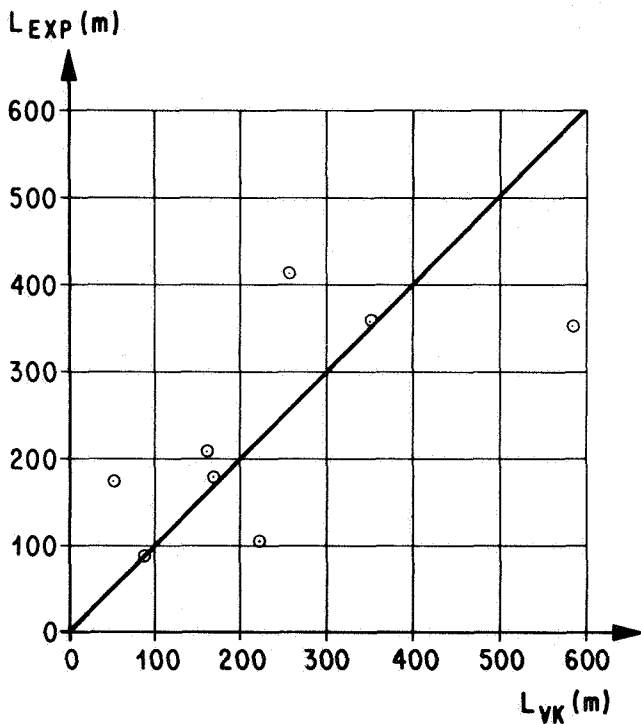


FIGURE 3. EXPERIMENTAL VALUES OF TURBULENCE VERSUS VON KÁRMÁN VALUES OF TURBULENCE

REFERENCES

1. Monin, A. S.; and Obukhov, A. M.: Basic Regularity Inturbulent Mixing in the Surface Layer of the Atmosphere. Trudy Geophysical Institute, ANSSSR, 24, 1954, p. 163.
2. Dutton, J. A.; and Fichtl, G. H.: Approximate Equations of Motion for Gases and Fluids. Unpublished manuscript.
3. Townsend, A. A.: The Structure of Turbulent Shear Flow. Cambridge at the University Press, Cambridge, Maryland, 1956.
4. Lumley, J. L.; and Panofsky, H. A.: The Structure of Atmospheric Turbulence. Interscience Publishers, New York, 1964.
5. Davenport, A. G.: The Spectrum of Horizontal Gustiness Near the Ground in High Winds. Quarterly Journal Ray Meteorological Soc., vol. 87, 1961, p. 194.
6. Monin, A. S.: Empirical Data on Turbulence in the Surface Layer of the Atmosphere. Journal of Geophysical Research, vol. 67, 1962, p. 3103.
7. Prasad, V.: Private communication, 1967.
8. Panofsky, H. A.: Private communication, 1967.
9. Daniels, G. E.; Scoggins, J. R.; and Smith, O. E.: Terrestrial Environment (Climatic) Criteria Guidelines for Use in Space Vehicle Development, 1966 Revision. NASA TM X-53328, NASA-Marshall Space Flight Center, Huntsville, Alabama, May 1, 1966.
10. Rice, S. O.: Mathematical Analysis of Random Noise. Bell System Technical Journal, vol. 23, 1944, p. 46.
11. Alexander, M.: Private communication, 1967.
12. Pritchard, F. E.; Casterbrook, C. G.; and McVehil, G. E.: Spectral and Exceedance Probability Models of Atmospheric Turbulence for Use in Aircraft Design. TR AFFDL-TR-65-122, Air Force Flight Dynamics Laboratory, Research and Technology Division, Air Force Systems Command, Wright-Patterson Air Force Base, Ohio, 1965.
13. Lappe, U. O.: Design of a Low Altitude Turbulence Model for Estimating Gust Loads on Aircraft. Technical Report AFFDL-TR-64-170, Air Force Flight Dynamics Laboratory, Research and Technology Division, Air Force Systems Command, Wright-Patterson Air Force Base, Ohio, 1965.
14. MacCready, P. B., Jr.: The Inertial Subrange of Atmospheric Turbulence, "Journal of Geophysical Research, vol. 67, 1962, p. 1051.
15. Taylor, G. I.: The Spectrum of Turbulence. Proc. Roy. Soc., A164, 1938, p. 476.
16. Webb, F. K.: Autocorrelations and Energy Spectra of Atmospheric Turbulence. Technical Paper No. 5, Melbourne, C. S. I. R. O., Div. Met. Physics, 1955.
17. Gault, J. D.: Low Altitude Atmospheric Turbulence, Lo-LoCat Mid-term Technical Data Analysis. Systems Engineering Group, Research and Technology Division, Air Force Systems Command, Wright-Patterson Air Force Base, Ohio, 1967.
18. Blackadar, A. K.: The Vertical Distribution of Wind and Turbulent Exchange in a Neutral Atmosphere. Journal of Geophysical Research, vol. 67, 1962, pp. 3095-3102.

WIND AND GUST CHARACTERISTICS IN THE LOWER 150 m OF THE ATMOSPHERE AT KSC, FLORIDA

By

Margaret Alexander,
Dennis W. Camp,
C. Kelly Hill, and
John W. Kaufman

SUMMARY

The results of recent research studies for improving our knowledge of the lower atmosphere at KSC, Florida, are presented. These studies involve data measurements obtained from NASA's 150-m meteorological tower located at KSC, Florida, close to Launch Complex 39A, the launch site for the Saturn vehicle. This proximity to the Saturn launch site makes the tower facility especially useful for obtaining ground wind information for input to Saturn design and launch criteria.

A gust factor is defined as the maximum wind speed during some finite period divided by the mean wind speed for the same period. Mean and maximum gust factors are plotted as a function of mean wind speeds for several different time-averaging periods and for six levels on the tower.

Relationships are shown between mean wind speeds and the standard deviations of wind speed and direction. Statistics of the frequency of occurrence of gusts versus their duration, obtained from data measurements on the tower, have been computed using large samples of gusts with periods of 4 to 6 sec.

Studies using these tower data provide new and pertinent information on peak wind speed profiles, gusts, and gust factors.

INTRODUCTION

Earlier measurements of lower atmospheric wind data for the KSC, Florida area were obtained from wind sensors installed at a single height above the ground. Such observations have been made at Patrick Air Force Base and at the Cape Kennedy Weather Station for several years. The lack of descriptive wind profile data, however, has severely limited the amount of research that could be undertaken to investigate lower atmospheric turbulence and its effects on Saturn vehicles during exposure to such winds while on the launch pad. Consequently, a 150-m meteorological tower was erected at KSC, Florida in the vicinity of Launch Complex 39 (Fig. 1) and has been in operation since December 1965. It has thus far been an excellent source of wind and temperature profile data and measurements of atmospheric pressure, humidity and radiation data. The capability of this facility to obtain measurements of both high resolution magnetic tape recorded wind profile data and paper strip chart data makes it extremely valuable for studying Saturn response characteristics to winds.

There are numerous acceptable ways to analyze NASA's 150-m meteorological tower data. Some of the more effective analytical approaches are discussed in this report. Although the results from these analyses of wind profile data are not final, they do give some valuable insight into the solution of problems dealing with ground winds for the design and launch of Saturn vehicles.

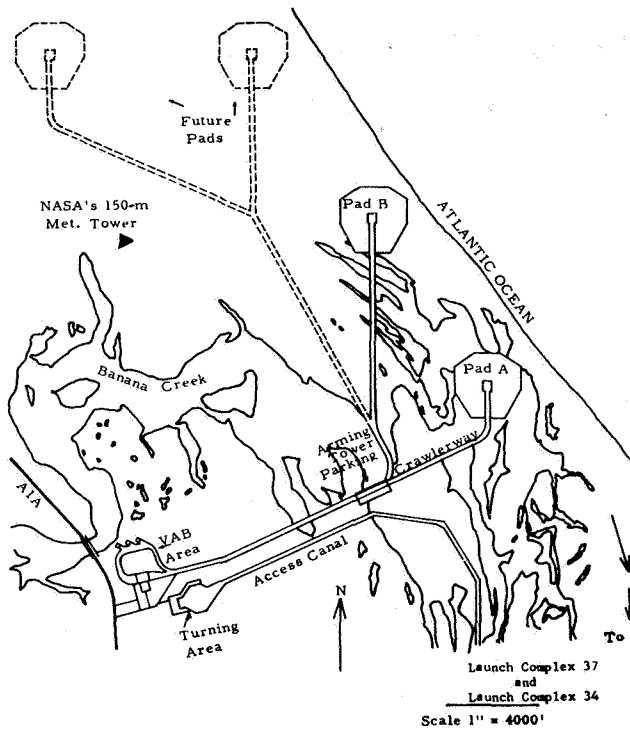


FIGURE 1. NASA LAUNCH COMPLEX 39, KSC, FLORIDA

NASA'S 150-m METEOROLOGICAL TOWER FACILITY

This important new source of lower atmospheric data [1] from KSC, Florida, now being used to develop wind and turbulence criteria for MSFC vehicle programs, is situated about 3 1/2 miles northwest of Launch Complex 39A and approximately 3 miles north of the Vehicle Assembly Building. Prominent topographical features in the vicinity of the tower include a creek about 150 m southwest and a line of palmetto trees oriented in a north-south position about 300 m west of the facility. Otherwise, the terrain around the tower is relatively flat with no large man-made structures nearby, other than the tower itself, which would cause significant changes in the local wind environment. The total facility consists of the 150-m tower, a smaller 18-m tower located 18 m northeast of the large tower, and a small building in which the wind, temperature, humidity, pressure and solar radiation data are recorded.

Wind data are measured by sensors on dual-mounted booms (3.66 m) positioned on the northeast and southwest sides of the large tower and on the northeast corner of the small tower. Figure 2 depicts the six positions of the wind sensors on the large tower (18, 30, 60, 90, 120, and 150 m) and two positions on the small tower (3, 18 m). The small tower is necessary to obtain a representative wind profile near the ground because the large tower significantly disturbs the flow and causes unrepresentative measurements below the 18-m level. Other meteorological measurements at this facility, including six levels of temperature (3, 18, 30, 60, 120, 150 m) and three levels of dewpoint (3, 60, 150 m), surface pressure and pyranometric measurements (direct and diffused solar radiation), are recorded inside the small building near the base of the tower. A 14-channel magnetic tape recorder also located in this building is used to record high resolution wind data either hourly or during special short selected periods for gust and turbulence studies. An automatic wind direction switching device that chooses the best exposed bank of wind instruments is incorporated into the tower facility.

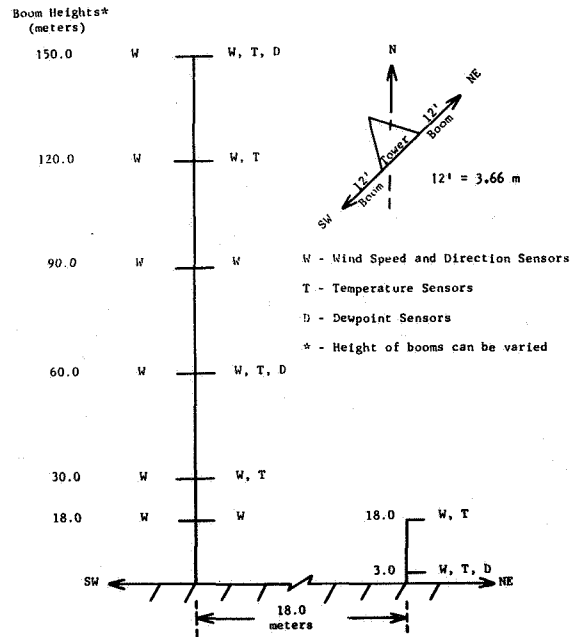


FIGURE 2. SCHEME FOR PLACEMENT OF METEOROLOGICAL SENSORS ON NASA'S 150-m METEOROLOGICAL TOWER, KSC, FLORIDA

This tower facility was purposely built near Launch Complex 39 for effective use of the wind statistics and related gust and turbulence information developed from the tower data in Saturn vehicle design and launch criteria.

CHARACTERISTICS OF WIND VELOCITY PROFILE DATA

VARIABILITY OF WIND SPEED AND DIRECTION

The variability of lower atmospheric wind speed and direction is often presented in the form of standard deviations (S. D. or sigma values). Figure 3 shows how the standard deviations of wind speed and direction behave as a function of wind speed. These mean sigma curves were "smoothed in" using approximately 80 S. D. values computed for each height represented (i. e., 18, 30, 60, 90, 120, and 150 m). The standard deviations were calculated from 5-min samples of data, which were recorded simultaneously during the afternoon when the thermal lapse rates were neutral to unstable. The mean wind speeds for these data samples fell within ranges of 2.0 to 15.0 m/sec for the lower level (18 m) and from 2.0 to about 25.0 m/sec for the higher levels (i. e., 90, 120, and 150 m).

As expected, the variability of wind speed increases with increasing wind speed and decreases as a function of height. Wind direction variability, however, decreases with increasing wind speed and decreases with height.

RATIO OF MAXIMUM WIND SPEEDS TO PEAK WIND SPEEDS

The question is often asked, "Can peak wind speeds for each individual height occur simultaneously in a given time interval over the entire length of the Saturn vehicle?" To gain some insight into this question, a direct approach was taken to determine if the simultaneously measured maximum wind speeds did closely approximate or equal the peak wind speeds. As an example, a 5-min sample of wind speed data was simultaneously recorded from anemometers located at the 18, 30, 60, 90, 120, and 150 m levels on NASA's 150-m meteorological tower. (Such data are actually digitized from analog magnetic tape recorded data at the rate of 10 samples/sec.)

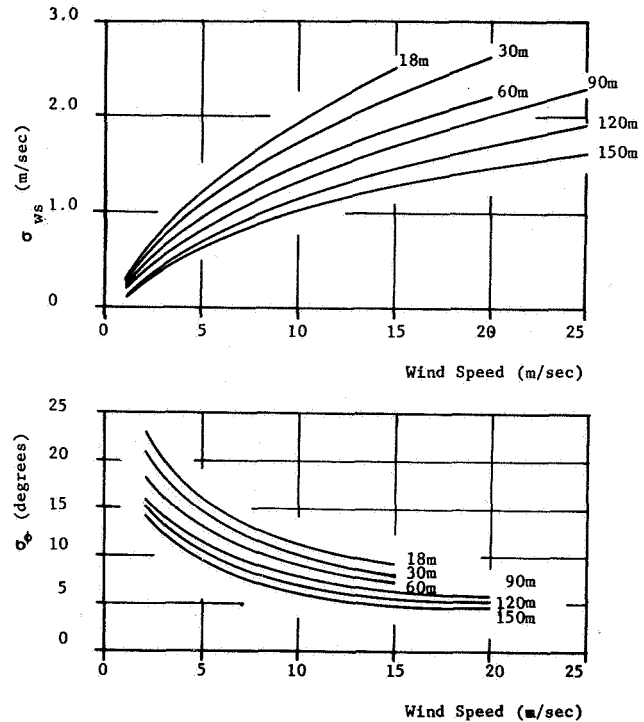


FIGURE 3. SIGMA (S. D.) CURVES OF WIND SPEED AND WIND DIRECTION VERSUS WIND SPEED COMPUTED FROM WIND VELOCITY DATA RECORDED AT NASA'S 150-m METEOROLOGICAL TOWER, KSC, FLORIDA

The arithmetic mean wind speed was then computed for these 5-min samples for each level. These mean values were then plotted, and a mean wind speed profile was drawn (Fig. 4). After the peak wind speed for the 5-min sample for each height was determined and plotted, a peak wind speed profile was established. It must be realized that the peak wind speeds over a finite time period seldom, if ever, occur simultaneously at all levels. The maximum integrated value of simultaneously measured wind speeds for this 5-min sample was determined by calculating an average wind speed (\overline{ws}) using digitized 0.1-sec wind speeds measured at the six levels. This 5-min sample, digitized at a rate of 10 samples/sec, provides 3,000 simultaneous wind profiles. The ratio of the average maximum wind speed profile (\overline{ws}_m) to the average of the peak wind speeds (\overline{ws}_p) was then determined; i. e., $\overline{ws}_m / \overline{ws}_p = 0.95$ for the sample shown in Figure 4.

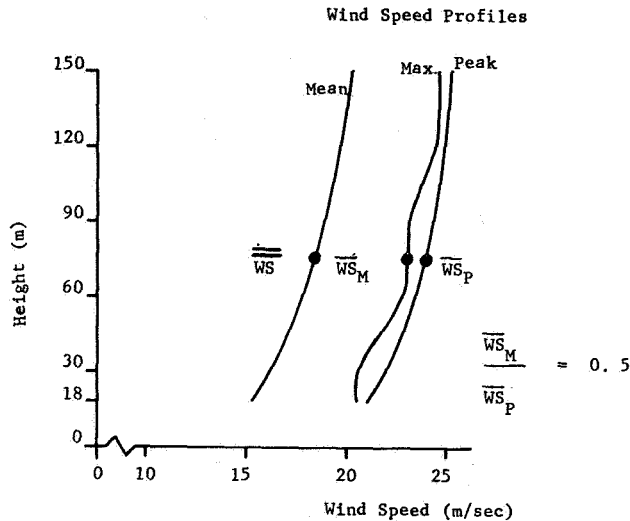


FIGURE 4. RATIO OF MAXIMUM WIND SPEEDS TO PEAK WIND SPEEDS COMPUTED FROM ONE 5-min SAMPLE OF DATA

Figure 5 shows 74 ratios of $\overline{ws}_m / \overline{ws}_p$ plotted as a function of the mean of mean wind speed profiles (\overline{ws}); i. e., the mean wind speeds computed for each of the six levels were simply averaged. From the relationship of the ratios of average maximum wind speeds (\overline{ws}_m) to average peak wind speeds, as shown in Figure 4, it can be seen that, although the maximum wind speeds did not equal the peak wind speeds, the maximum instantaneously measured winds can very closely approximate the peak wind. Ratios up to 0.97 were computed for the mean of mean wind speeds (\overline{ws}) beginning at approximately 7.0 m/sec speed and above (Fig. 5). Consequently, it is justifiable to design vehicles to withstand peak wind speed conditions; this has been the policy followed by MSFC/NASA space vehicle engineers in the past [2].

WINDS ASSOCIATED WITH A THUNDERSTORM

During a thunderstorm in the vicinity of NASA's 150-m meteorological tower at KSC, Florida, on May 9, 1967, at approximately 1418 Z wind profile data were recorded from 7 anemometer levels (i. e., 3, 18, 30, 60, 90, 120, and 150 m). Wind speed data recorded and digitized from analog magnetic tape recordings were plotted for every 15 sec and for each of the 7 levels. From this, a

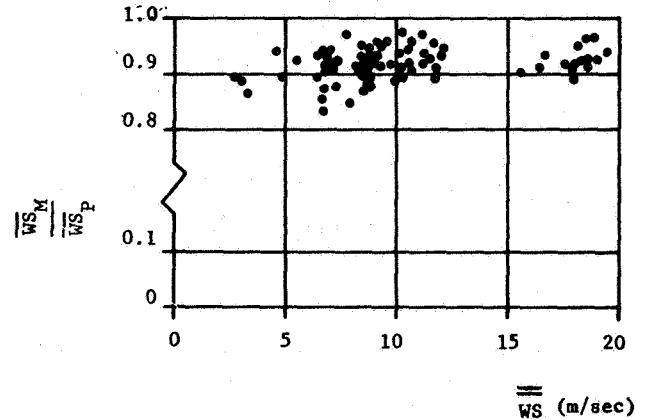


FIGURE 5. RATIO OF MAXIMUM WIND SPEEDS TO PEAK WIND SPEEDS AS A FUNCTION OF MEAN WIND SPEED BASED ON 74 5-min SAMPLES OF WIND SPEED PROFILE DATA

height-time cross section of a 10-min period which included these thunderstorm winds (Fig. 6) showed that (1) the wind speeds increased (decreased) to their maximum (minimum) values in about a 15- to 30-sec time period, (2) wind speed increases and decreases were in the order of 6 to 9 m/sec, (3) two maximum wind speed regimes were characterized (one between the 120- and 150-m level and the other between the heights of 18 and 60 m), (4) generally, the maximum winds occurred at the top levels first, then worked down to the lower levels, and (5) the maximum winds did not occur simultaneously (see the time of occurrence of maximum wind speeds at different levels as shown on Figure 6). Two other sets of wind profile data similarly measured during the passage of thunderstorms at the tower site, but are not shown here, strongly support comments (4) and (5) above.

The variability of wind velocity profile data is, indeed, fascinating both from its relationship to vehicle structural design and from a purely academic viewpoint. This section has discussed the measurement and analysis of conditions in the lower 150 m of the atmosphere, and an anomaly of winds associated with a thunderstorm. Several research projects are in progress which hopefully will provide a better understanding of the winds in the lower atmosphere. Lower atmospheric data are being continuously recorded at the KSC, Florida launch area for use in these studies.

* HEIGHT (m)	TIME (zulu)	WS PEAK (m/sec)
150	14:18:10.5	17.9
120	14:18:10.2	17.5
90	14:18:0.8	13.5
60	14:17:52.3	16.3
30	14:18:14.4	16.5
18	14:18:14.7	16.8
3	Missing	Missing

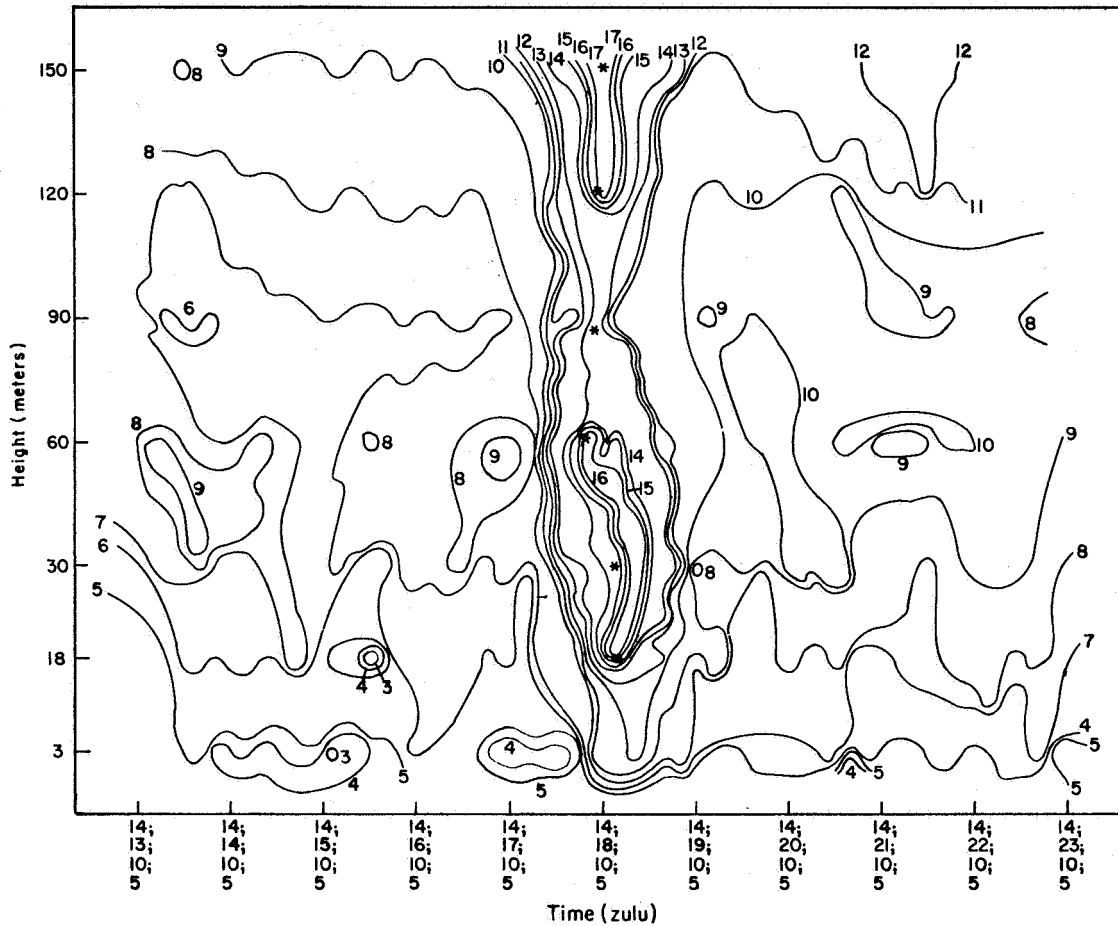


FIGURE 6. HEIGHT-TIME CROSS SECTION OF WIND ASSOCIATED WITH A THUNDERSTORM AS OBSERVED AT 150-m METEOROLOGICAL TOWER, KSC, FLORIDA, ON MAY 9, 1967 (14:13:10.5 - 14:23:10.5 ZULU) TEST NUMBER 150094; ws-m/sec

GUST FACTOR ANALYSIS

Marshall Space Flight Center has adopted a gust factor of 1.4 [2] for Saturn vehicle design and operational problems at KSC, Florida. The general practice has been to treat the gust as acting over the

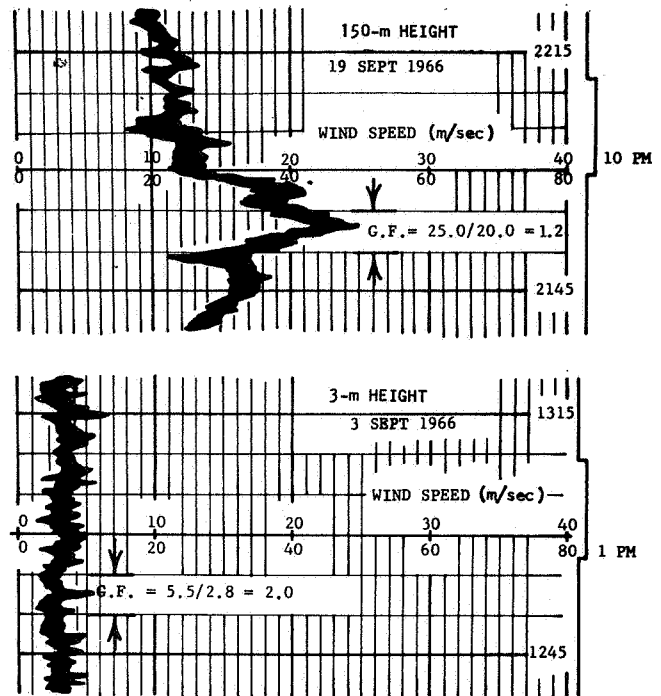
entire length of the vehicle. However, numerous questions regarding vehicle response calculations for drag and lateral lifting forces resulted in initiating a more detailed gust factor analysis. The gust factor represents a maximum wind speed fluctuation about a steady state speed and is a function of steady state or mean wind speed, the

length of time used to obtain the mean wind, the prevailing stability conditions, terrain features, and height.

To more precisely determine the gust factor to a height of 150 m, analyses have been made relating gust factor to height, mean wind speed, and various time averaging periods to define the mean wind speed. Data used in these studies were recorded during September 1966 through August 1967 at NASA's 150-m meteorological tower facility located in the vicinity of Launch Complex 39 at KSC, Florida, Florida.

A gust factor is computed by dividing the peak wind speed which occurs over a finite period by the mean wind speed for the same time period. Figure 7 shows how the gust factor is computed using wind data recorded on paper strip charts during September 1966 at the 3- and 150-m heights. The 3-m sample occurred on the third of September about noon; the 150-m sample occurred on September 19 about 10 pm EST. In both cases, a mean wind speed averaging period of five minutes was used. At 3 m, a peak wind speed of 5.5 m/sec and a mean wind speed of 2.8 m/sec give a gust factor of 2.0, while a 25 m/sec peak wind speed at the 150-m height and a 20 m/sec mean wind speed give a gust factor of 1.2. In other words, a large gust factor is not necessarily the result of a high peak gust.

Results of the analysis of 63 one-hour samples of data recorded on magnetic tape during hours when the atmosphere is generally unstable (daytime data) are presented in Figures 8 and 9. How the mean gust factors vary as a function of height (18, 30, 60, 90, 120, and 150 m), mean wind speed (2 through 24 m/sec), and mean wind speed averaging period (0.5, 1, 2, 5, and 10 min) is illustrated in Figure 8. A similar illustration for maximum gust factors is presented in Figure 9. Between 4570 and 7028 gust factors were computed for each mean gust factor curve in Figure 8 for mean wind speeds ranging from 2 to 24 m/sec. Figure 9 shows the maximum gust factor curves obtained by enveloping the extreme gust factors associated with the mean gust factors of Figure 8. Both figures illustrate that the mean and maximum gust factors decrease with height, increasing wind speeds, and shorter averaging periods for mean wind speed.



$$G. F. = \frac{WS_{max}}{\overline{WS}}$$

where

G. F. is gust factor

WS_{max} is maximum wind speed during a 5 minute period

\overline{WS} is mean wind speed for the 5 minute period

FIGURE 7. EQUATION FOR COMPUTING GUST FACTOR WITH TWO EXAMPLES

The MSFC environmental criteria value of 1.4 for gust factor over an averaging period for mean wind speed of two minutes appears to be a representative one. This fact is indicated by comparing this 1.4 value to the two-minute averaged curves for the 18-through 150-m heights. The analysis of gust factor, however, is continuing with emphasis on deriving a general equation (most likely an exponential one) for gust factor with variables of time, height and mean wind speed. Results will be documented in the near future.

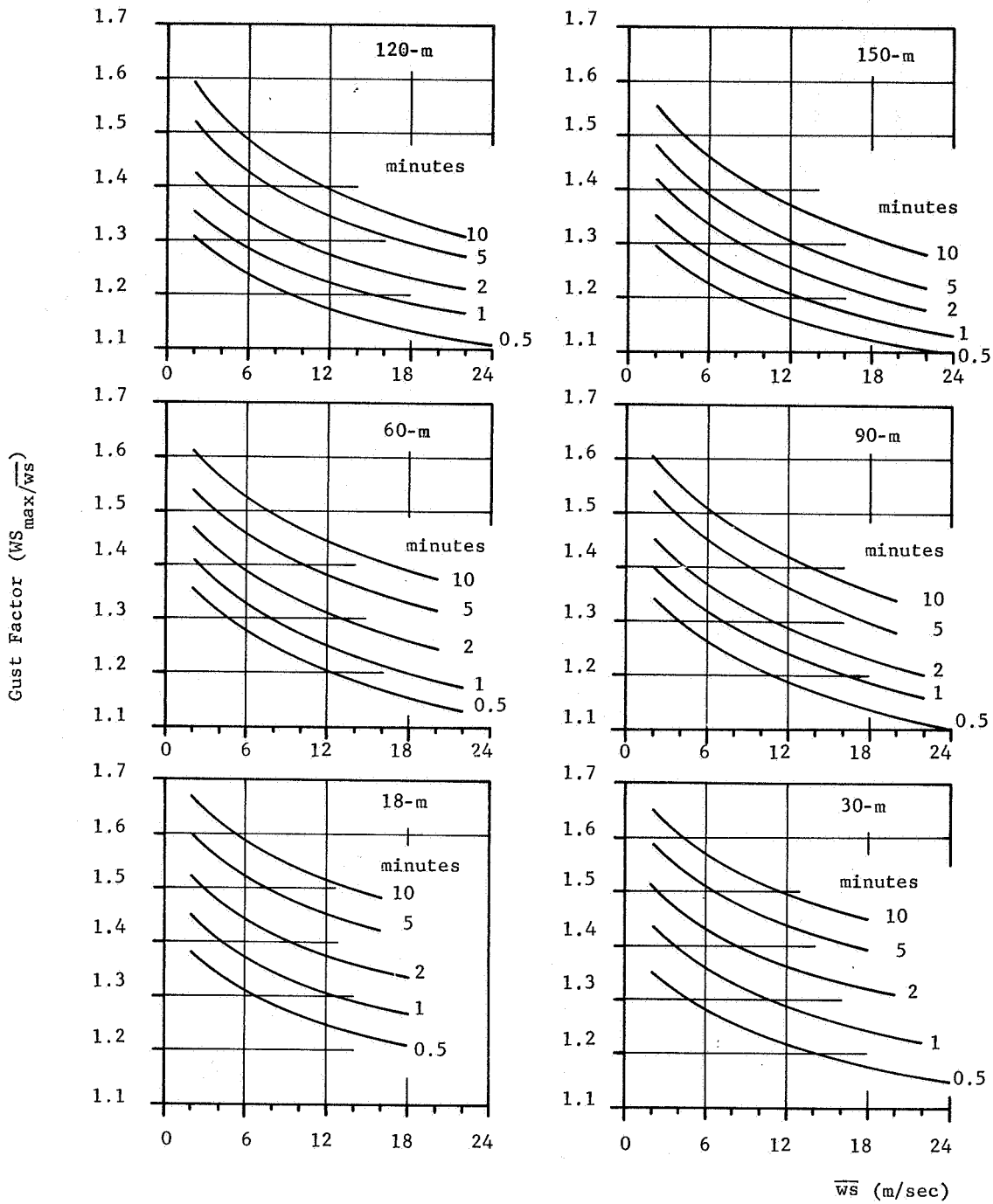


FIGURE 8. MEAN GUST FACTOR FOR SIX HEIGHTS AS A FUNCTION OF MEAN WIND SPEED AND FIVE MEAN WIND SPEED AVERAGING PERIODS FROM DATA RECORDED AT NASA'S 150-m METEOROLOGICAL TOWER, KSC, FLORIDA

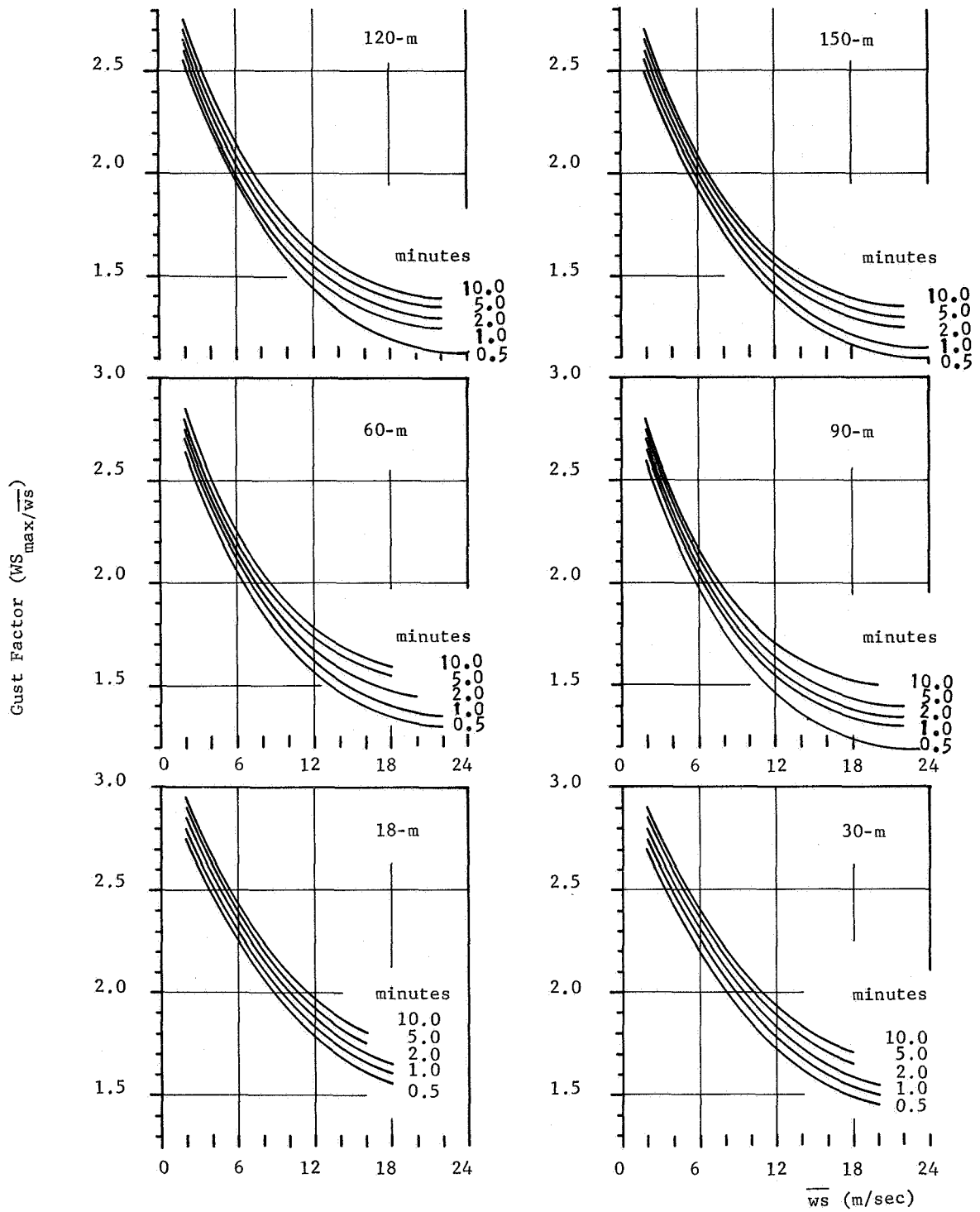


FIGURE 9. MAXIMUM GUST FACTOR FOR SIX HEIGHTS AS A FUNCTION OF MEAN WIND SPEED AND FIVE MEAN WIND SPEED AVERAGING PERIODS FROM DATA RECORDED AT NASA'S 150-m METEOROLOGICAL TOWER, KSC, FLORIDA

GUST CHARACTERISTICS

Before discussing the characteristics of a gust, it is necessary to define the wind gust as used in this analysis. A wind gust is defined as a build-up in the measured instantaneous wind speed above a two-minute arithmetic mean wind speed to an amplitude equal to or greater than 0.5 m/sec and a decay back to the mean wind speed (Fig. 7). With this definition of a wind gust, two characteristics of the gust were considered: (1) percentage of occurrence of gusts for various gust period durations and (2) a statistical gust for various gust duration periods.

Figure 10 illustrates the percentage of occurrence of gusts for various gust duration periods based on 1400 gusts recorded at the 18-m level on NASA's 150-m meteorological tower. As expected, gusts having the shorter duration periods occur more frequently. Almost identical percentage-of-occurrence distributions were obtained for the other tower levels. A more detailed presentation of the percentage of occurrence of various gusts will be published soon. A statistical gust is illustrated in Figure 11, where the 50, 90, 95, and 99 percentile values, determined from a cumulative frequency distribution of 583 measured wind gusts having a period of 4.0 to 6.0 sec, are plotted. Superimposed on the statistical curves is an actually measured wind gust. This observed gust has been plotted for every 0.2 sec. Statistical gusts for the levels above 18 m were similar to the ones shown in Figure 11, but the magnitudes of the gusts were smaller.

CONCLUSIONS

The tower data from NASA's 150-m facility at KSC, Florida are now contributing significantly to MSFC's Saturn vehicle research efforts through the application of results from studies of lower atmospheric wind profiles and turbulence. As additional tower data become available, improvements are expected in the relationships of the shape of wind profiles and their characteristic fluctuations in speed and direction. The conclusions pertaining to wind gusts and gust factors are vitally important in the establishment of vehicle design and launch guidelines for Saturn vehicles. Deriving a general equation for the gust factor and determining the function which most nearly defines the gust shape will be emphasized in future studies.

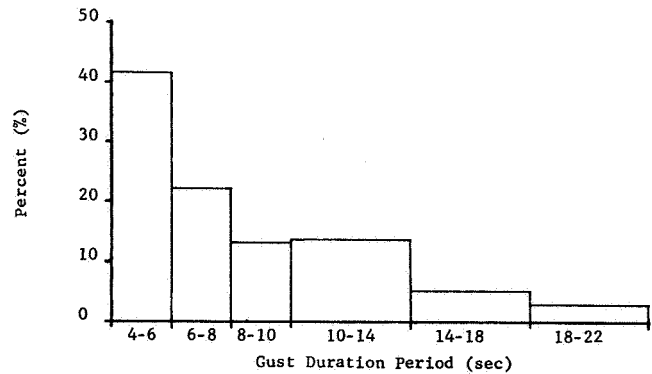


FIGURE 10. PERCENTAGE OF OCCURRENCE OF GUSTS HAVING VARIOUS DURATIONS BASED ON 1400 GUSTS RECORDED AT THE 18-m LEVEL ON NASA'S 150-m METEOROLOGICAL TOWER, KSC, FLORIDA

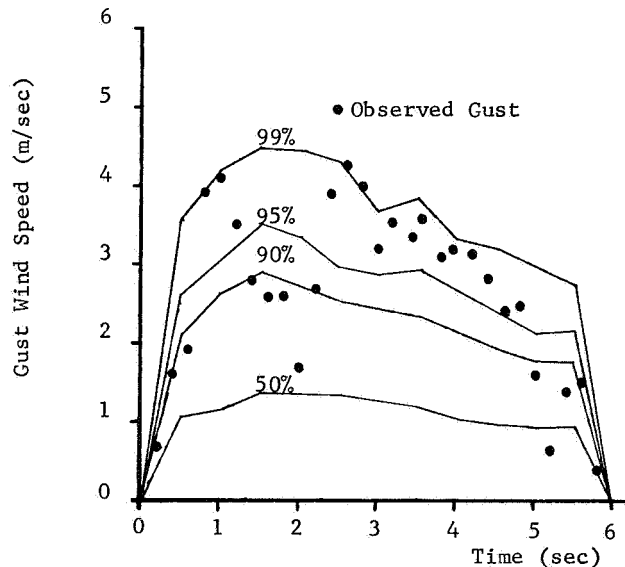


FIGURE 11. PERCENTILE GUST SHAPES BASED ON 583 GUSTS OF TIME DURATION OF 4 TO 6 sec OCCURRING AT THE 18-m LEVEL

REFERENCES

1. Kaufman, John W.; and Keene, Lester, F.: NASA's 150-m Meteorological Tower Located at Cape Kennedy, Florida. TM X-53259, Marshall Space Flight Center, May 12, 1965.
2. Daniels, Glenn E.; Scoggins, James R.; and Smith, Orvel E.: Terrestrial Environment (Climatic) Criteria Guidelines for Use in Space Vehicle Development, 1966 Revision. TM X-53328, Marshall Space Flight Center, May 1, 1966.



A STATISTICAL ANALYSIS OF WINDS FOR AEROSPACE VEHICLE DESIGN , MISSION PLANNING, AND OPERATIONS

By

Orvel E. Smith, Lee W. Falls, and S. Clark Brown

SUMMARY

Several statistical concepts in the analysis of a time ordered data sample are presented in terms of wind statistics applicable to aerospace vehicle design and operational problems. These concepts include extreme values, calculated risk, exposure period probabilities, exceedance probabilities, persistence, runs, and conditional probabilities. Examples of the resulting wind statistics for these probabilities, using a sample of hourly peak winds and eight years of serially complete winds aloft records for Cape Kennedy, Florida, are presented.

INTRODUCTION

The statistical analysis of a variable such as wind speed is difficult because of the extreme variability of this atmospheric element in time and space. Statistical methods of analysis may be divided into two general categories, descriptive and analytical, both of which depend primarily on the basic laws of probability. Descriptive methods reduce large amounts of data to a few meaningful "statistics" such as measures of location (mean, mode) and measures of variation (variance, standard deviation). A theoretical statistical model is assumed for the observations, and analytical methods are used to determine how well the empirical data fit this model. Thus, the analytical procedures determine the "goodness-of-fit" between theory and observation.

The many estimates of peak wind speed probabilities derived from empirical statistics in the past have not been completely satisfactory. Classical statistical methods are not adequate when the variable of interest is the largest in a set of observations.

The theory of extreme values developed by the late E. J. Gumbel [1] was found to be an efficient and adequate statistical model for the analysis of extreme surface winds for vehicle launch and mission planning purposes.

After considering the range of the winds aloft and the rather high time correlation between observations, it was decided to develop empirical statistics from this data sample. Consequently, all probability statements concerning the winds aloft are empirical statistics.

EXTREME VALUE THEORY

In a set of N independent extremes, x_1, x_2, \dots, x_n , each being the extreme of one of N sets of n observations (where the N extremes are unlimited, exponentially distributed variables), as both N and n grow large the cumulative probability that any of these N extremes will be less than any chosen quantity, x , approaches

$$\Phi(x) = \exp[-e^{-y}] \quad (1)$$

where

$$y = \alpha(x - \mu), \text{ or } x = \mu + \frac{y}{\alpha} \quad (2)$$

for largest extremes. In eq.(2), α is a measure of concentration about the mode μ ; i. e., α is a scale parameter and μ is a location parameter.

By the theory of least squares, α and μ can be estimated from the sample by

$$\alpha = \frac{\pi}{S_x \sqrt{6}} \quad \text{and} \quad \mu = \bar{x} - \frac{\gamma}{\alpha} \quad (3)$$

where $\gamma = \text{Euler's constant} = 0.57722$, and \bar{x} and S_x are the mean and standard deviation of the set of N observed extremes.

We define return period, T_x , as

$$T_x = \frac{1}{1 - \Phi(x)}, \quad (4)$$

which may be interpreted as the average interval between recurrences of an event in a particular series of trials.

From eqs. (2) and (3), we obtain an expression for x :

$$x = \bar{x} + \frac{S_x \sqrt{6}}{\pi} (y - \gamma). \quad (5)$$

Figure 1 is an extreme probability graph on which y is one of the scales on the abscissa. There is also a scale of $\Phi(x)$ from eq.(1) and of return period, T_x , from eq.(4). The ordinate is a linear scale of the random variable, x , in our case, wind speed.

Equation (5) produces a straight line on this graph paper. This represents a best fit curve to the data sample by the least-squares method. The set of the N observed extremes furnishes values for the calculation of S_x and \bar{x} in eq.(5).

In some cases, the scatter of the observations about the least-squares line of eq.(5) is so fine that the theory can be accepted on the basis of a visual inspection. In other cases, the deviations about the theoretical line may be such that the question arises whether the observations are compatible with the theory. To decide the question of how far the observations can deviate without invalidating the theory, control curves are constructed showing upper and lower limits within which the values can vary with a prescribed probability of, say, 0.68. This level is chosen because it corresponds to the one standard

deviation limit for the normal distribution. This gives a graphical criterion for the "goodness-of-fit" between theory and observations. For example, Figure 1 shows the probability of a maximum peak wind associated with a thunderstorm on any day in July being less than or equal to 22 m/sec (42 knots) (10-m reference level) is approximately 0.99. Also, the average interval of recurrence (T_x) of this 22 m/sec (42 knot) peak wind in July is approximately 100 days.

Now, let P = probability of an event not occurring in any of N trials, and P_1 = probability of an event occurring at least one time in N trials. We now introduce the concept of calculated risk, U , which is the probability of encountering a peak wind speed (referenced to 10-m level) at least one time in N trials (days, hours, etc.). Thus, our event of interest in P_1 above is peak wind speed, and from the definition of multiple event probability,

$$U = P_1 = 1 - [\Phi(x)]^N,$$

or from eqs. (1) and (2),

$$U = 1 - \exp[-Ne^{-\alpha(x-\mu)}], \quad (6)$$

where x = wind speed, and N = the number of trials or the exposure time of a vehicle on the launch pad. The parameters α and μ are defined by eq.(3).

The function $\Phi(x)$ given by eq. (1) is a member of a class of statistical functions called extreme value distributions and is the appropriate type of statistical model for investigation in the analysis of a variable such as extreme wind speed. Fisher and Tippett [2] discovered that the limiting extreme value distribution can take only three forms, Types I, II, and III, which are illustrated in Figures 2, 3, and 4, respectively. The Fisher-Tippett Type I, the distribution defined by eq. (1), is the one used by Gumbel [1]. Also, Type I is the limiting form of Types II and III. Type I is unbounded at both ends, Type II is bounded below at zero, and Type III is bounded above at zero. Since wind speed has a physical lower bound at zero, it may be desirable to investigate distribution Type II for our statistical model. Thom [3] uses the Fisher-Tippett Type II distribution for ground wind distributions.

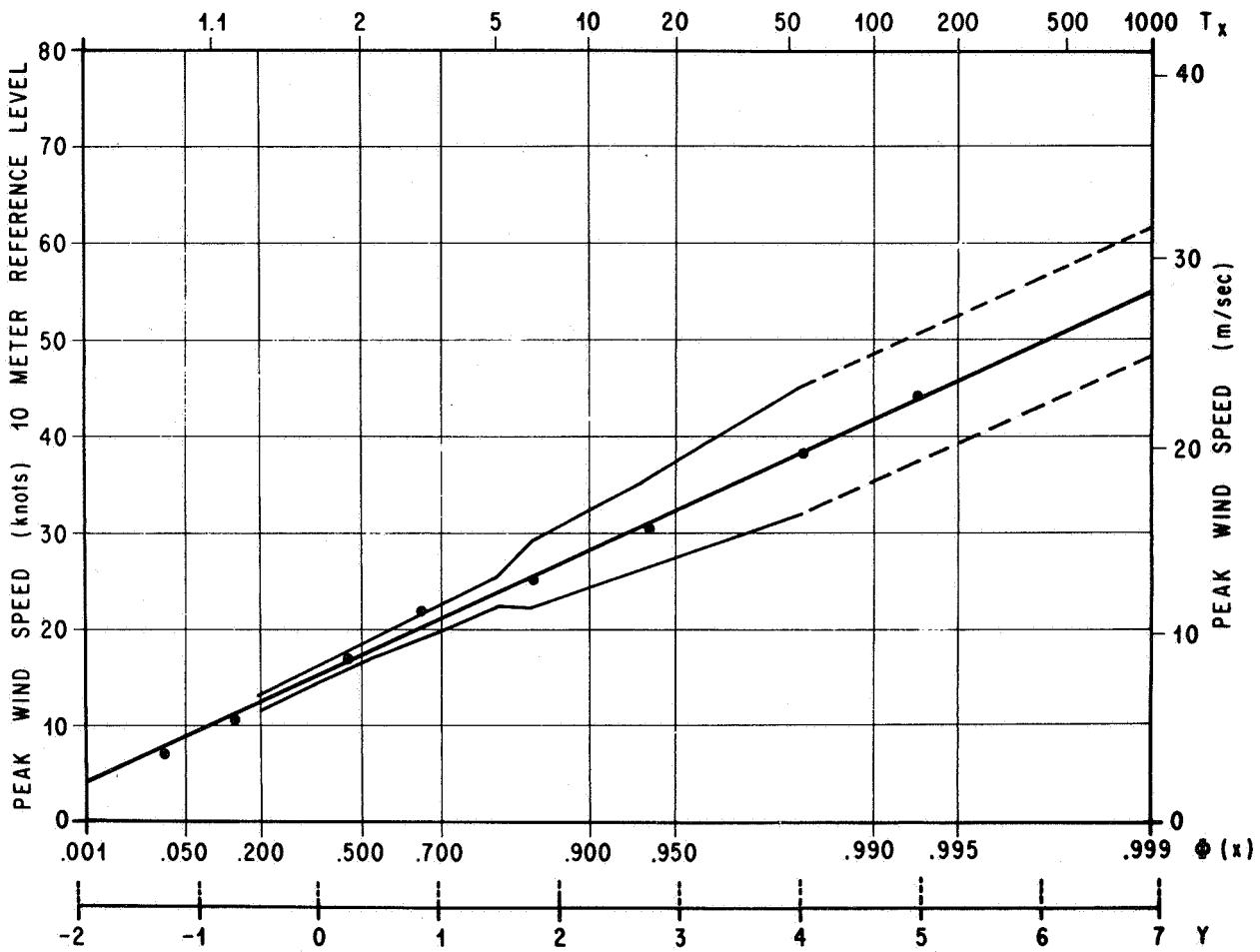


FIGURE 1. PROBABILITY OF MAXIMUM DAILY PEAK THUNDERSTORM WINDS AT CAPE KENNEDY, FLORIDA

$$\Phi(x) = \exp \left[- \exp \left[-a(x - \mu) \right] \right], \quad -\infty < x < \infty$$

TRANSFORMATION: $x = \mu + y/a$

DENSITY: $\phi(x) = a \exp \left[-a(x - \mu) \right] \Phi(x)$

$$\Phi(x) = \exp \left[- \left(\frac{x - \epsilon}{\mu - \epsilon} \right)^k \right], \quad x \geq \epsilon, \quad \mu > \epsilon, \quad k > 0$$

TRANSFORMATION: $x = \epsilon + (\mu - \epsilon) \exp \left[y/k \right]$

DENSITY: $\phi(x) = \left(\frac{k}{\mu - \epsilon} \right) \left(\frac{x - \epsilon}{\mu - \epsilon} \right)^{k-1} \Phi(x)$

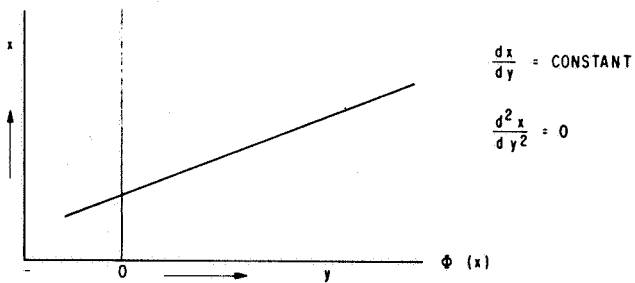


FIGURE 2. FISHER-TIPPETT TYPE I DISTRIBUTION (GUMBEL DISTRIBUTION)

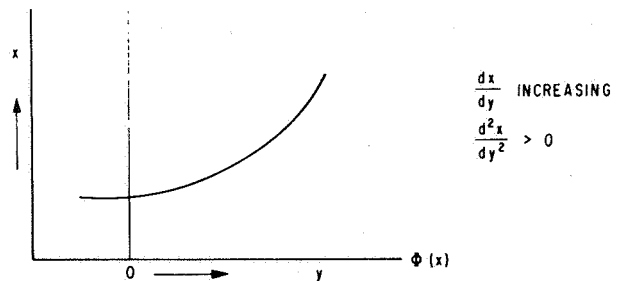


FIGURE 3. FISHER-TIPPETT TYPE II DISTRIBUTION

$$\Phi(x) = \exp \left[- \left(\frac{\omega - x}{\omega - \mu} \right)^k \right], \quad x \leq \omega, \quad \mu < \omega, \quad k > 0$$

$$\text{TRANSFORMATION: } x = \omega - (\omega - \mu) \exp \left[-y/k \right]$$

$$\text{DENSITY: } \phi(x) = \left(\frac{k}{\omega - \mu} \right) \left(\frac{\omega - x}{\omega - \mu} \right)^{k-1} \Phi(x)$$

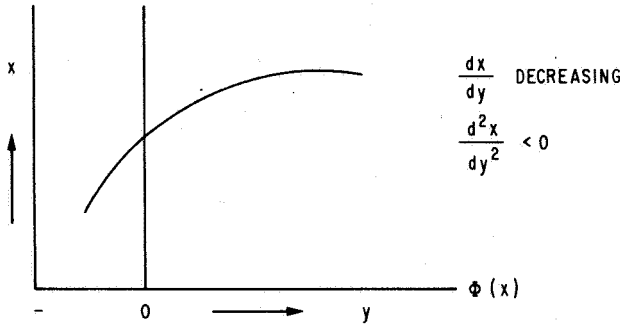


FIGURE 4. FISHER-TIPPETT TYPE III DISTRIBUTION

The concept of calculated risk has been proposed by Court [4] as wind design criteria for facilities. Gumbel [1] uses Court's term "calculated risk" in this connection. In other terms and applications, the fundamental principles have a long history stemming from early statisticians who were interested in the probability theory of games. In this paper, the calculated risk concept is extended to analyze time ordered data which vary systematically with time and which may be highly correlated with respect to time. This extension to calculated risk is called exposure period probability when used in reference to the probability that the vehicle will experience ground winds while exposed to the natural elements; e. g., while being readied for launch on the pad.

An exposure period probability is an empirical statistic of ground winds derived from a time-ordered sample of winds and involves counting the occurrences of wind speeds equal to or greater than specified magnitudes in all possible combinations. Thus, an exposure period statistic expresses the probability that an event will occur one or more times in k -consecutive time intervals. The probability of the event may vary with respect to time (from trial to trial) without invalidating any fundamental principle. Calculated risk requires that the probability of the event remain constant with respect to time (from trial to trial). With special attention given to the effects of uncompleted runs at the ends of a finite sample series, exceedance probabilities can be derived from the probability of runs and therefore from exposure period probabilities.

WIND DATA SAMPLES FOR CAPE KENNEDY

HOURLY PEAK WIND SAMPLE

The surface (~ 10 -m level) wind data normally available for statistical analysis from the Environmental Science Services Administration, National Weather Records Center, Asheville, North Carolina, are in the form of card deck 144 taken from Standard Form WBAN-10. These records contain, among other measurements and observations, wind measurements averaged over one minute taken at hourly intervals. In general, these records are referred to as hourly observations. After several attempts at adjusting these hourly wind data failed to yield consistent statistical results between hourly peak winds and daily peak winds, it was considered necessary to read the original anemometer chart records (continuous recorder traces) to produce a data sample of hourly peak winds. This tedious task of reading the original chart records was performed by the National Weather Records Center, supported by the NASA-MSFC Aero-Astroynamics Laboratory, Aerospace Environment Division with funds both from Program and Supporting Research. (The serially-complete winds-aloft records to be described subsequently were also produced and sponsored by the same organizations.)

From the continuously recording charts, the highest instantaneous indicated wind speed (and associated direction) that occurred during each hour was selected for the data sample. If more than one maximum (peak) wind speed of equal magnitude occurred during a given hour, only the first occurrence was selected. The resulting data sample of hourly peak wind speeds (and associated directions) exist only for Cape Kennedy, Florida. The reference height for these data is 10 m above natural grade. The period of record is from September 1958 to December 1966 with missing data from March 1961 to November 1961, and from November 29, 1962, to March 31, 1963.

This is the first report on the analysis of hourly peak winds for Cape Kennedy. The analysis is incomplete only in that all statistics of interest for the aerospace vehicle programs have not been derived to date. The validity and adequacy of conclusions made from numerical data depend upon the accuracy and reliability of the data sample. In this case, statistical conclusions and interpretations based upon this hourly peak sample will be valid and reasonable.

DAILY PEAK WIND SAMPLE

From an hourly peak wind sample, a daily peak wind sample, a monthly peak wind sample, and a yearly peak wind sample can be derived, provided that records exist for all hours. The sample size becomes proportionately smaller for each larger reference period; e. g., a sample size of daily peak winds would be 1/24 that of an hourly peak wind sample. Statistical analysis of samples derived from hourly peak winds have not been completed to date.

For this report, a daily peak wind sample was derived from records previously used in NASA TM X-53116 [5] which consists of fifteen years of daily peak wind speeds for Cape Kennedy. The original sample consists of three types of measurements: Type I, peak gust; Type II, observed gust; and Type III, hourly wind. The daily peak wind for each day of the fifteen years of record is from one of these three types. To obtain an unbiased representative sample of the population of daily peak surface wind speeds for Cape Kennedy, the available fifteen-year sample was reduced by choosing the latter part of the record in which all wind measurements were significantly Type I, peak gust. These measurements were obtained from continuously recording charts, and thus provide a true daily peak wind value. This revised daily peak sample consists of 2,525 measurements, and the period of record is from February 1, 1959, through June 30, 1966.

WINDS ALOFT SAMPLE

The winds aloft sample is composed of radiosonde observations made twice daily (at 0000Z and 1200Z) at Cape Kennedy covering the period from January 1, 1956, through December 31, 1963. The observations are serially complete with wind direction and speed recorded at 1 km intervals from 0 to 27 km altitude. The total number of observations is 5,844. This data sample is described in References 6 and 7, and is available from the National Weather Records Center as Card Deck 600. This data sample, which has been generally accepted by the aerospace industries for certain space vehicle applications, is being used extensively for the Saturn program. Extension of several statistical techniques using this data sample promises to yield even broader applications to advanced NASA programs such as AAP (Apollo Applications Program) and Voyager.

ANALYSIS

PEAK WIND SPEEDS AT 10-m REFERENCE HEIGHT ABOVE NATURAL GRADE

Peak Ground Winds. It has been estimated that only a few seconds are required for the wind to produce steady drag loads on the vehicle while it is on the pad. Because of vortex shedding, a steady wind as low as 9 m/sec for 15 or more seconds may introduce dynamic loads on the Saturn V vehicle in some configurations. To overcome dynamic wind loads, dynamic dampers supported by the launch umbilical tower and the mobile service structure are attached to the Saturn V vehicle. When the damper is attached to the vehicle, the total wind loading capability of the vehicle system is increased, thus decreasing the risk of structurally compromising the vehicle. However, during certain operations, the dampers must be retracted, making the vehicle more susceptible to structural damage from ground winds. The Saturn V ground wind criteria for vehicle launch have been defined in terms of the peak wind at the 18.3-m (60-ft) reference level above natural grade. Therefore, it is the occurrence of peak wind that becomes the important and meaningful statistic to be used in systems design and operational considerations. If an operation requires, say, one hour to complete, and if the critical wind loads on the vehicle can be defined in terms of the peak wind, then it is the probability of occurrence of the peak wind during one hour that gives a measure of the probable risk of structurally damaging the vehicle.

To serve as a convenient reference in the following discussion, the NASA-MSFC design ground wind profile for Cape Kennedy is reproduced from NASA TM X-53328 [8] as Table I. This study is restricted to determining statistics of peak wind speeds taken at one height, namely, at the 10-m reference height above natural grade at Cape Kennedy. There is still the problem of relating these wind statistics of peak winds at a specific height to the wind profile. The two previous articles in this review are devoted to the problem of defining the wind profile structure near the ground.

Empirical Statistics. A first step in making a statistical summary from a sample is to arrange the data into homogeneous groups. From the hourly peak wind sample, the smallest possible groupings are by hour of day. Winds associated with the hurricanes

TABLE I. PEAK DESIGN WIND PROFILES

Height Above Natural Grade		95 Percentile		99 Percentile		99.9 Percentile	
m	ft	m/sec	knots	m/sec	knots	m/sec	knots
3.0	10	10.1	19.6	13.3	25.8	16.6	32.2
<u>9.1</u>	<u>30</u>	12.6	<u>24.4</u>	16.5	<u>32.1</u>	20.7	<u>40.2</u>
<u>18.3</u>	<u>60</u>	14.4	<u>28.0</u>	18.9	<u>36.8</u>	23.7	<u>46.1</u>
30.5	100	16.0	31.1	21.0	40.9	26.3	51.1
61.0	200	18.4	35.7	24.1	46.9	30.2	58.7
91.4	300	19.9	38.6	26.1	50.8	32.7	63.6
121.9	400	21.1	41.0	27.7	53.9	34.6	67.3
152.4	500	22.0	42.8	29.0	56.3	36.2	70.4

have been eliminated from this sample to further assure a homogeneous sample. It is assumed that such winds belong to a separate and distinct population. Winds associated with thunderstorms are, however, included in the sample. If the means and variances of two or more groupings (or subsamples) are not significantly different, then the subsamples may be further grouped into a larger sample. Cumulative percentage frequencies of hourly peak winds, grouped by like hour and all hours combined, were computed for monthly reference periods. Examples of the empirical cumulative percentage frequencies for January and July are shown on normal probability graph paper in Figures 5 and 6, respectively.

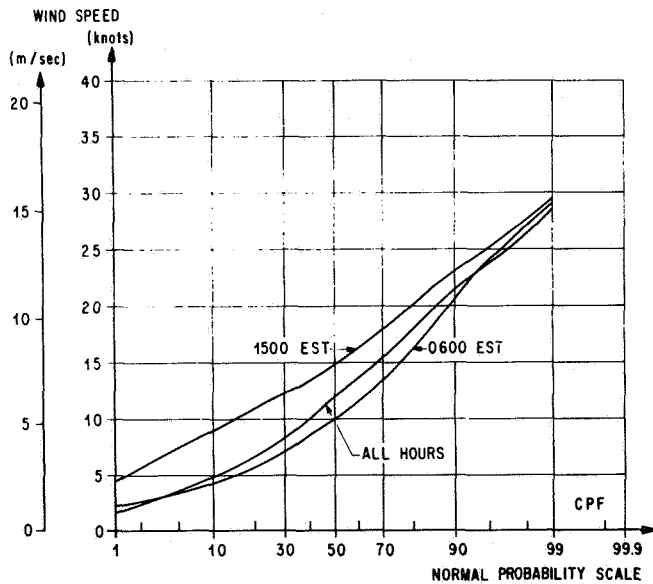


FIGURE 5. JANUARY HOURLY PEAK WIND SPEED CUMULATIVE PERCENTAGE FREQUENCY (10-m LEVEL) AT CAPE KENNEDY, FLORIDA

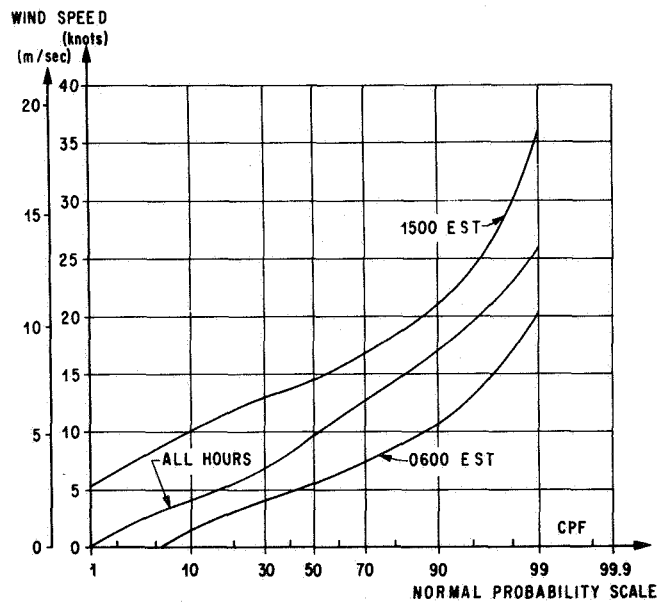


FIGURE 6. JULY HOURLY PEAK WIND SPEED CUMULATIVE PERCENTAGE FREQUENCY (10 m LEVEL) AT CAPE KENNEDY, FLORIDA

From the empirical cumulative percentage frequencies, any desired percentile value can be interpolated. The resulting percentiles for hourly groupings of hourly peak winds are illustrated in Figures 7 and 8 for January and July. From these figures, it is seen that the time of day to conduct an operation to avoid the probability of encountering high wind speeds is after 2100 EST and before 0700 EST, provided that it takes one or less hours to complete the operation. Furthermore the diurnal amplitude of all percentiles for July is greater than the corresponding percentiles for January. The

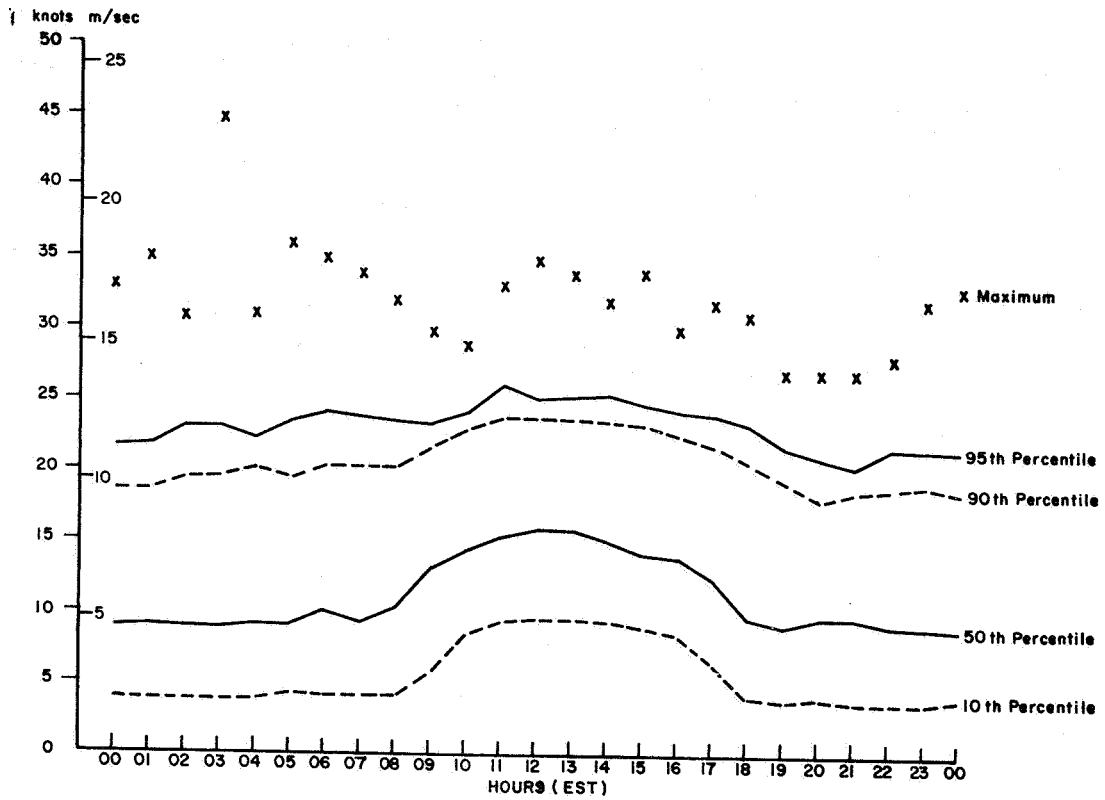


FIGURE 7. JANUARY HOURLY PEAK WIND SPEED PERCENTILES VERSUS TIME OF DAY (10-m LEVEL) AT CAPE KENNEDY, FLORIDA

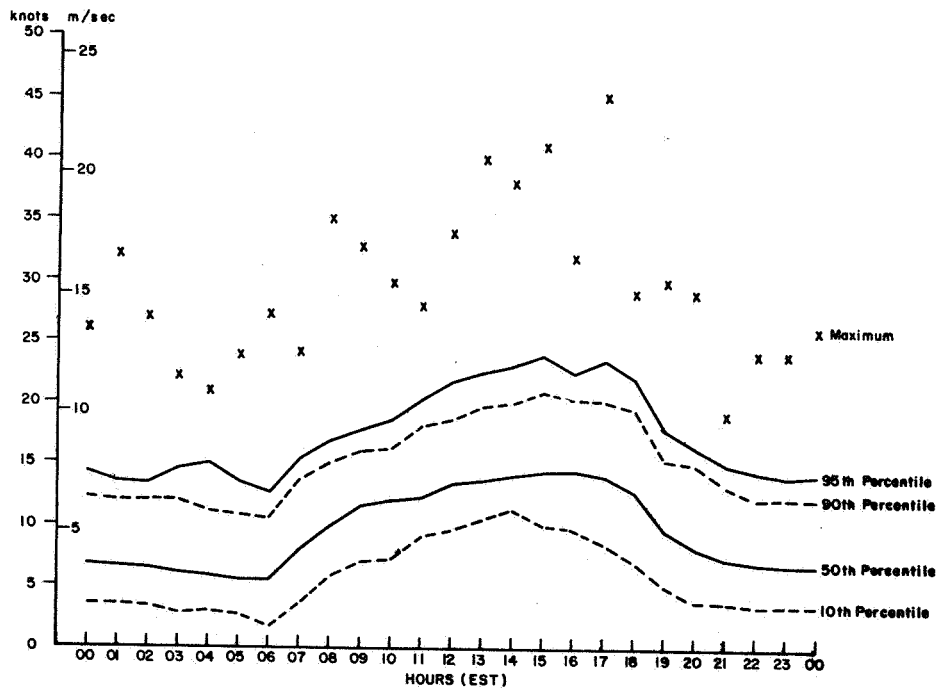


FIGURE 8. JULY HOURLY PEAK WIND SPEED PERCENTILES VERSUS TIME OF DAY (10-m LEVEL) AT CAPE KENNEDY, FLORIDA

diurnal amplitude also increases with higher percentiles during July, whereas the amplitude decreases with increasing percentiles during January. This feature is attributed to the high frequency of air mass (afternoon) thunderstorms during July (or in general, during the summer months) in contrast to the occurrence of frontal thunderstorms during January (or in general, during winter and spring) which may produce high winds at any time of the day.

If it is not known what time of day an operation is to take place, the statistics for all hours combined for monthly reference periods may be used. A comparison of the monthly and annual percentiles of hourly peak winds for all hours is presented in Figure 9. It must be recognized that this grouping is a very inhomogeneous sample. There are some hours of the day (primarily the afternoon hours) during which there is a higher probability of the wind exceeding these percentiles, and other hours (primarily early morning

hours) for which there is a lower probability for the indicated percentiles. The principal conclusion to be drawn by a comparison of Figures 7 and 8 with Figure 9 is that the amplitude of the median (50th percentile) wind over a 24-hr period is greater than the seasonal amplitude at this percentile.

Thunderstorm Winds. Thunderstorms are a recognized special weather phenomenon, and the high frequency of thunderstorms during the summer months is the cause of much concern relative to vehicle operations at Cape Kennedy. Standard weather observing practice is to report the occurrence of a thunderstorm for the observing station if thunder is heard. Thus, the occurrence of a thunderstorm is determined by an observational method. An observer can hear thunder over a radius of approximately 25 km. The frequency at which thunderstorms were observed on the hour (at standard reporting times) for each hour versus

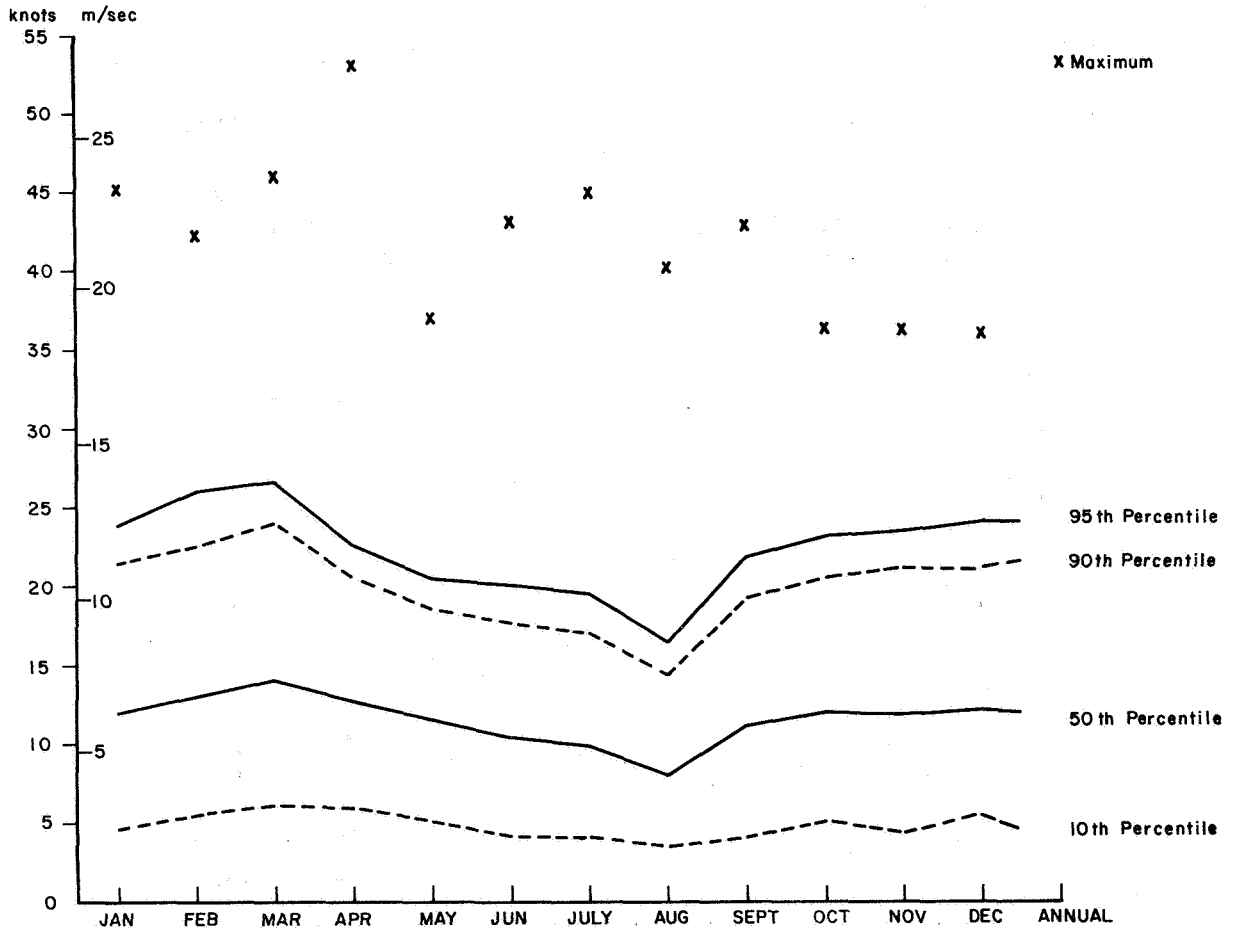


FIGURE 9. MONTHLY PERCENTILES (ALL HOURS) HOURLY PEAK WIND SPEED (10-m LEVEL) AT CAPE KENNEDY, FLORIDA

month is given in Figure 10. For example, there is a 24 percent chance that thunder will be heard at 1600 EST during July from a single observing point at Cape Kennedy. One or more thunderstorms may occur within the observing range at a given time and during some time interval. From NASA TM X-53635 [9], there is a 44.1 percent chance that one or more thunderstorms will occur during any arbitrary afternoon (1200 - 1959 EST) in July. There is a 45.2 percent chance that one or more thunderstorms will occur on any arbitrary day in July. To determine the probability of thunderstorm winds striking the vehicle, a sample of daily peak thunderstorm winds was obtained. For July, this sample as fitted to the Fisher-Tippett Type I (or Gumbel [1]) distribution function is shown in Figure 1.

The theoretical distribution of Figure 1 is reproduced in Figure 11 to compare with the distribution of daily peak winds. It is concluded from Figure 11 that there is only a 1 percent chance that a daily peak thunderstorm wind greater than 22 m/sec (42 knots) will occur at a specific point over Cape Kennedy; i. e., strike the vehicle at the 10-m reference height during any day in July even though there is a high probability, 0.452 [9], that one or more thunderstorms will occur during any day in July over the Cape Kennedy area (over a radius of approximately 25 km).

Now compare the distribution of daily peak thunderstorm winds with daily peak winds for July

(Fig. 11). Notice that the slopes of these curves are not the same; this indicates that on some days the peak wind for the day was greater than the maximum observed peak wind during a thunderstorm observation.

Because of the excellent fit of the daily peak thunderstorm winds to the theoretical distribution function, and recalling from Section II that the theory of extreme values requires independence in the data sample, it may be assumed that the occurrence of peak thunderstorm winds at a specific location on Cape Kennedy is a random phenomenon. It certainly cannot be assumed that the daily occurrence of thunderstorms is random. In fact, given that a thunderstorm occurred on a specific date, there is a 70 percent chance that a thunderstorm will occur on the next day. A study on thunderstorm persistence at Cape Kennedy, NASA TM X-53635 [9], concludes that "a first order Markov model may be used to approximate the distribution of sequences of summer afternoons with thunderstorms. The second order Markov model may be used to approximate the distribution of sequences of summer afternoons without thunderstorms."

Theoretical Probabilities. The extreme value theory has been applied to these surface wind samples to provide probability statements of a critical wind speed striking the launch vehicle during a specified exposure period.

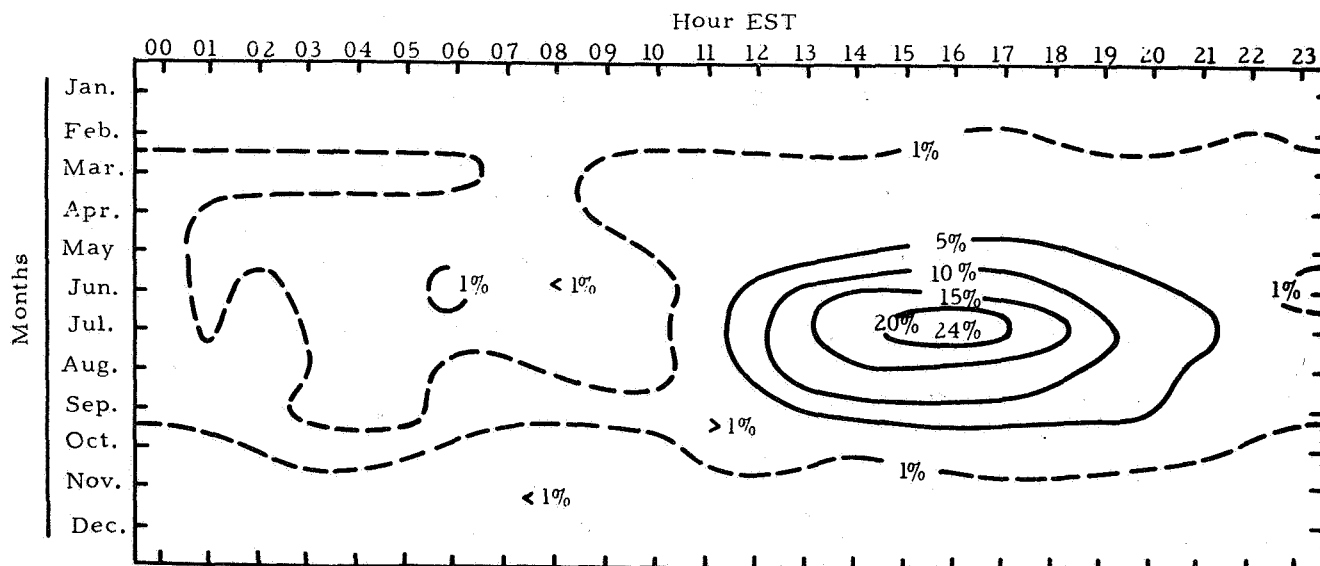


FIGURE 10. PROBABILITY (%) OF OCCURRENCE OF THUNDERSTORMS BY MONTHS VERSUS TIME OF DAY IN THE CAPE KENNEDY AREA FOR THE PERIOD JANUARY 1957 - DECEMBER 1962

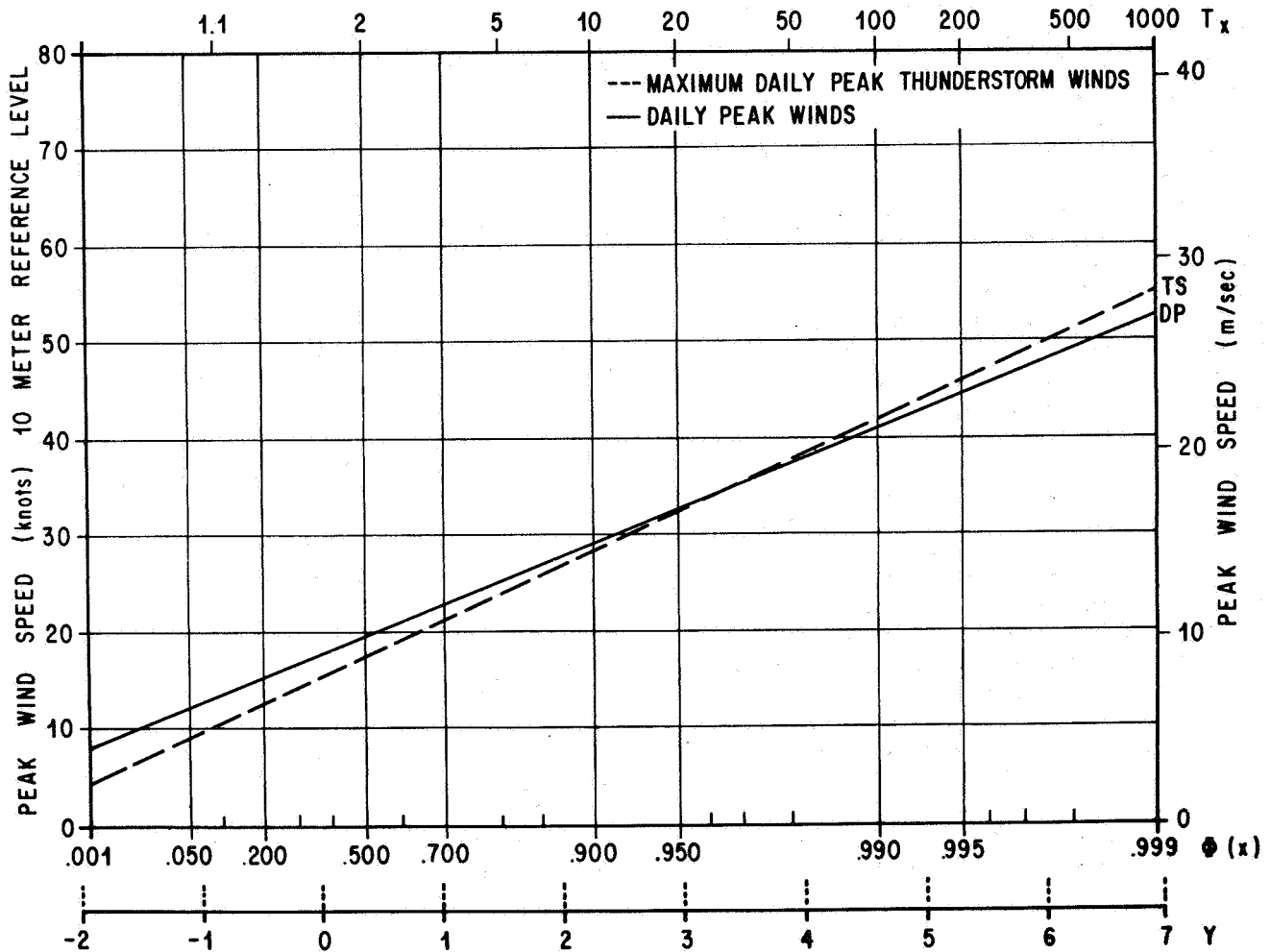


FIGURE 11. COMPARISON OF DAILY PEAK WINDS WITH MAXIMUM DAILY PEAK THUNDERSTORM WINDS IN JULY

The calculated risk probabilities answer probabilistic statements such as the probability of the event (peak wind) occurring at least one time during a continuous time interval, N , which begins at any time in a continuous time interval, k . For convenience, we make probability statements in reference to monthly periods; i. e., k is approximately 30 days, and N ranges from 1 day to 90 days. Since N is defined in this wide range of continuous time, it would not be proper to group our data sample by monthly periods alone. For example, consider the question: "What is the probability of encountering a certain peak wind at least one time beginning on any day in January for an exposure period of 90 days?" Obviously, since there are only 31 days in January, if we begin a 90-day exposure of a vehicle on the last day of January, the exposure time will extend into February, March, and April.

For this reason, the probabilities presented in Figures 12 (July) and 13 (October) were computed from eq. (6) by grouping the revised daily peak wind speed sample for Cape Kennedy into monthly, bi-monthly, trimonthly, and quadmonthly reference periods; i. e., monthly reference periods are (January), (February), . . . , (December); bi-monthly reference periods are (January, February), (February, March), (March, April), . . . , (December, January); trimonthly reference periods are (January, February, March), (February, March, April), (March, April, May), . . . , (December, January, February); quadmonthly reference periods are (January, February, March, April), (February, March, April, May), (March, April, May, June), . . . , (December, January, February, March).

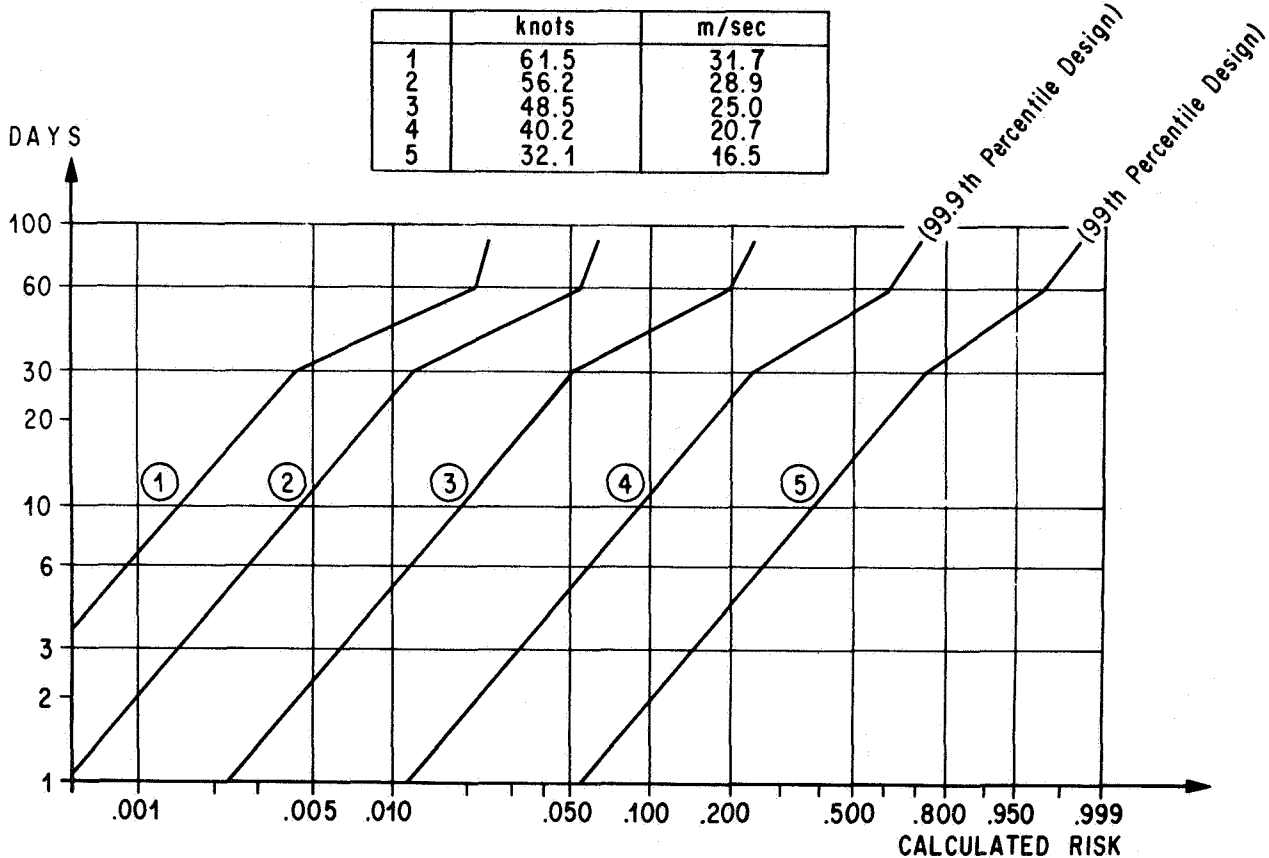


FIGURE 12. CALCULATED RISK VERSUS EXPOSURE TIME WITH PEAK WIND SPEED REFERENCED TO 10-m (30 ft) LEVEL AT CAPE KENNEDY, FLORIDA IN JULY

In Figures 12 and 13, exposure times of one day ($N = 1$) were computed from the monthly reference periods; exposure times of 30 days ($N = 30$) were computed from the bimonthly reference periods; exposure times of 60 days ($N = 60$) were computed from the trimonthly reference periods; and exposure times of 90 days ($N = 90$) were computed from the quadmonthly reference periods. For each month of the year and a given wind speed, these points were connected by a straight line on \ln versus $\ln \ln$ graph paper. Since $\ln N$ versus $\ln[-\ln(1 - U)]$ is a linear function, computer programs were written and used to generate all calculated risks U_i for all N_i based upon eq. (6). The method described imparts the proper connotation to our probabilistic statements in regard to convenient monthly time periods.

For example, Figure 12 shows that the calculated risk of encountering a 25.0 m/sec (48.5 knot) peak

wind speed (referenced to 10-m height) at least one time in 30 days beginning on any day during the month of July at Cape Kennedy, Florida, is 0.050. Figure 13 shows that the calculated risk of encountering a 16.5 m/sec (32.1 knot) peak wind speed (referenced to 10-m height) at least one time in 20 days beginning on any day during the month of October at Cape Kennedy is 0.550.

Figure 14 illustrates the distributions for October peak winds taken for different reference periods. From this graph, the probability of the peak winds for the indicated reference periods can be read. For example, the probability that the peak wind for the hour indicated as 0600 EST will be > 16.5 m/sec (32 knots) is 0.003 (i. e., $1 - 0.997 = 0.003$). In symbols, this statement is expressed as $P\{W \leq 16.5 \text{ m/sec}\}$ for hourly peak wind during the period from 0530 to 0630 EST is 0.997. Therefore, the

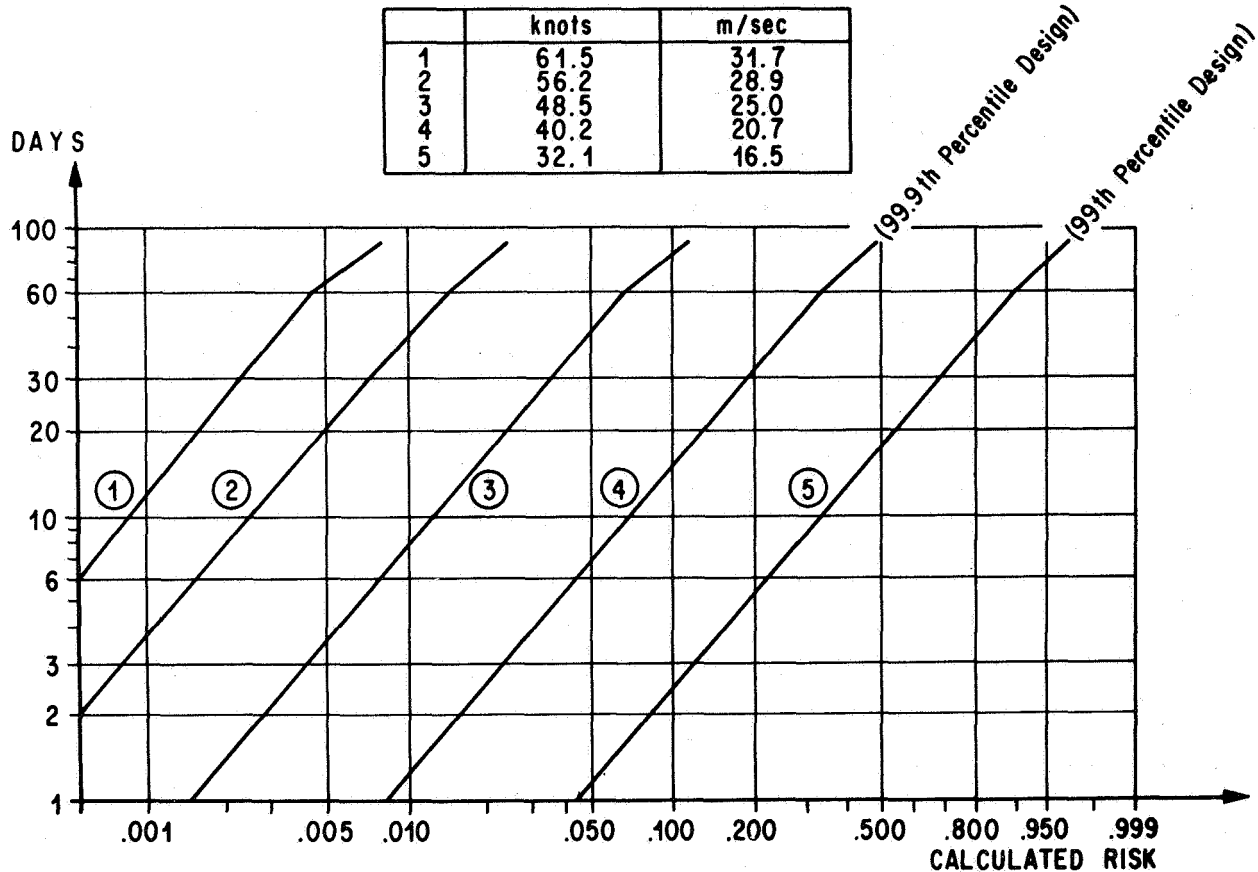


FIGURE 13. CALCULATED RISK VERSUS EXPOSURE TIME WITH PEAK WIND SPEED REFERENCED TO 10-m (30 ft) LEVEL AT CAPE KENNEDY, FLORIDA IN OCTOBER

$P\{W > 16.5 \text{ m/sec}\}$ is 0.003. Similar probability statements can be made for other reference periods and wind speeds.

Figure 15 represents the calculated risk of encountering peak ground wind speeds for hourly exposure periods for the month of October at Cape Kennedy. This is a cross-plot taken from the probabilities illustrated in Figure 14. The dashed line (0600 EST) and the solid line (1500 EST) graphically illustrate the diurnal change of the probability of encountering a given wind speed of 16.5 m/sec (32 knots at the 10-m level) if the exposure time begins on specified hours over the twenty-four hour day. The heavy dashed lines (calculated risk) indicate the unrealistic change of probability with exposure time where the probability in eq. (6) for each successive hour in the exposure period is assumed constant. Also included on Figure 15 is the calculated risk for exposure periods from 1 to 3 days.

Exposure Period Probabilities. The term "exposure period probability" is used to express the risk the vehicle would have in encountering a critical wind speed when exposed on the launch pad for k-consecutive hours, days, or even months. A computer counting procedure is used to determine the probability that the wind speed will equal or exceed specified values (critical wind magnitudes to the vehicle or any value of interest) at least one time in k-consecutive time increments. This empirical statistic is thus seen to fall into the general class of probabilities referred to as exceedance probabilities. To derive exposure period probabilities requires serially complete data records. The advantage of exposure period probabilities over calculated risk probabilities is that the probability from trial to trial may change without invalidating any fundamental principle. The resulting statistics are more realistic for a variate that changes systematically or which is highly correlated with respect to time, such as winds near the ground taken on an hourly basis. The

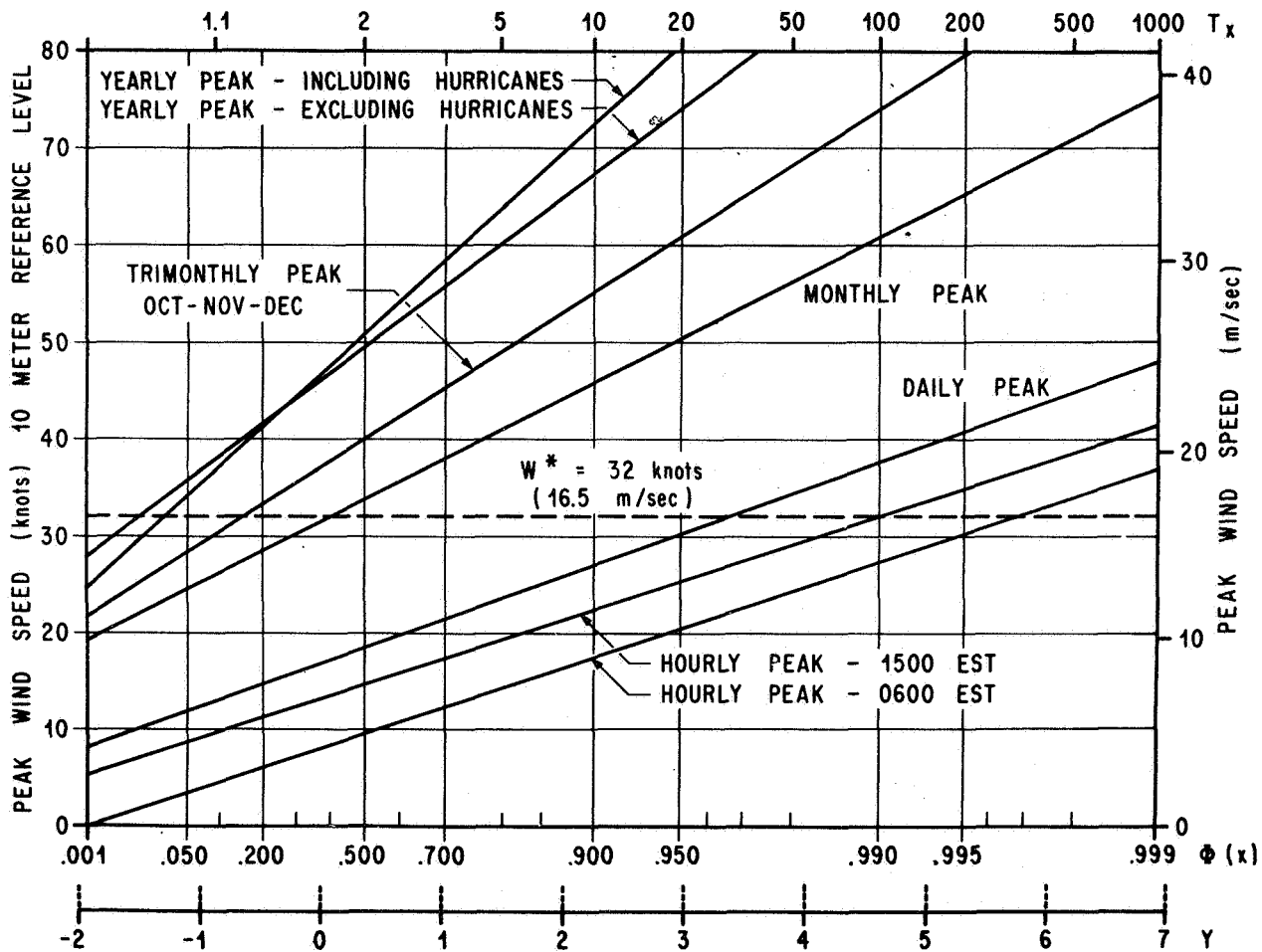


FIGURE 14. FISHER-TIPPETT TYPE I DISTRIBUTION COLLATED TO PEAK WIND SPEED SAMPLES AT CAPE KENNEDY, FLORIDA IN OCTOBER

single disadvantage of exposure period probabilities is that statistics are empirical. Estimates outside the observed range of the variate cannot be obtained.

To emphasize the importance of extreme value statistics, Gumbel [1] quips, "Some day the improbable will happen . . ." In our terms, the longer the vehicle is exposed to the natural elements, the higher the probability is that the vehicle will experience a high wind.

WINDS ALOFT ANALYSIS

Selection of the Maximum Wind Speed in the 10-15 km Layer. The following discussion is devoted to the statistical analysis of winds aloft taken from the data sample described previously under

"Winds Aloft Sample." A unique presentation of the probability that winds aloft will equal or exceed a given magnitude versus altitude and month is presented for wind speeds ≥ 50 m/sec and ≥ 75 m/sec in Figures 16 and 17, respectively. Figure 16 shows a 5 percent chance and greater that winds will be ≥ 50 m/sec over the altitude region from 7 km to 16 km from the latter part of October to the first part of May. Figure 17 shows that wind speeds ≥ 75 m/sec occur between 11 and 14 km altitude during February to the first part of March with a frequency of 5 percent or greater. This is in excellent agreement with the MSFC winds aloft design criteria [8] which were based on a much earlier and less complete wind sample.

EXPOSURE TIME N

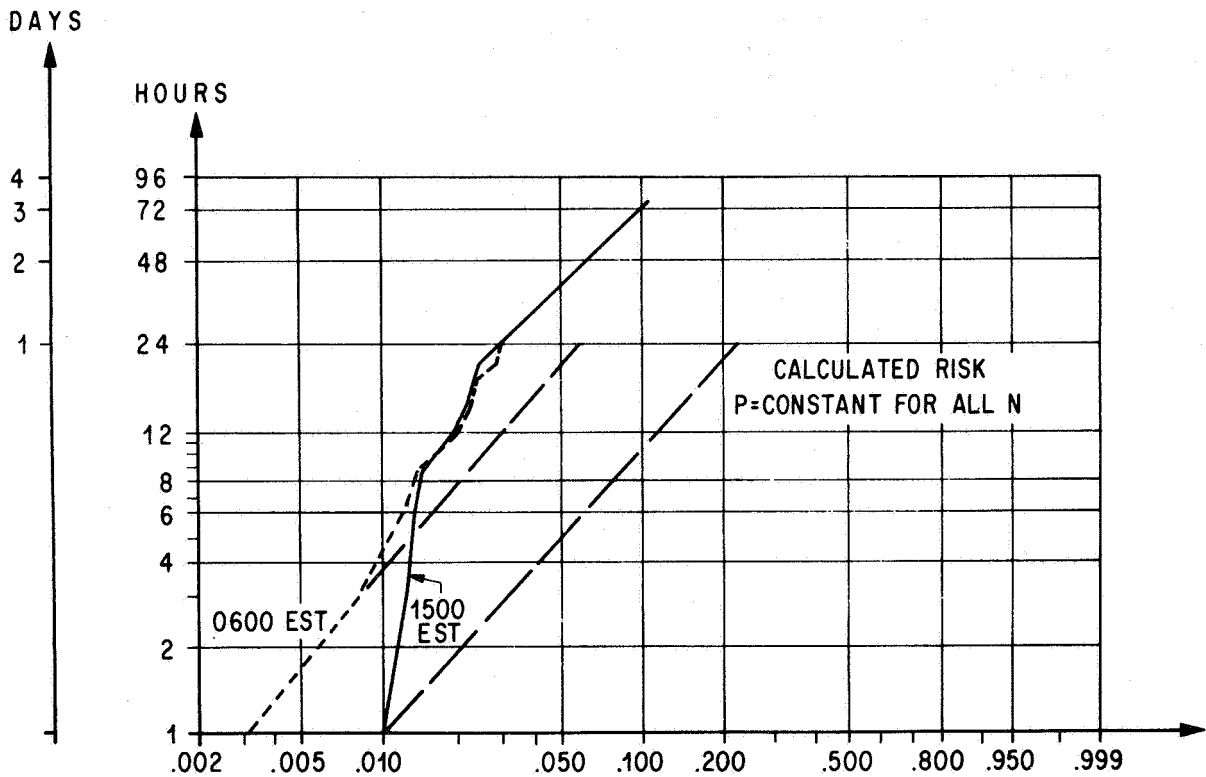


FIGURE 15. HOURLY EXPOSURE PERIOD PROBABILITY FOR PEAK WIND SPEED BEING > 32 KNOTS (10-m LEVEL) AT CAPE KENNEDY, FLORIDA IN OCTOBER

To depict the data sample from which a number of useful statistics for aerospace mission analysis are derived, a serial plot of the twice daily maximum wind speeds that occurred in each profile at 10 km through 15 km altitude for eight years of serially complete rawinsonde records is presented in Figure 18. This graph makes for an interesting subjective analysis, and many words could be written to describe these data. This plot (Fig. 18) represents the complete data sample from which all of the following statistics are derived. After giving some justification for the use of this sample of maximum wind speeds in the 10-15 km layer, some representative statistics will be presented.

The arguments for using the maximum wind speed within the 10-15 km layer rather than the winds at a discrete altitude are as follows:

- (1) The most critical altitude for wind loads are not always known during early design phases of a vehicle development program. It is reasonable to assume that the critical altitude will be near that of maximum dynamic pressure; and for large boosters, this altitude is, in general, within 10-15 km altitude.
- (2) The maximum winds, particularly during the winter, occur in the 10-15 km layer.
- (3) The individual wind measurements are considered representative of quasi-steady state wind values averaged over approximately 600-m altitude. These are winds determined from rawinsonde using standard data reduction methods.
- (4) The standard MSFC flight performance and structural load procedures require the use of an embedded gust superimposed on the synthetic design wind profiles [8].

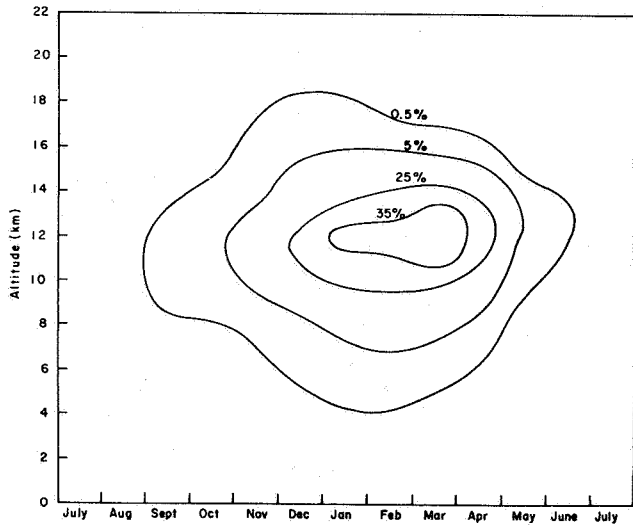


FIGURE 16. FREQUENCY OF SCALAR WIND SPEED EXCEEDING 50 m/sec AS A FUNCTION OF ALTITUDE AND MONTHS FOR THE YEARS 1956-1963 AT CAPE KENNEDY, FLORIDA

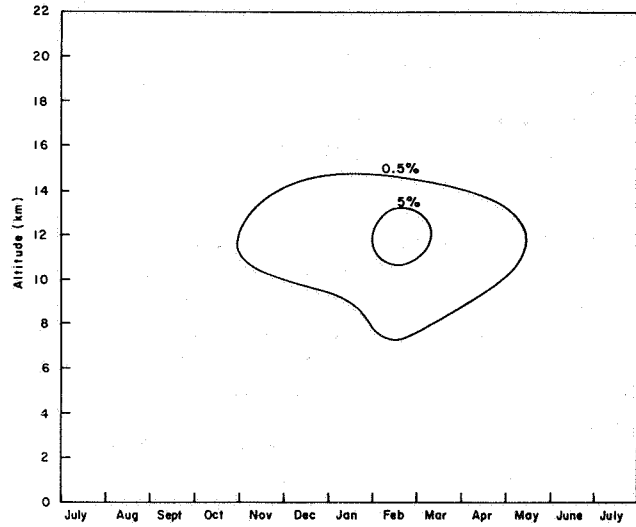


FIGURE 17. FREQUENCY OF SCALAR WIND SPEED EXCEEDING 75 m/sec AS A FUNCTION OF ALTITUDE AND MONTHS FOR THE YEARS 1956-1963 AT CAPE KENNEDY, FLORIDA

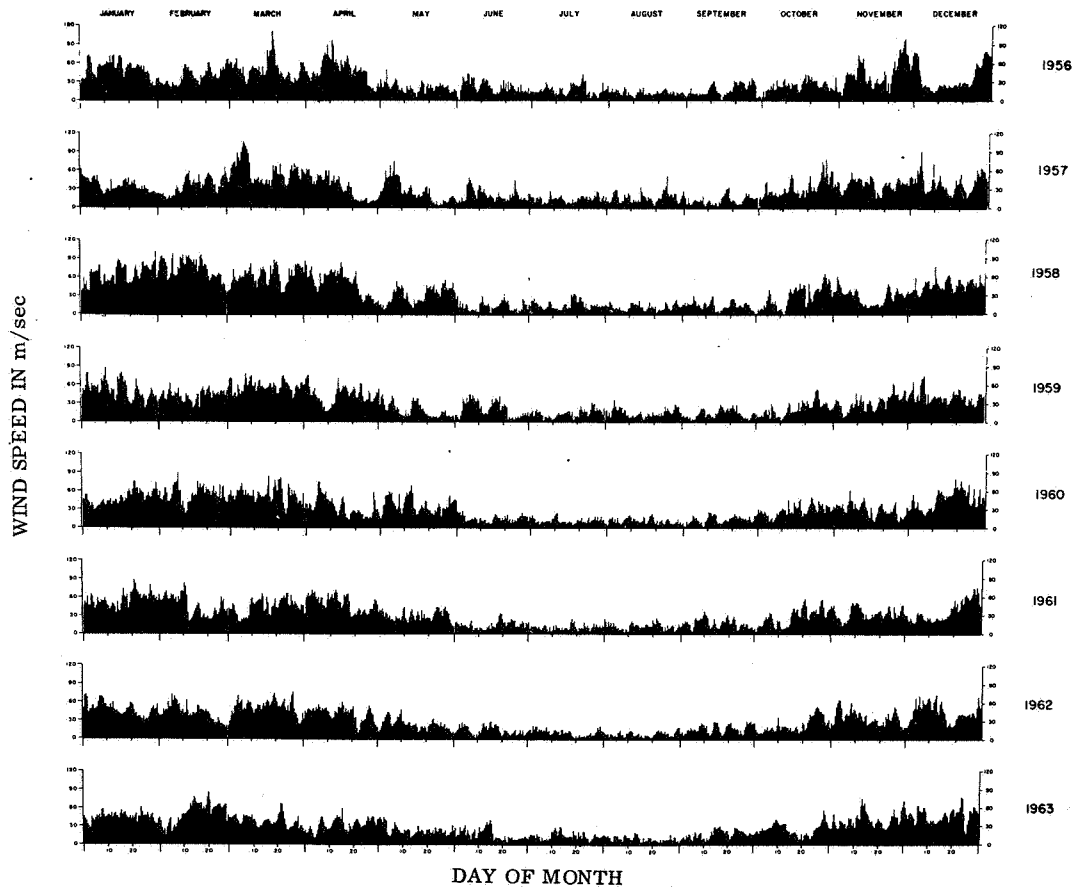


FIGURE 18. TWICE DAILY MAXIMUM WIND SPEED IN THE 10-15 km LAYER AT CAPE KENNEDY, FLORIDA

(5) The resulting statistics from a sample of the maximum wind in the 10-15 km layer yield higher percentile values than the corresponding percentile values of the wind at discrete altitudes or the envelope of the percentiles determined at discrete altitudes. A comparison is presented as Table II.

(6) It is considered that predictions of the maximum wind speed within the 10-15 km layer can be made more reliable than predictions at discrete altitudes. The use of the maximum wind for the 10-15 km layer as the data sample for mission analysis and the envelope of percentile values taken at discrete altitudes for design studies and design criteria introduces a double standard: one data sample for design and another for mission analysis.

This double standard is not unreasonable when viewed from the standpoint that the critical wind loads may be considered to occur anywhere within the 10-15 km altitude region. On the other hand, the maximum wind in the 10-15 km layer data sample cannot be used to construct synthetic wind profiles because the sample is selective; i. e., extremes for the layer are used and this would introduce a fictitious discontinuity in the profile.

Serial Correlation Coefficients. That many meteorological parameters are persistent is certainly well known, in fact, many forecast schemes are based on persistence. As a measure of the persistence of the Cape Kennedy winds aloft, serial correlation coefficients were computed for each month of each year by Kendall's formulation

TABLE II. COMPARISON OF THE 90TH AND 95TH PERCENTILE DESIGN WIND SPEED AT 10-14 km ALTITUDE WITH MAXIMUM WIND SPEED FOR THE 10-15 km LAYER AT CAPE KENNEDY, FLORIDA

	From Design Envelopes 10-14 km		From Maximum wind 10-15 km layer	
	90th- m/sec	95th-Percentiles m/sec	90th- m/sec	95th-Percentiles m/sec
Jan	66.0	72.0	71.0	76.8
Feb	68.0	75.0	72.8	84.9
Mar	68.0	75.0	73.2	80.0
Apr	61.0	66.0	65.3	71.0
May	44.0	50.0	45.9	52.2
June	28.0	34.0	32.8	37.8
July	19.0	23.0	23.0	26.9
Aug	19.0	22.0	21.2	24.3
Sept	23.0	26.0	27.8	30.3
Oct	41.0	47.0	45.5	52.2
Nov	47.0	53.0	52.5	62.0
Dec	57.0	63.0	65.0	70.9

$$r_k = \frac{\frac{1}{N-k} \sum_{j=1}^{N-k} (X_j X_{j+k}) - \frac{1}{(N-k)^2} \left(\sum_{j=1}^{N-k} X_j \right) \left(\sum_{j=1}^{N-k} X_{j+k} \right)}{\left[\frac{1}{N-k} \sum_{j=1}^{N-k} X_j^2 - \frac{1}{(N-k)^2} \left(\sum_{j=1}^{N-k} X_j \right)^2 \right]^{\frac{1}{2}} \left[\frac{1}{N-k} \sum_{j=1}^{N-k} X_{j+k}^2 - \frac{1}{(N-k)^2} \left(\sum_{j=1}^{N-k} X_{j+k} \right)^2 \right]^{\frac{1}{2}}}$$

$$X_j = X_1, X_2, \dots, X_{n-1} \quad X_{j+1} = X_2, X_3, \dots, X_n$$

The mean monthly correlation coefficient was obtained by first performing the Z' transformation

$$Z' = \frac{1}{2} \ln \frac{1 + r_k}{1 - r_k}$$

for each r_k , then computing \bar{Z}' from

$$\bar{Z}' = \frac{\sum_{k=1}^{k=N/2} Z'_k (N - k - 3)}{\sum_{k=1}^{k=N/2} (N - k - 3)}$$

and finally determining \bar{r}_k from

$$\bar{r}_k = \tanh \bar{Z}'_k$$

Although the correlation coefficients vary widely from year to year (Fig. 19) in the mean, the January wind speeds show a significant positive correlation for approximately 6 twelve-hour periods (3 days).

Empirical Exceedance Probabilities. By considering the wind speeds as a step-wise continuous (over 12-hr intervals) time series, a number of useful statistics have been derived which have very important applications to the design, mission planning, and ultimately launch operations of aerospace vehicles. The assumption of constant wind over

12-hr intervals is imposed because rawinsonde wind measurements were not made routinely at closer intervals for the eight years of record. Therefore, the basic wind records were serially completed only for wind profiles twice daily for Cape Kennedy. For most purposes, this assumption does not greatly handicap the statistical analysis, but in the case of time-dependent statistics, inferences for the initial time period less than 12 hr are precluded. For time periods after the initial 12-hr increment, the time-dependent probabilities may be considered continuous and interpolations would be valid.

The probability of the maximum wind speed (W) in the 10-15 km layer exceeding (and not exceeding) specified values of wind speed (W^*) one or more times in k-consecutive 12-hr periods is presented in Table III (parts A and B). The computational method used in deriving these statistics was a combinational counting procedure. Identical results can also be derived from an analysis of runs (a run is a succession of like events). Furthermore, the probability of a run of length k can be derived from Table III.

The probability of runs and conditional probabilities can be derived from the exceedance probabilities (Table III). An example is presented below, and the following definitions are helpful.

Let $P\{B\} = P[W \geq W^*]$ denote the probability that $W \geq W^*$ one or more times in k-consecutive 12-hr periods (these statistics are given in Table IIIB); then $[1 - P\{B\}] = P\{B'\}$ is the probability that $W < W^*$ for k-consecutive 12-hr periods. The probability $P\{B'\}$ is also the probability of a run below W^* of length k in units of 12-hr periods.

TABLE III. PROBABILITY (%) THAT THE MAXIMUM WIND SPEED, W, IN THE 10-15 km LAYER WILL OCCUR ONE OR MORE TIMES LESS THAN (EQUAL TO OR GREATER THAN) SPECIFIED VALUES, W*, FOR K-CONSECUTIVE 12-HR PERIODS AT CAPE, KENNEDY, FLORIDA

W*	SPEED												MONTH--JANUARY									
	---less than---05, 10, . . . 110---m/sec												Number of Observations---496									
	05	10	15	20	25	30	35	40	45	50	55	60	65	70	75	80	85	90	100	110	Min. Speed	No. Occ.
(A) W**	.0	.0	.0	.0	.0	6.3	12.5	21.0	34.3	49.6	64.9	76.4	84.1	88.9	94.0	96.6	98.4	99.8	100.0	100.0	21	1
K 1	.0	.0	.0	.0	3.0	8.9	16.3	27.0	42.7	58.5	73.0	83.5	88.5	93.1	96.4	98.0	99.4	100.0	100.0	100.0	21	1
K 2	.0	.0	.0	.0	4.0	10.7	19.4	31.9	49.0	65.3	79.0	87.9	91.5	95.8	98.0	99.4	99.8	100.0	100.0	100.0	21	1
K 3	.0	.0	.0	.0	5.0	12.5	22.2	36.1	54.2	69.8	83.1	91.1	93.8	96.8	99.8	100.0	100.0	100.0	100.0	100.0	21	2
K 4	.0	.0	.0	.0	6.0	14.1	24.4	39.9	58.3	73.6	86.3	93.5	95.2	97.4	99.4	100.0	100.0	100.0	100.0	100.0	21	3
K 5	.0	.0	.0	.2	7.1	15.7	26.6	43.1	61.5	76.4	88.5	95.4	96.4	97.8	99.8	100.0	100.0	100.0	100.0	100.0	15	1
K 6	.0	.0	.0	.6	8.3	17.1	28.8	46.4	64.3	79.0	90.1	96.6	97.2	98.2	100.0	100.0	100.0	100.0	100.0	100.0	15	1
K 7	.0	.0	.0	1.0	9.3	18.5	30.8	49.0	66.5	81.3	91.3	97.6	98.0	98.6	100.0	100.0	100.0	100.0	100.0	100.0	15	1
K 8	.0	.0	.2	1.4	10.3	20.0	32.9	51.4	68.5	83.3	92.3	98.4	98.6	99.0	100.0	100.0	100.0	100.0	100.0	100.0	13	1
K 9	.0	.0	.4	1.8	11.3	21.4	34.5	53.2	70.4	84.7	93.1	99.2	99.2	99.4	100.0	100.0	100.0	100.0	100.0	100.0	13	1
(B) W**	05	10	15	20	25	30	35	40	45	50	55	60	65	70	75	80	85	90	100	110	Max. Speed	No. Occ.
K 1	100.0	100.0	100.0	100.0	98.0	93.8	87.5	79.0	65.7	50.4	35.1	23.6	15.9	11.1	6.0	3.4	1.6	.2	.0	.0	101	1
K 2	100.0	100.0	100.0	100.0	98.8	96.4	91.3	84.5	73.8	59.5	44.2	30.8	20.6	15.5	8.5	5.4	2.6	.4	.0	.0	101	1
K 3	100.0	100.0	100.0	100.0	99.4	97.6	94.0	87.3	78.2	65.3	50.8	35.9	24.4	19.0	10.9	7.7	3.9	.6	.0	.0	101	1
K 4	100.0	100.0	100.0	100.0	99.6	97.8	95.6	89.1	80.8	69.4	55.4	39.7	28.0	22.4	12.9	9.5	4.8	1.0	.8	.0	101	1
K 5	100.0	100.0	100.0	100.0	99.6	98.0	96.4	90.7	83.5	72.2	58.9	42.9	31.3	25.2	14.0	11.3	5.8	1.2	1.0	.0	101	1
K 6	100.0	100.0	100.0	100.0	99.6	98.2	97.2	92.1	85.7	74.4	61.5	45.8	34.7	27.8	16.5	12.9	6.9	1.4	1.2	.0	101	1
K 7	100.0	100.0	100.0	100.0	99.6	98.2	97.6	93.1	87.3	76.6	63.7	48.4	37.9	30.6	18.1	14.5	7.9	1.6	1.4	.0	101	1
K 8	100.0	100.0	100.0	100.0	99.6	98.2	97.8	93.8	88.7	78.2	65.7	50.4	40.3	33.1	19.8	16.1	8.9	1.8	1.6	.0	101	1
K 9	100.0	100.0	100.0	100.0	99.6	98.2	98.0	94.4	89.7	79.8	67.5	52.0	42.5	35.3	21.2	17.5	9.9	2.0	1.8	.0	101	1
K 10	100.0	100.0	100.0	100.0	99.6	98.2	98.0	95.0	90.7	80.8	69.2	53.2	44.2	37.3	22.0	18.8	10.7	2.2	2.0	.0	101	1

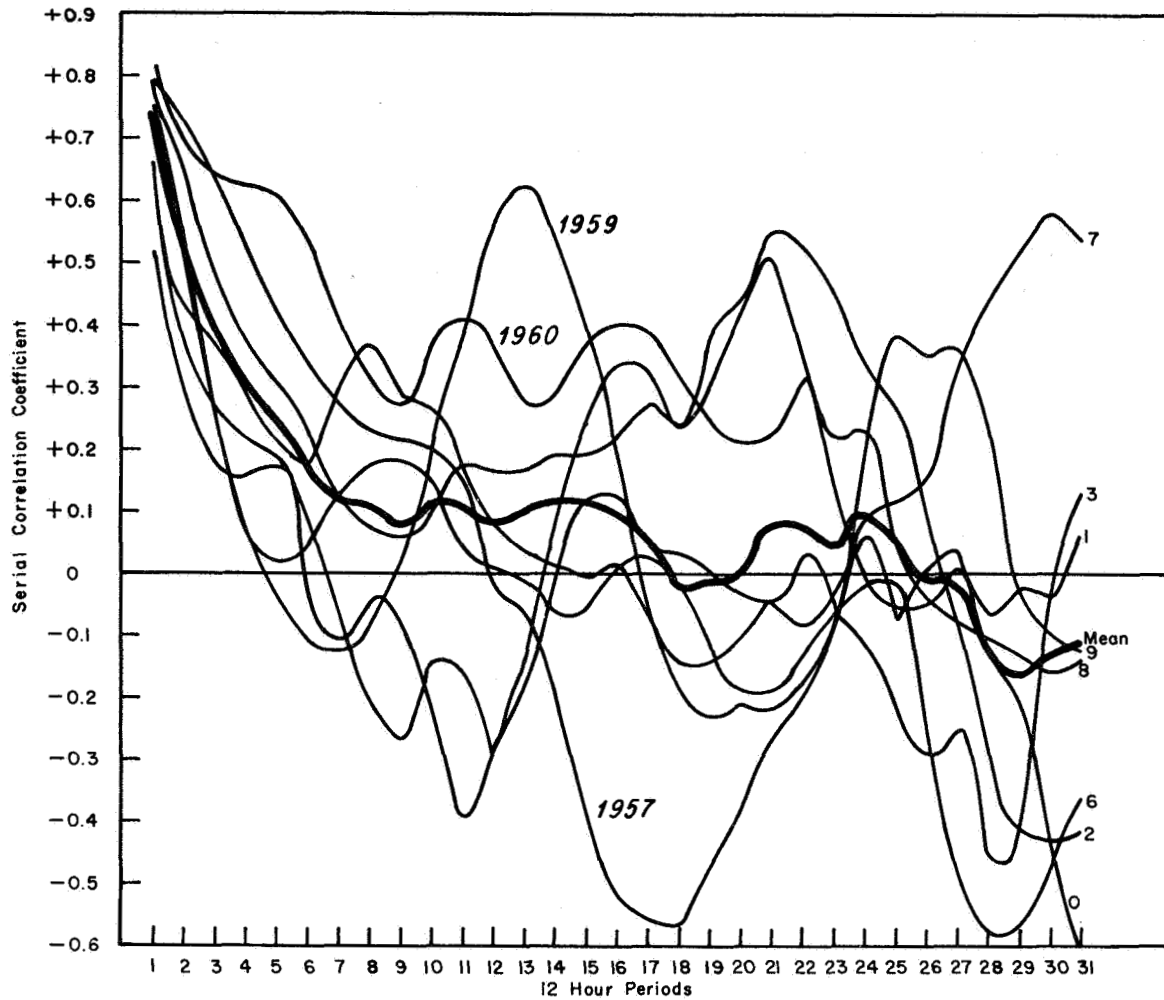


FIGURE 19. PLOT OF MAXIMUM WIND SPEED IN THE 10-15 km LAYER FOR THE YEARS 1956-1963 DURING JANUARY AT CAPE KENNEDY, FLORIDA

Let $P\{A\} = P[W < W^*]$ denote the probability that $W < W^*$ one or more times in k -consecutive 12-hr periods (these statistics are given in Table IIIA); then $[1 - P\{A\}] = P\{A'\}$ is the probability that $W \geq W^*$ for k -consecutive 12-hr periods. The probability $P\{A'\}$ is also the probability of a run above W^* of length k in units of 12-hr periods.

Using 50 m/sec for W^* from Table III, the January statistics, and the above definitions, the probability of a run above 50 m/sec and a run below 50 m/sec of length k in units of 12-hr periods is illustrated in Table IV. The computational procedure to derive conditional probabilities from $P\{B'\}$ is also illustrated in Table IV. The conditional probabilities from $P\{A'\}$ can also be computed in like fashion.

When W^* is defined as the critical wind speed prohibiting the launch of a vehicle, several statistical inferences in terms of vehicle operations can be made.

1. The probability of $P\{B\} = P[W \geq W^*]$ as previously defined is the probability of no-launch at least one time in k -consecutive 12-hr periods. From Table IIIB for $W^* = 50$ m/sec, the probability is 0.504 for $k=1$. Stated in another way, there is a 50.4 percent chance of no-launch during any arbitrary 12-hr period during January under the assumption that when the wind is critical, it is critical for 12 hr. There is an 80.8 percent chance of no-launch at least one time in 10 consecutive 12-hr periods (or 5 days). This probability is also read from Table III.

TABLE IV. AN EXAMPLE FOR JANUARY IN THE COMPUTATION OF PROBABILITIES OF RUNS AND CONDITIONAL PROBABILITIES FOR MAXIMUM WIND IN THE 10-15 km LAYER AT CAPE KENNEDY, FLORIDA

k-12 hr periods (k)	P{B}	P{A}	P{B'}	P{A'}	Comparison with a random variable	Conditional Probabilities (%), from P{B'}			
	P[W ≥ 50*] (%)	P[W < 50*] (%)	[1-P{B}] (%)	[1-P{A}] (%)		P _k /P _i , i ≤ k.			
						i= 1	i= 2	i= 3	i= 4
1	50.4	49.6	49.6	50.4	50.0	100			
2	59.5	58.5	40.5	41.5	25.0	82	100		
3	65.3	65.2	34.7	34.7	12.5	70	86	100	
4	69.4	69.8	30.6	30.2	6.25	62	76	88	100
5	72.2	73.6	27.8	26.4	3.12	56	69	80	91
6	74.4	76.4	25.6	23.6	1.56	52	63	74	84
7	76.6	79.0	23.4	21.0	0.78	47	58	67	76
8	78.2	81.3	21.8	18.8	0.39	44	54	63	71
9	79.8	83.3	20.2	16.7	0.20	41	50	58	66
10	80.8	84.7	19.2	15.3	0.10	39	47	55	63
	From Table III. B	From Table III. A	runs below	runs above					

* Units, m/sec

2. The probability $P\{A\} = P[W < W^*]$ as previously defined is the probability of launch at least one time in k-consecutive 12-hr periods. From Table IIIA for $W^* = 50$ m/sec, this probability for $k = 10$ consecutive 12-hr periods is 0.847.

3. The probability $P\{B'\} = [1 - P\{B\}]$, which can be computed from Table IIIB or taken directly from Tables V and VI, is the probability of launch for k-consecutive 12-hr periods. From Table IV for January for $W^* = 50$ m/sec, there is a 19.2 percent chance that the wind will not be critical for launch for 10 consecutive 12-hr periods or for a 5-day period.

4. The probability $P\{A'\} = [1 - P\{A\}]$, which can be computed from Table IIIA or taken directly from Tables VI and VII, is the probability of no-launch for k-consecutive 12-hr periods. From Table IV for January for $W^* = 50$ m/sec, there is a 15.3 percent chance that the wind will be critical for launch for 10 consecutive 12-hr periods or for a 5-day period.

5. Conditional probabilities can be readily computed from the run statistics ($P\{B'\}$ and $P\{A'\}$), as illustrated in Table IV or taken directly from Tables V-VIII). The January statistics for wind speed ≥ 50 , < 50 , ≥ 75 , and < 75 m/sec for the

probabilities of runs above and runs below these specified wind speed values and the resulting conditional probabilities are presented in Tables V, VI, VII, and VIII, respectively. The explanation for the columns for these tables is as follows:

Column 1 is the length of a run in increments of 12-hr periods; i. e., k - 12-hr periods.

Column 2 is the number of runs of length k (denote this column as N_{rk}). (This is the absolute frequency of a run of length k .)

Column 3 is the number of observations of length k or greater. (This is the cumulative absolute frequency of runs of length k ; denote this column by N_k .)

Column 4 is the number of observations in the sample. This is a fixed value for each month corresponding to the number of observations for the given month in the eight-year data sample.

Column 5 is the probability of having a run of length k or greater. Denote this column by P_k , where

$$P_k = \frac{N_k}{N}$$

Column 6 and all other columns are the conditional probabilities:

$$P_{c(k,i)} = \frac{N_k}{N_i}, \quad \begin{array}{l} i \leq k \\ i = 1, 2, 3 \dots \end{array}$$

where column 6 is for $i = 1$, column 7 is for $i = 2$, etc.

For vehicle mission analysis and launch planning, conditional probabilities give answers to such questions as, "What is the probability that the winds will remain critical for launch, given that they are critical at 24 or 12 hr prior to the scheduled launch?" Conversely, given that the winds are not critical at 24 or 12 hr before launch, "what is the probability that they will remain not critical up to the scheduled launch?"

From Table IV at 24 hr before launch, suppose that the wind is below critical limits (< 50 m/sec) for the first time in a series of wind measurements, then there is a 70 percent chance that the wind will remain below critical limits at launch time. Suppose wind measurements at 12 hr before launch revealed that the magnitudes are still below the critical limits; now the conditional probability for launch time is

0.86, or there is an 86 percent chance that the winds will be below critical limits at launch time. This conditional probability is read from Table IV at $k = 3$ and $i = 2$.

Clearly, if the wind is observed to be less than 50 m/sec, the probability of this event occurring at a given time is 1.00, or as indicated in Table IV, 100 percent. Based on this information, the predicted occurrence of the event two days hence is 56 percent (read from Table IV at $i = 1$ and $k = 5$); whereas, there was only a 49.6 percent chance of the wind being less than 50 m/sec on any arbitrary observation during the month. To continue the example, suppose the wind is observed 12 hr later (corresponding to $i = 2$) and it is still below 50 m/sec; then, the probability that the wind will be below 50 m/sec 24 hr in the future is 76 percent. This value is read from the table at $i = 2$, $k = 4$. Now, compare the probabilities at k_2i_1 , k_3i_2 , etc. (or the values above the diagonal); these probabilities increase but will later decrease and even fluctuate as the computations are carried out further. In a similar manner, the conditional probabilities can be carried out for $P\{A'\}$ and corresponding interpretations can be made. The meteorologist terms this behavior of an atmospheric variable with respect to time as "persistence." In principle, the conditional probabilities could be used in conjunction with other meteorological information to make a deterministic wind prediction. Another possible application of the conditional probabilities would be to serve as base-line values for wind forecast verifications.

By comparing $P\{B'\}$ and $P\{A'\}$ with the statistics of a random variable (see Table IV), it is concluded that the wind sample is not stochastically independent. What happens to the conditional probabilities for the random series? The conditional probabilities remain 0.50.

Probability of Runs and Conditional Probabilities. From an analysis independent of that for exceedance probabilities, the run probabilities and conditional probabilities for the same data sample (the maximum wind speed 10-15 km over Cape Kennedy) were computed for specified wind speeds. Since these statistics were determined at different times and using different techniques, the notation is slightly different. The most satisfying feature is that the resulting statistics are identical, thus giving rise to confidence in the correctness of the computation processes, as well as providing an independent approach to the same problem. Figure 20 is a useful graphical form to display the probabilities of runs.

TABLE V. RUNS AND CONDITIONAL PROBABILITIES FOR THE MAXIMUM WIND IN THE 10-15 km LAYER BEING < 50 m/sec (JANUARY, CAPE KENNEDY, FLORIDA)

k	N _{rk}	N _k	P _k	P _{c1}	P _{c2}	P _{c3}	P _{c4}	P _{c5}	P _{c6}	P _{c7}	P _{c8}	P _{c9}	P _{c10}	P _{c11}	P _{c12}	P _{c13}	P _{c14}	P _{c15}	P _{c16}	
1	16	246	.496	1.0																
2	9	201	.405	.82	1.0															
3	7	172	.347	.70	.86	1.0														
4	3	152	.306	.62	.76	.88	1.0													
5	0	138	.278	.56	.69	.80	.91	1.0												
6	3	127	.256	.52	.63	.74	.84	.92	1.0											
7	1	116	.234	.47	.58	.67	.76	.84	.91	1.0										
8	3	108	.218	.44	.54	.63	.71	.78	.85	.93	1.0									
9	1	100	.202	.41	.50	.58	.66	.72	.79	.86	.93	1.0								
10	0	95	.192	.39	.47	.55	.63	.69	.75	.82	.88	.95	1.0							
11	0	91	.183	.37	.45	.53	.60	.66	.72	.78	.84	.91	.96	1.0						
12	1	87	.175	.35	.43	.51	.57	.63	.69	.75	.81	.87	.92	.96	1.0					
13	0	83	.167	.34	.41	.48	.55	.60	.65	.72	.77	.83	.87	.91	.95	1.0				
14	1	80	.161	.33	.40	.47	.53	.58	.63	.69	.74	.80	.84	.88	.92	.96	1.0			
15	1	77	.155	.31	.38	.45	.51	.56	.61	.66	.71	.77	.81	.85	.89	.93	.96	1.0		
16	0	75	.151	.30	.37	.44	.49	.54	.59	.65	.69	.75	.79	.82	.86	.90	.94	.97	1.0	

k = Number of 12-hr periods (run).
 N_{rk} = Number of runs of exact length k.
 P_k = The probability that run of length k or greater will occur.
 N_k = Number of occurrences of runs equal to or greater than k.
 N = Number of possible outcomes.
 P_c = Conditional probability

TABLE VI. RUNS AND CONDITIONAL PROBABILITIES FOR THE MAXIMUM WIND IN THE
10-15 km LAYER BEING < 75 m/sec (JANUARY, CAPE KENNEDY, FLORIDA)

k	N_{rk}	N_k	P_k	P_{c1}	P_{c2}	P_{c3}	P_{c4}	P_{c5}	P_{c6}	P_{c7}	P_{c8}	P_{c9}	P_{c10}	P_{c11}	P_{c12}	P_{c13}	P_{c14}	P_{c15}	P_{c16}	
1	1	466	496	.940	1.0															
2	2	454	496	.915	.97	1.0														
3	0	442	496	.891	.95	.97	1.0													
4	2	432	496	.871	.93	.95	.98	1.0												
5	0	422	496	.851	.91	.93	.95	.98	1.0											
6	0	414	496	.835	.89	.91	.94	.96	.98	1.0										
7	1	406	496	.819	.87	.89	.92	.94	.96	.98	1.0									
8	0	398	496	.802	.85	.88	.90	.92	.94	.96	.98	1.0								
9	0	391	496	.788	.84	.86	.88	.91	.93	.94	.96	.98	1.0							
10	0	384	496	.774	.82	.85	.87	.89	.91	.93	.95	.96	.98	1.0						
11	2	377	496	.760	.81	.83	.85	.87	.89	.91	.93	.95	.96	.98	1.0					
12	1	370	396	.746	.79	.81	.84	.86	.88	.89	.91	.93	.95	.96	.98	1.0				
13	1	365	496	.736	.78	.80	.83	.84	.86	.88	.90	.92	.93	.95	.97	.99	1.0			
14	1	361	496	.728	.77	.80	.82	.84	.86	.87	.89	.91	.92	.94	.96	.98	.99	1.0		
15	0	358	496	.722	.77	.79	.81	.83	.85	.86	.88	.90	.92	.93	.95	.97	.98	.99	1.0	
16	0	355	496	.716	.76	.78	.80	.82	.84	.86	.87	.89	.91	.92	.94	.96	.97	.98	.99	1.0

k = Number of 12-hr periods (run).
 N_{rk} = Number of runs of exact length k.
 P_k = The probability that run of length i or greater will occur.
 N_k = Number of occurrences of runs equal to or greater than k.
 N = Number of possible outcomes.
 P_c = Conditional probability.

TABLE VII. RUNS AND CONDITIONAL PROBABILITIES FOR THE MAXIMUM WIND IN THE 10-15 km LAYER BEING ≥ 50 m/sec (JANUARY, CAPE KENNEDY, FLORIDA)

k	N_{rk}	N_k	P_k	P_{c1}	P_{c2}	P_{c3}	P_{c4}	P_{c5}	P_{c6}	P_{c7}	P_{c8}	P_{c9}	P_{c10}	P_{c11}	P_{c12}	P_{c13}	P_{c14}	P_{c15}	P_{c16}	
1	11	250	.496	.504	1.0															
2	12	206	.496	.415	.82	1.0														
3	3	172	.496	.347	.69	.83	1.0													
4	5	150	.496	.302	.60	.73	.87	1.0												
5	1	131	.496	.264	.52	.64	.76	.87	1.0											
6	2	117	.496	.236	.47	.57	.68	.78	.89	1.0										
7	1	104	.496	.210	.42	.50	.60	.69	.79	.89	1.0									
8	3	93	.496	.188	.37	.45	.54	.62	.71	.79	.89	1.0								
9	1	83	.496	.167	.33	.40	.48	.55	.63	.71	.80	.89	1.0							
10	2	76	.496	.153	.30	.37	.44	.51	.58	.65	.73	.82	.92	1.0						
11	0	70	.496	.141	.28	.34	.41	.47	.53	.60	.67	.75	.84	.92	1.0					
12	0	66	.496	.133	.26	.32	.38	.44	.50	.56	.63	.71	.80	.87	.94	1.0				
13	1	62	.496	.125	.25	.30	.36	.41	.47	.53	.60	.67	.75	.82	.89	.94	1.0			
14	2	58	.496	.117	.23	.28	.34	.39	.44	.50	.56	.62	.70	.76	.83	.88	.94	1.0		
15	0	55	.496	.111	.22	.27	.32	.37	.42	.47	.53	.59	.66	.72	.79	.83	.89	.95	1.0	
16	0	54	.496	.109	.22	.26	.31	.36	.41	.46	.52	.58	.65	.71	.77	.82	.87	.93	.98	1.0

k = Number of 12-hr periods (run).
 N_{rk} = Number of runs of exact length k .
 P_k = The probability that run of length k or greater will occur.
 N_k = Number of occurrences of runs equal to or greater than i .
 N = Number of possible outcomes.
 P_c = Conditional probability.

TABLE VIII. RUNS AND CONDITIONAL PROBABILITIES FOR THE MAXIMUM WIND IN THE 10-15 km LAYER BEING ≥ 75 m/sec (JANUARY, CAPE KENNEDY, FLORIDA)

k	N_{rk}	N_k	N	P_k	P_{c1}	P_{c2}	P_{c3}	P_{c4}	P_{c5}	P_{c6}
1	4	30	496	.060	1.0					
2	4	18	496	.036	.60	1.0				
3	1	10	496	.020	.33	.56	1.0			
4	1	6	496	.012	.20	.33	.60	1.0		
5	1	3	496	.006	.10	.17	.30	.50	1.0	
6	1	1	496	.002	.03	.06	.10	.17	.33	1.0

k = Number of 12-hr periods (run).
 N_{rk} = Number of runs of exact length k .
 P_k = The probability that run of length i or greater will occur.

N_k = Number of occurrences of runs equal to or greater than k .
 N = Number of possible outcomes.
 P_c = Conditional probability.

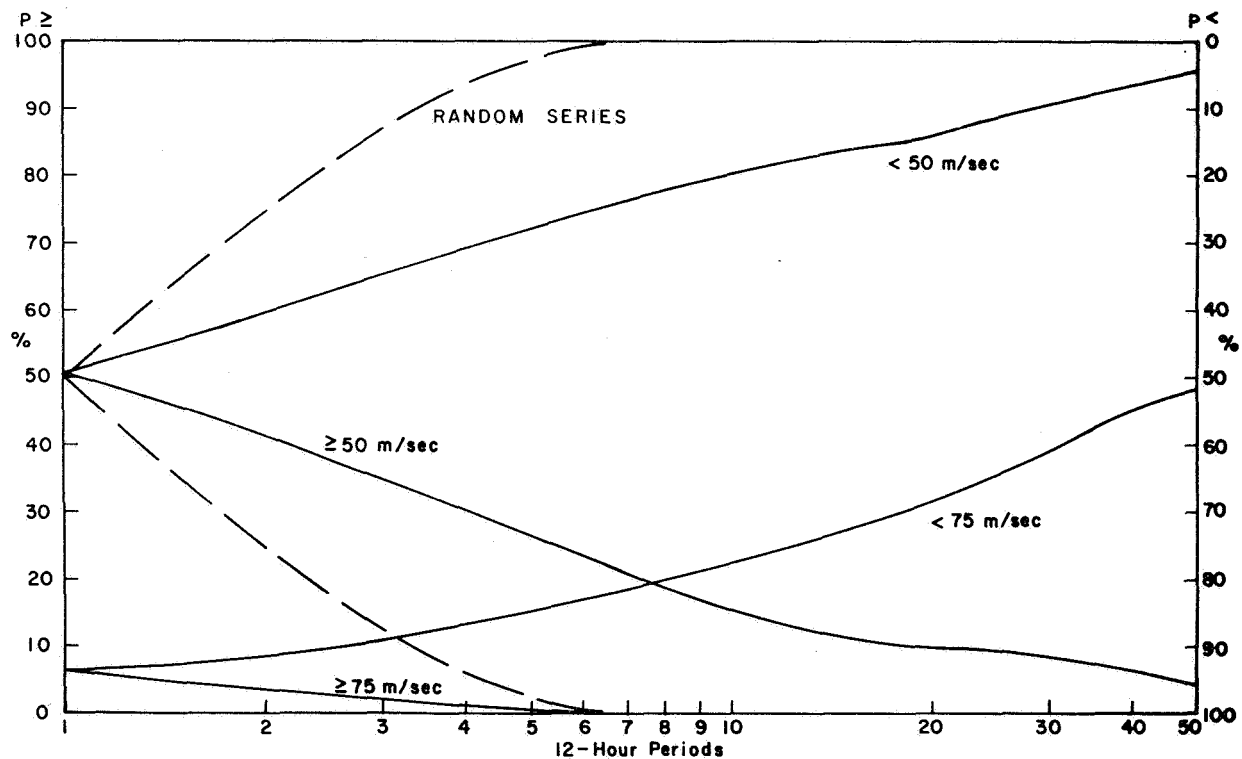


FIGURE 20. PROBABILITY OF THE MAXIMUM WIND SPEED IN THE 10-15 km LAYER BEING \geq AND $<$ SPECIFIED VALUES FOR k 12-HR PERIODS DURING JANUARY AT CAPE KENNEDY, FLORIDA

From the definitions presented in the section "Empirical Exceedance Probabilities," an inverse operation can be performed to calculate the exceedance probabilities from the probabilities of runs given in Tables V-VIII. For example, the probability that the maximum wind speed in the 10-15 km layer will exist for 10 consecutive 12-hr periods at a magnitude ≥ 50 m/sec in January (Table VII, column 5, corresponding to $k = 10$) is 0.153. In symbols, this statement is expressed as $P\{W \geq 50 \text{ m/sec}\}$ for 10 consecutive 12-hr periods is 0.153.

The probability that the wind speed will not exceed 50 m/sec at least one time in 10 consecutive 12-hr periods is 0.847 ($1 - 0.153 = 0.847$). The probability that the wind speed will exceed 50 m/sec at least one time in 10 consecutive 12-hr periods in January is obtained from Table V, $1 - 0.192 = 0.808$.

Empirical Multiple Exceedance Probabilities. The longest succession of maximum wind speed in the 10-15 km layer with wind speeds ≥ 75 m/sec occurred during the winter of 1958. This year would be referred to as a high wind year. In terms of runs, the longest runs ≥ 75 m/sec by months are as following:

Max. Length of Run in 12-hr Periods	Year/Month	Dates and Times Inclusive
6	1958/Jan.	25, 12Z - 27, 12Z
14	1958/Feb.	10, 00Z - 16, 12Z
7	1958/Mar.	28, 12Z - 31, 12Z
3	1958/Apr.	15, 12Z - 16, 12Z

(There were no values ≥ 75 m/sec for May - October)

6	1956/Nov.	25, 03Z - 27, 15Z
4	1956/Dec.	29, 03Z - 30, 15Z

The counting rule for runs is as follows: If a run begins in one month and extends into a following month, it is counted as a run for the month in which it begins.

Beginning at 12Z on January 25, 1958, the wind blew at a speed ≥ 75 m/sec for fifty-three 12-hr periods (26 1/2 days) with only 6 exceptions: There were two single breaks, i.e., twice that the wind dropped below 75 m/sec; twice the wind dropped below 75 m/sec for two 12-hr periods; and twice the

wind dropped below 75 m/sec for three 12-hr periods. For this particular sample period of 53, there was a 77 percent chance that the wind was equal to or greater than 75 m/sec. Yet, for the entire sample of eight Januaries, there was a 6 percent chance that the wind speed was equal to or greater than 75 m/sec in the 10-15 km layer.

Now return to the discussion on the probabilities $P\{B\}$ and $P\{A\}$; i.e., the probability that $W \geq W^*$ and $W < W^*$ one or more times in k -consecutive 12-hr periods. To base an entire mission on the probability of having at least one opportunity to launch because of a winds-aloft constraint in k -consecutive 12-hr periods, even though this probability can be well above a 95 percent chance of launch within the launch opportunity period, may be a rather high risk to the project in view of the consequences: loss of the mission. For this reason, the computations have been extended to derive the probability of 2, 3, 4, . . . i , ($i = 20$) launch opportunities (because of arbitrary winds-aloft constraints) in k -consecutive 12-hr periods. These latter statistics are referred to as the probability of i successes in j periods: $P\{i \text{ successes in } j \text{ periods}\}$. The extreme approach would be to base the probability of mission success on the probability that the winds aloft would be below the launch constraint value continuously for k -consecutive 12-hr periods. These statistics will find immediate application to multiple vehicle launches such as will be required for AAP in the concept of "cluster vehicles." Where the mission successes depend upon getting two or more vehicles launched at intervals from 1 to 3 days separation.

The probable number of launch opportunities (wind speed < critical) in a given number of periods expressed in terms of i successes (where success is the occurrence of wind speed < critical) in j periods is shown in Table IX. For example, suppose a mission has a 4-day launch window in January, and the vehicle is constrained to wind speeds less than 50 m/sec. Of concern to the mission planner is the probability that at least one observation of wind speeds < 50 m/sec (one launch opportunity) will occur during the launch window (eight 12-hr periods). This probability, 0.813, is read from Table IX, line 8, column 1. If, however, after considering other factors, it is decided that 4 successes in the 8 periods are required, that probability, 0.550, is read from line 8, column 4. Table X contains similar probability statements except here it is required that the successes be consecutive. With this additional restriction, the probability of success will naturally be lower. Using the example above, one obtains 0.431 from Table X versus 0.550 from Table IX.

TABLE IX. P{I SUCCESSES IN J PERIODS} MAXIMUM WIND BEING < 50 m/sec IN THE
10-15 km LAYER (JANUARY, CAPE KENNEDY, FLORIDA)

J 12-hr periods	1	2	3	4	5	6	7	8	9	10	11	12	13	14	15	16
1	.496	-	-	-	-	-	-	-	-	-	-	-	-	-	-	-
2	.585	.405	-	-	-	-	-	-	-	-	-	-	-	-	-	-
3	.653	.488	.347	-	-	-	-	-	-	-	-	-	-	-	-	-
4	.698	.560	.427	.306	-	-	-	-	-	-	-	-	-	-	-	-
5	.736	.599	.504	.379	.278	-	-	-	-	-	-	-	-	-	-	-
6	.764	.631	.540	.464	.341	.256	-	-	-	-	-	-	-	-	-	-
7	.790	.649	.577	.506	.423	.313	.234	-	-	-	-	-	-	-	-	-
8	.813	.669	.591	.550	.468	.399	.280	.218	-	-	-	-	-	-	-	-
9	.833	.690	.605	.565	.516	.450	.369	.258	.202	-	-	-	-	-	-	-
10	.847	.714	.619	.583	.530	.498	.425	.343	.236	.192	-	-	-	-	-	-
11	.859	.732	.641	.593	.548	.510	.480	.403	.315	.220	.183	-	-	-	-	-
12	.867	.754	.655	.611	.558	.524	.492	.468	.379	.288	.208	.175	-	-	-	-
13	.875	.774	.671	.621	.577	.534	.506	.482	.454	.351	.268	.198	.167	-	-	-
14	.883	.790	.692	.631	.589	.548	.520	.494	.470	.431	.325	.254	.188	.161	-	-
15	.889	.806	.702	.653	.599	.560	.532	.510	.482	.458	.399	.308	.240	.181	.155	-
16	.891	.825	.712	.667	.617	.569	.546	.520	.500	.472	.429	.383	.288	.232	.175	.151

TABLE X. P {I CONSECUTIVE SUCCESSES IN J PERIODS} MAXIMUM WIND BEING < 50 m/sec
IN THE 10-15 km LAYER (JANUARY, CAPE KENNEDY, FLORIDA)

J 12-hr periods	1	2	3	4	5	6	7	8	9	10	11	12	13	14	15	16
1	.496	-	-	-	-	-	-	-	-	-	-	-	-	-	-	-
2	.585	.405	-	-	-	-	-	-	-	-	-	-	-	-	-	-
3	.653	.466	.347	-	-	-	-	-	-	-	-	-	-	-	-	-
4	.698	.528	.393	.306	-	-	-	-	-	-	-	-	-	-	-	-
5	.736	.577	.440	.399	.278	-	-	-	-	-	-	-	-	-	-	-
6	.764	.611	.484	.371	.304	.256	-	-	-	-	-	-	-	-	-	-
7	.790	.637	.518	.401	.331	.282	.234	-	-	-	-	-	-	-	-	-
8	.813	.653	.540	.431	.355	.308	.256	.218	-	-	-	-	-	-	-	-
9	.833	.667	.563	.460	.379	.333	.278	.238	.202	-	-	-	-	-	-	-
10	.847	.681	.575	.482	.401	.357	.298	.258	.216	.192	-	-	-	-	-	-
11	.859	.696	.585	.504	.423	.379	.319	.276	.230	.204	.183	-	-	-	-	-
12	.867	.706	.595	.518	.442	.401	.337	.294	.244	.216	.196	.175	-	-	-	-
13	.875	.716	.605	.530	.460	.423	.355	.310	.258	.228	.208	.188	.167	-	-	-
14	.883	.726	.615	.542	.472	.442	.373	.327	.270	.240	.220	.200	.177	.161	-	-
15	.889	.736	.625	.554	.482	.460	.391	.343	.282	.250	.232	.212	.188	.171	.155	-
16	.891	.746	.635	.567	.494	.472	.407	.359	.294	.260	.242	.224	.198	.181	.165	.151

The data shown here were extracted from tables covering all months for wind speeds \geq and $<$ 5, 10, 15, . . . 90 m/sec, where $i = 1, 2, 3, \dots, 20$, and $j = 1, 2, 3, \dots, 40$.

Since a large number of statistics can be derived from the statistics like those presented in Tables III and V-VIII, these tables can serve as basic inputs to computer simulation programs for mission analysis purposes. However, transitional conditional probabilities cannot be derived from these tables. The winds can change with time from critical for launch to noncritical several times during a mission opportunity or during a long countdown. For example, there are 20 possible combinations for conditional probabilities of critical and noncritical winds in only five consecutive periods. Because of the large volume of resulting statistics, the presentation of all possible conditional probabilities must take the form of mathematical statistical models. The most suggestive forms are to be found in order statistics involving Markov processes.

The message in these winds aloft launch probability statements is: "If you don't first succeed, try and try again, but beware that the longer you try and don't succeed, the probability becomes greater that something else will cause a problem." The application of this thought is inherent in such areas as trade-off studies, mission analysis, systems engineering analysis, etc.

Wind Bias Profiles. Two alternatives are, in principle, feasible to lower the probability of launch delays caused by winds aloft, particularly during the winter months. One is to use wind bias profiles, and the other is to develop an advance guidance system for wind load relief. Based on monthly median pitch plane wind component profiles, the vehicle tilt program is biased to yield a small angle of attack and thus reduce structural loads. This procedure could also be applied to the yaw plane, but it has not been used to date. When properly applied, the wind bias technique lowers the probability of launch delay from winds aloft. Wind bias profiles have been used for a number of Saturn flights; e.g., SA-4 launched March 28, 1963; SA-5 launched January 29, 1964; SA-9 launched February 16, 1965; AS-201 launched February 22, 1966; and

Saturn 501 launched November 9, 1967. The SA-6, launched May 28, 1964, was wind biased to intentionally introduce a larger angle of attack and thus greater structural loads than would otherwise be likely from the natural occurrence of the wind profile during that time of year. Because of the nature of some missions, it is expected that the use of wind-biased techniques would be operationally more complicated than for these flights. If the launch azimuths have large range during a launch window, a system to update the wind bias would be required. The merits of the wind-biased technique must be analyzed for each mission. The information needed for the analysis includes:

1. Launch opportunities - dates.
2. Launch windows - hours within the launch opportunities.
3. Launch azimuth versus launch windows.

CONCLUSIONS

Through the use of examples, the importance of ground winds and winds aloft statistics to the aerospace vehicle programs has been presented. There is still much work to be done to extend this study to improve the theoretical probability models and to present the resulting statistics in a form amenable for use in management decisions involving systems engineering. A number of statistical concepts have been advanced relative to the application of wind statistics to aerospace vehicle design, operational, and mission problems. The determination of the probability of launch as a function of several atmospheric launch constraints (e.g., ground winds, winds aloft, and clouds) taken simultaneously and in combination is the subject of a separate study. The proper balance in supporting research funds and program funds to continue these efforts will serve to the mutual benefit of several interests within all NASA Centers. The realization of the importance of these and similar studies will become more apparent with the changing role of the MSFC space program from that of research and development of large boosters to that of space exploration and application.

REFERENCES

1. Gumbel, E. J.: Statistics of Extremes, Columbia University Press, New York, 1958.
2. Fisher, R. A.: Contributions to Mathematical Statistics, John Wiley and Sons, Inc., New York, 1950.
3. Thom, H. C. S.: Distribution of Extreme Winds in the United States. Journal of the Structural Division Proceedings of the American Society of Civil Engineers, April, 1960.
4. Court, Arnold: Some New Statistical Techniques in Geophysics. Advances in Geophysics, New York, Academic Press, 1952, pp. 45-85.
5. Lifsey, J. David: An Empirical Analysis of Daily Peak Surface Wind at Cape Kennedy, Florida for Project Apollo. NASA TM X-53116, August 27, 1964.
6. Canfield, N. L.; Smith, O. E.; and Vaughan, W. W.: Progress in Circumventing Limitations of Upper Wind Records. Journal of Applied Meteorology, vol. 5, no. 3, June 1966, pp. 301-303.
7. Canfield, N. L.; Smith, O. E.; and Vaughan, W. W.: Serial Completion of Upper Wind Records. Journal of Geophysical Research, vol. 72, no. 4, pp. 1389-1392.
8. Daniels, G. E.; Scoggins, J. R.; and Smith, O. E.: Terrestrial Environment (Climatic) Criteria Guidelines for Use in Space Vehicle Development, 1966 Revision. NASA TM X-53328
9. Lee, R. F.; Ownbey, J. W.; and Quinlan, F. T.: Thunderstorm Persistence at Cape Kennedy, Florida. To be published as NASA TM X-53635.

DIURNAL VARIATION OF DENSITY AND TEMPERATURE IN THE UPPER ATMOSPHERE

By

Robert E. Smith

SUMMARY

Results of six rocket-launched probes instrumented to measure neutral molecular nitrogen densities and electron densities and temperature between 140 and 325 km are presented and compared with current atmospheric models. Measured N_2 number densities are substantially lower than model value predictions.

DIURNAL VARIATIONS IN ATMOSPHERIC DENSITIES

Since atmospheric drag is the largest force acting on a vehicle in low-earth orbit, the selection of the model most representative of the upper atmosphere of the earth is very important to MSFC program activities. Current models of the earth's upper atmosphere are based solely upon:

1. Density values deduced from analyses of satellite orbital decay. Analyses of satellite orbital decay show that the upper atmosphere expands outward in response to heating from the sun. This outward expansion, referred to as the diurnal bulge, results in a maximum density at all satellite altitudes at about 2 p. m. with a minimum density at about 4 a. m.
2. Time invariant single values for all model parameters at an altitude of 120 km.

Our investigations of the various atmospheric models combined with the orbital dynamics and lifetime studies in which they were to be used at MSFC pointed out that the shape of this diurnal bulge of the atmosphere was just as important as the absolute magnitudes of the density values.

Our investigations also showed that (1) density measurements made by satellite or rocket-borne probes differ from orbital decay analyses values by a factor of 2 to 3 and (2) no attempt had been made to define the shape of this diurnal curve in the 100-200 km altitude region where rocket-launched probes are required. To correct this omission, on January 24, 1967, personnel of the MSFC and the University of Michigan launched six payloads from Cape Kennedy, Florida (Fig. 1).

The payloads were instrumented to measure the neutral molecular nitrogen density with an omegatron mass analyzer located in one end of the cylinder and the electron temperature and density with a Langmuir probe located in the central part of the cylinder. The payloads were ejected at about 70 km with a coast up to an apogee of about 325 km. Measurements were made on both up- and down-legs of the flight.

Figure 2 shows the six vertical N_2 density profiles compared with the Community on Space Research International Reference Atmosphere (CIRA) 1965 Model No. 4 values [1]. The measured values are substantially lower than the corresponding model values.

Figure 3 is a plot of the N_2 number densities versus time at four specific altitudes. The crosses are the measured data points that are connected here by the solid lines. The dashed line connects N_2 values predicted by Jacchia's [2] 1964 static diffusion model for the same geophysical conditions, while the circles are values predicted by the CIRA 1965 Model No. 4. It is readily apparent that the measured values are substantially lower than the model values at all altitudes and all times of the day. At 300 km, the afternoon maximum is about 3.3 times

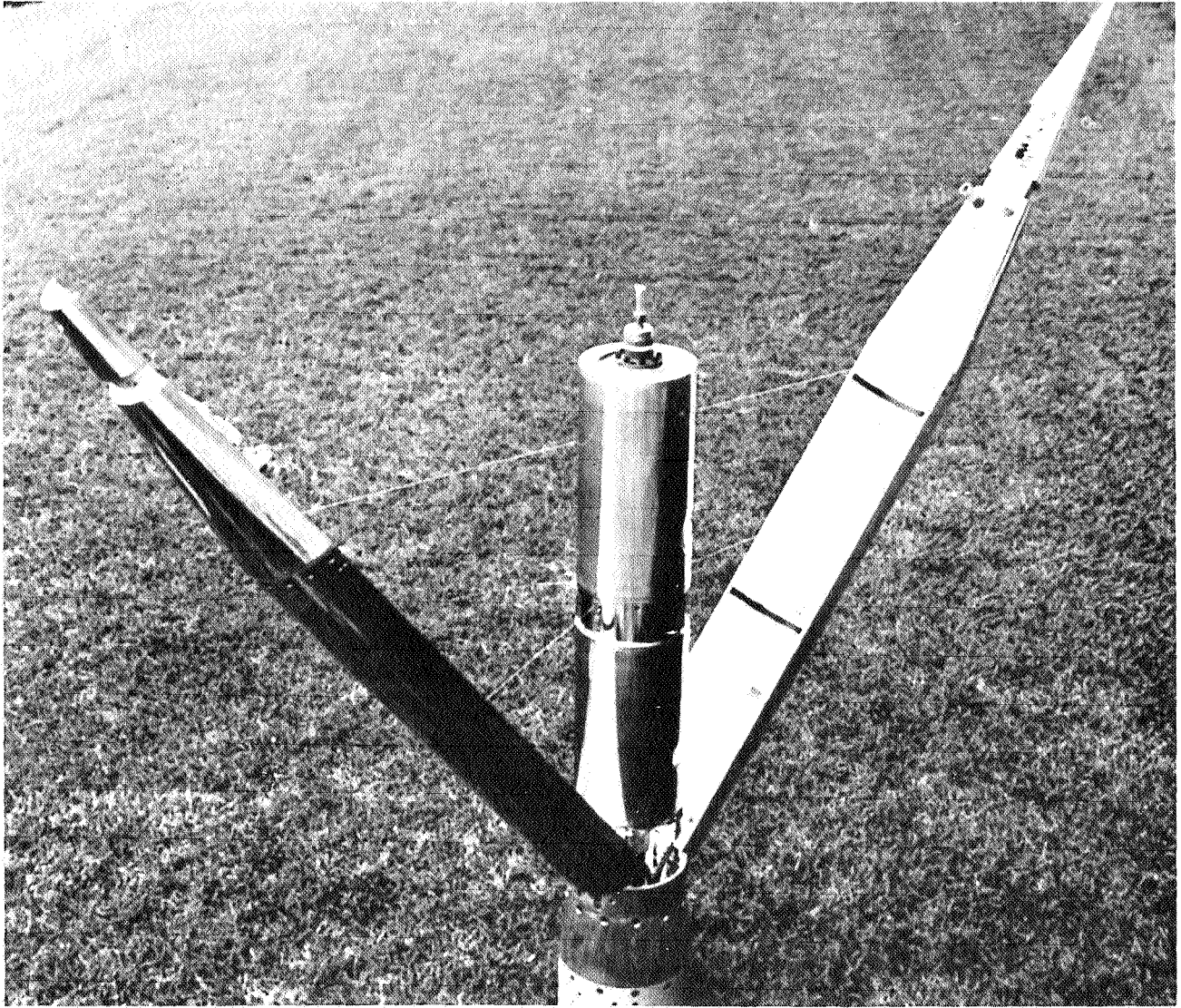


FIGURE 1. THERMOSPHERE PROBE

the morning minimum. At 150 km, this ratio decreases to 1.25. The data clearly show a greater diurnal variation at the lower altitudes than predicted by either model since both models assume single fixed boundary conditions at 120 km. The gauges used in this survey were cross calibrated four at a time on the same system, and special care was taken to insure that all had identical post-calibration histories. For this reason, it is believed that the total uncertainty in the relative values are ± 7 percent.

Figure 4 shows the six vertical profiles of N_2 temperature obtained through a downward integration of the density profiles according to the hydrostatic equation. The maximum temperature occurred at

2 p. m. at all altitudes above 145 km; however, the minimum temperature above 240 km occurred at 6:30 a. m. (just after sunrise). Between 170 and 240 km the minimum temperature occurred at 9:30 p. m.; while below 170 km, the minimum temperature occurred at 3:30 a. m.

Figure 5 shows N_2 temperature versus time at selected altitudes compared once again with the Jacchia 1964 static diffusion model for the appropriate geophysical conditions. Gauge sensitivity does not affect the temperature derivation; thus the ± 5 percent error bars are conservative, assuming diffusive equilibrium. Agreement between model and derived temperature values is very good with the most notable

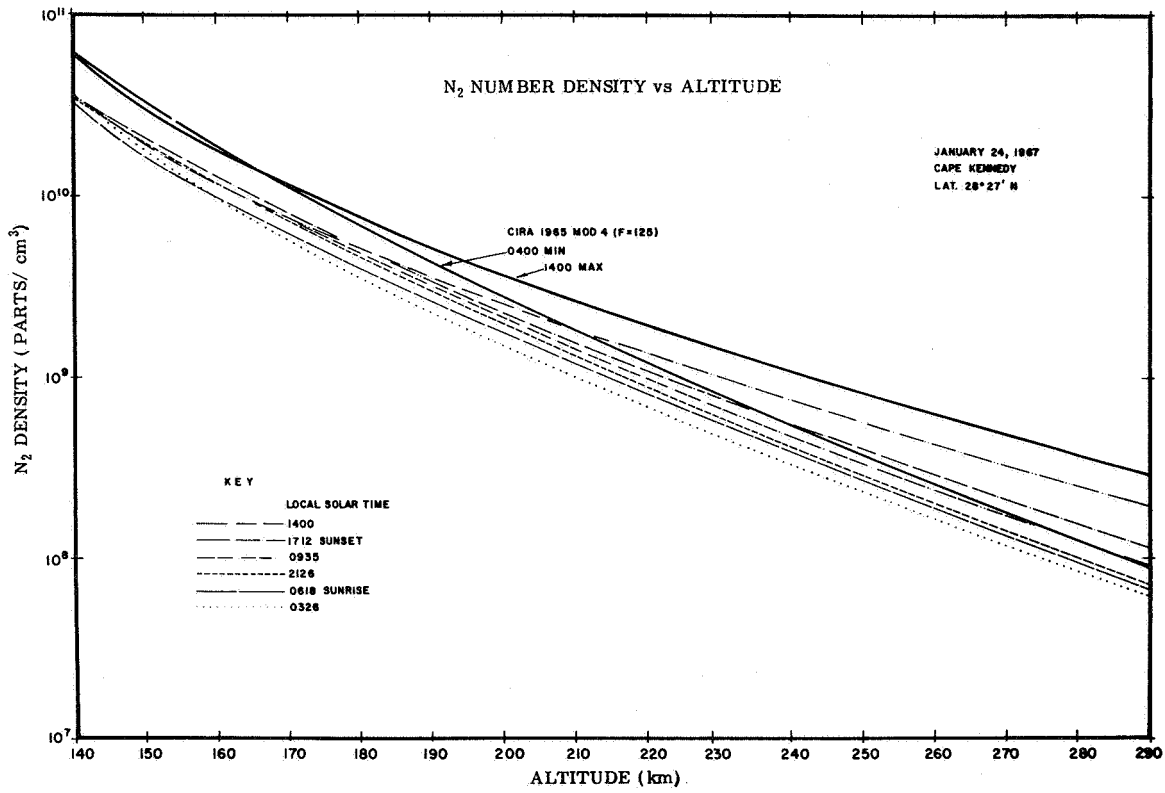


FIGURE 2. DIURNAL SURVEY OF THE THERMOSPHERE

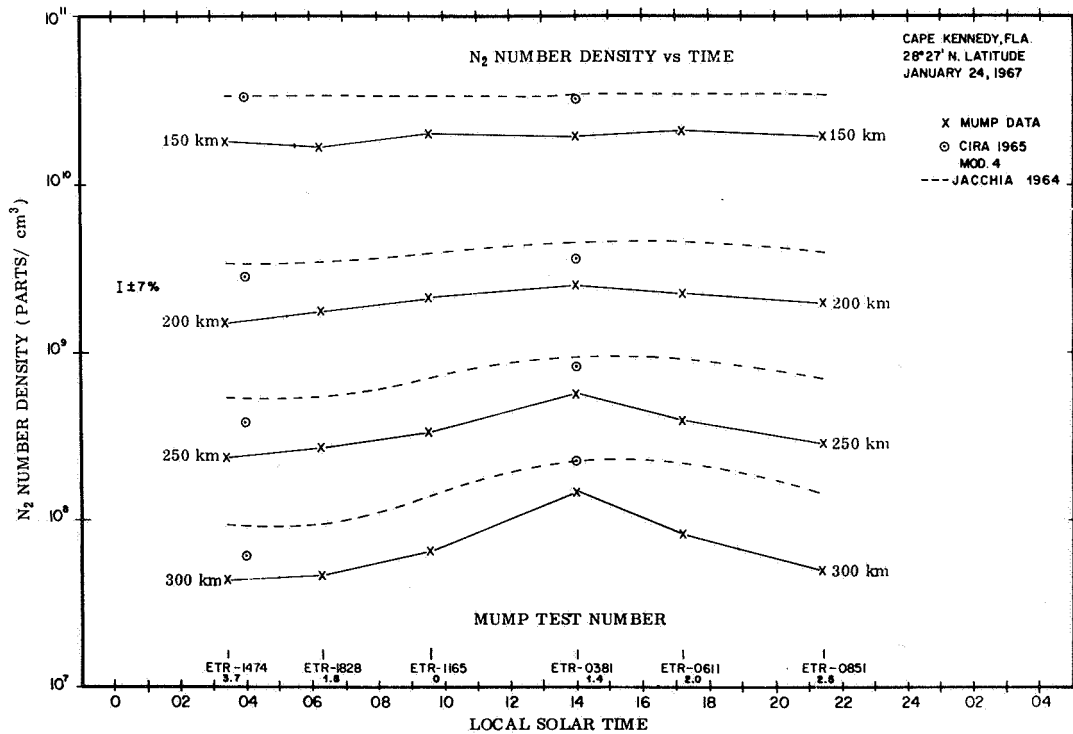


FIGURE 3. MARSHALL - UNIVERSITY OF MICHIGAN PROBE (MUMP) DIURNAL SURVEY OF THE THERMOSPHERE

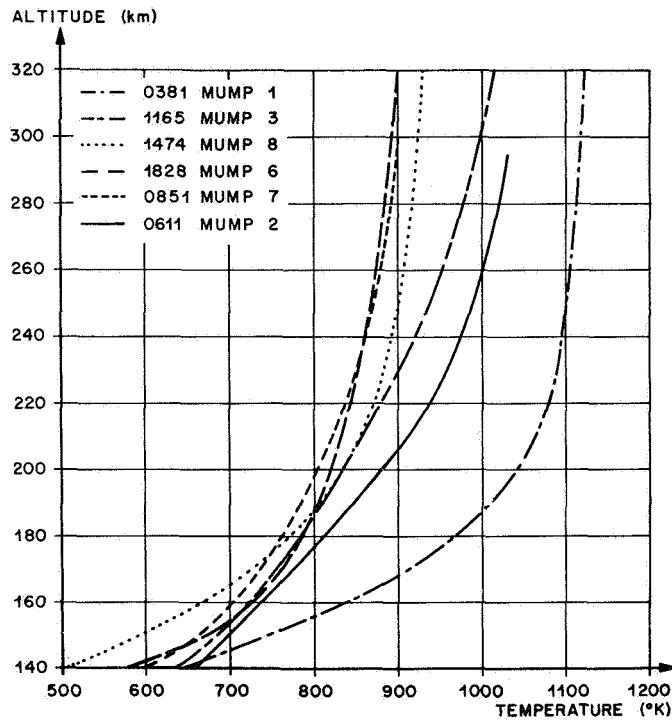


FIGURE 4. TEMPERATURE - HEIGHT PROFILES

difference being the steeper slope of the afternoon-derived temperature decrease. There is a very interesting agreement between this model and the derived temperature in regard to the decrease in the exospheric temperature between 3:30 a. m. and sunrise. According to the model, this is caused by a decrease in the geomagnetic index, a_p , from 3.7 to 1.8. The disagreement at the lower altitudes during the corresponding time period is unexplained so far.

CONCLUSIONS

The six atmospheric probes produced results that:

1. Reaffirmed the discrepancy of a factor of 2 to 3 between gauge measured densities and densities deduced from orbital decay analyses.
2. While confirming that the models provide a fair representation of the general behavior of

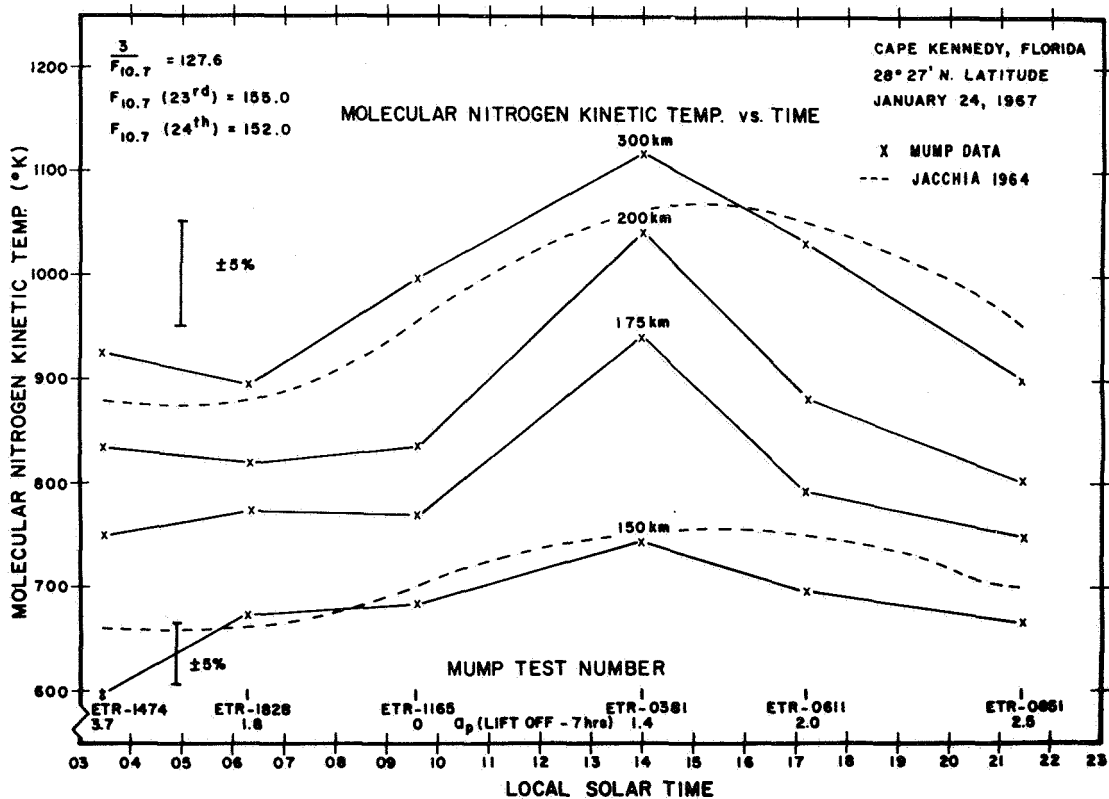


FIGURE 5. MUMP DIURNAL SURVEY OF THE THERMOSPHERE

the upper atmosphere, also pointed out that (1) the upper atmosphere is much more variable than the models predict, (2) the lower boundary condition cannot be time invariant, (3) much additional information is required concerning atmospheric reaction times, and (4) there is still a possibility that the diurnal maximum atmospheric temperature occurs later in the afternoon, as recent Thomson [3] backscatter results have indicated.

FUTURE ACTIVITIES

Future efforts in the program will be directed toward making (1) measurements between 80-140 km, the altitude region containing the postulated lower boundary, and (2) a series of probe launches at approximately one-hour intervals during the late afternoon to more exactly determine the time of occurrence of the afternoon maximum atmospheric density and temperature.

REFERENCES

1. Harris, I.; and Priester, W.: The Upper Atmosphere in the Range from 120 to 800 km. Institute for Space Studies, Goddard Space Flight Center, New York, New York, August 25, 1964.
2. Jacchia, L. G.: Static Diffusion Models of the Upper Atmosphere with Empirical Temperature Profiles. Smithsonian Contribution to Astrophysics, vol. 8, no. 9, 1965, pp. 215-257.
3. Nisbet, J. S.: Neutral Atmospheric Temperatures from Incoherent Scatter Observations. Ionospheric Research Laboratory, The Pennsylvania State University, University Park, Pennsylvania, February 16, 1967.



IONOSPHERIC DISTURBANCES CAUSED BY GROUND BASED ACOUSTIC ENERGY SOURCES

By

William T. Roberts

SUMMARY

Traveling ionospheric disturbances (TID) have long been observed through ionospheric measurements. Ionospheric radio measurements have revealed that these ionospheric movements occur at all geophysical locations and at virtually all heights. These upper atmospheric motions were formerly thought to result solely from solar-terrestrial interactions, but in recent years there has been increasing evidence to indicate that many of the sources for these traveling waves may be ground based. Traveling ionospheric disturbances have definitely been observed to result from atmospheric nuclear blasts and large earthquakes. Recently, the suggestion has been made that atmospheric gravity waves may be generated as a matter of course in such natural events as thunderstorms [1]. There is also some reason to believe that static test firings of large rocket engines and boosters generate sufficient acoustic energy in the low frequency bandwidths to propagate to ionospheric heights and create large disturbances. An analogy has often been made of the similarity between ionospheric traveling disturbances and ripples generated in a smooth pond when a rock is thrown into the water.

IONOSPHERIC DISTURBANCES

The Space Environment Branch is currently engaged in a study of these traveling ionospheric disturbances caused by ground-based acoustic energy sources such as static test firings of large rocket boosters and high energy meteorological

phenomena such as thunderstorms. Since the Space Environment Branch is the Marshall Space Flight Center group responsible for the development of atmospheric models, it has a responsibility as well as a deep interest in the dynamics of the upper atmosphere. The three primary purposes of the program are (1) to collect data to show that ground-based acoustic energy sources do generate pressure waves which can and do propagate to ionospheric heights, (2) to study the propagation of these waves, taking into account winds, temperature profiles, acoustic frequency cutoff regions caused by atmospheric density stratification, absorption, defocusing caused by large temperature gradients such as those that exist at the base of the thermosphere, etc., and (3) to formulate the theoretical mechanisms through which neutral motions in the upper atmosphere are coupled to the ionospheric electrons.

The third purpose has extremely interesting implications. If the coupling relationship can be established with consideration to the magnetic field and the production and loss rates, it may then be possible to determine the neutral motions of the upper atmosphere from the motions of the ionospheric electrons. The electron dynamics may be derived by a relatively simple array of ground-based transmitters and receivers. The main method presently used to measure upper atmospheric winds is to observe the motions of chemiluminescent clouds produced through the release of vapor trails by rockets launched to high altitudes. A second method used to investigate upper atmospheric winds is to observe the decay in satellite inclinations. This method, however, is useful only for altitudes over 200 km and relies heavily on estimated values for the drag coefficient and average cross-sectional area of the satellite.

Funding for this program was provided by the Office of Space Science and Applications following a similar inhouse study on the effects of vehicle launches on the ionosphere [2] .

The current site arrangement is shown in Figure 1. Each transmitter site is equipped with three transmitters broadcasting on different frequencies. The frequencies are regulated by crystal-controlled oscillators stable to within one part in 10^8 per day. Any Doppler shift of the received signal thus results from changes in the ionospheric reflection point and not transmitter drifting. The frequencies were selected so that the frequency separation from one site to another would be on the order of 6 Hz. The received signals are recorded on magnetic tape and processed by a Rayspan analog spectrum analyzer. All signals which fall outside ± 10 Hz of the center frequency are filtered from the data.

The signals are assumed to reflect at the midpoint of the lines joining the transmitter to the receiver, and the distances d_1 , d_2 , and d_3 are the distances from the static test stand to these three midpoints. Since $d_1 < d_2 < d_3$, the horizontal velocities of traveling waves may be measured by determining the time at which the wavefront passes each point. Discrepancies in wave passage caused by the intervening winds and temperature profiles are considered in the data reduction.

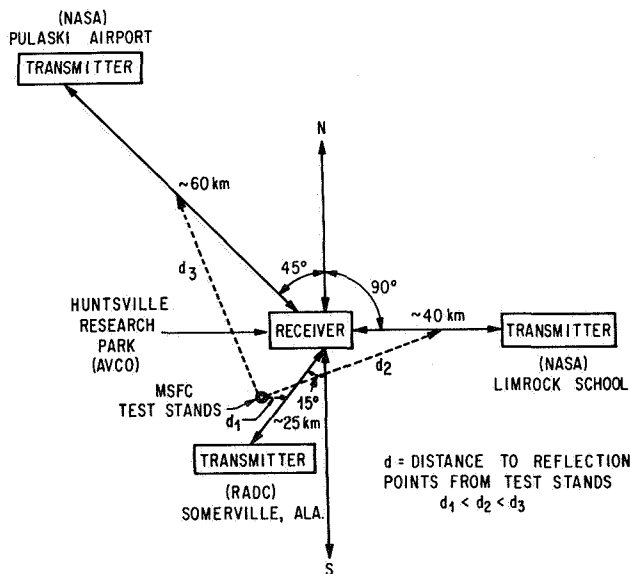


FIGURE 1. PHASE-PATH SOUNDER SITE ARRANGEMENT

The transmitter sites are equipped with Heathkit DX-60 A's modified with crystal-controlled oscillators, which provide ultra-stable frequency references to drive the transmitters. The six oscillators were purchased from Biley Mfg. Co. and cut to the following frequencies: 1998482 Hz, 2731992 Hz, 4080992 Hz, 5734992 Hz, 4759992 Hz, and 6184992 Hz. The site is also equipped with a microbarograph to measure pressure changes as low as 0.6 N/m^2 ($6 \mu\text{bars}$) with periods in the order of 0.1 min to 6.0 min. The microbarograph is composed mainly of a Sanborn differential gas pressure transducer and transducer converter insulated from the atmosphere except for the testing values [3] .

Figure 2 shows the antenna array at the Pulaski site. The towers are Rohn Mfg. Co. 22.9-m (75-ft) crank-up towers which support three inverted vee antennas. The guys for the antennas are polypropylene ropes to avoid interference with the antenna pattern. At one site, nylon rope was used by mistake and after the first large storm the towers were found lying on the ground with the guy ropes still tied.

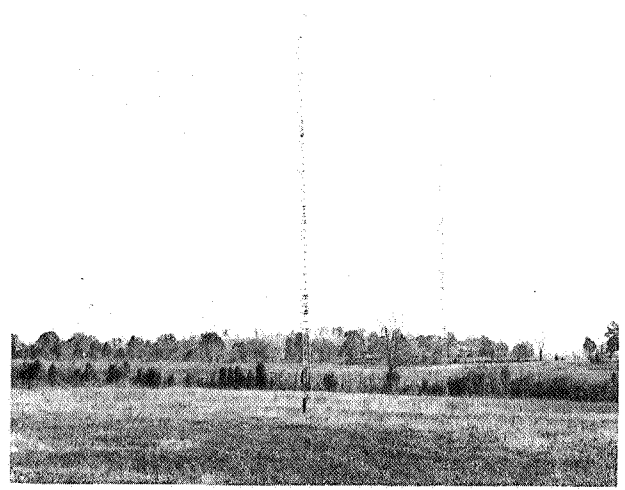


FIGURE 2. PULASKI, TENNESSEE SITE ANTENNA TOWERS

Figure 3 is a photo of the receiver site equipment. There are three SP-600JX receivers operating from a common 455 kHz local oscillator. Each receiver has its own crystal-controlled first-conversion oscillator at a frequency which places the received output at a nominal second IF center frequency of 90 Hz. Each receiver signal is recorded on a separate channel as are the 90 Hz reference output and a WWV timing signal. The tape recorder

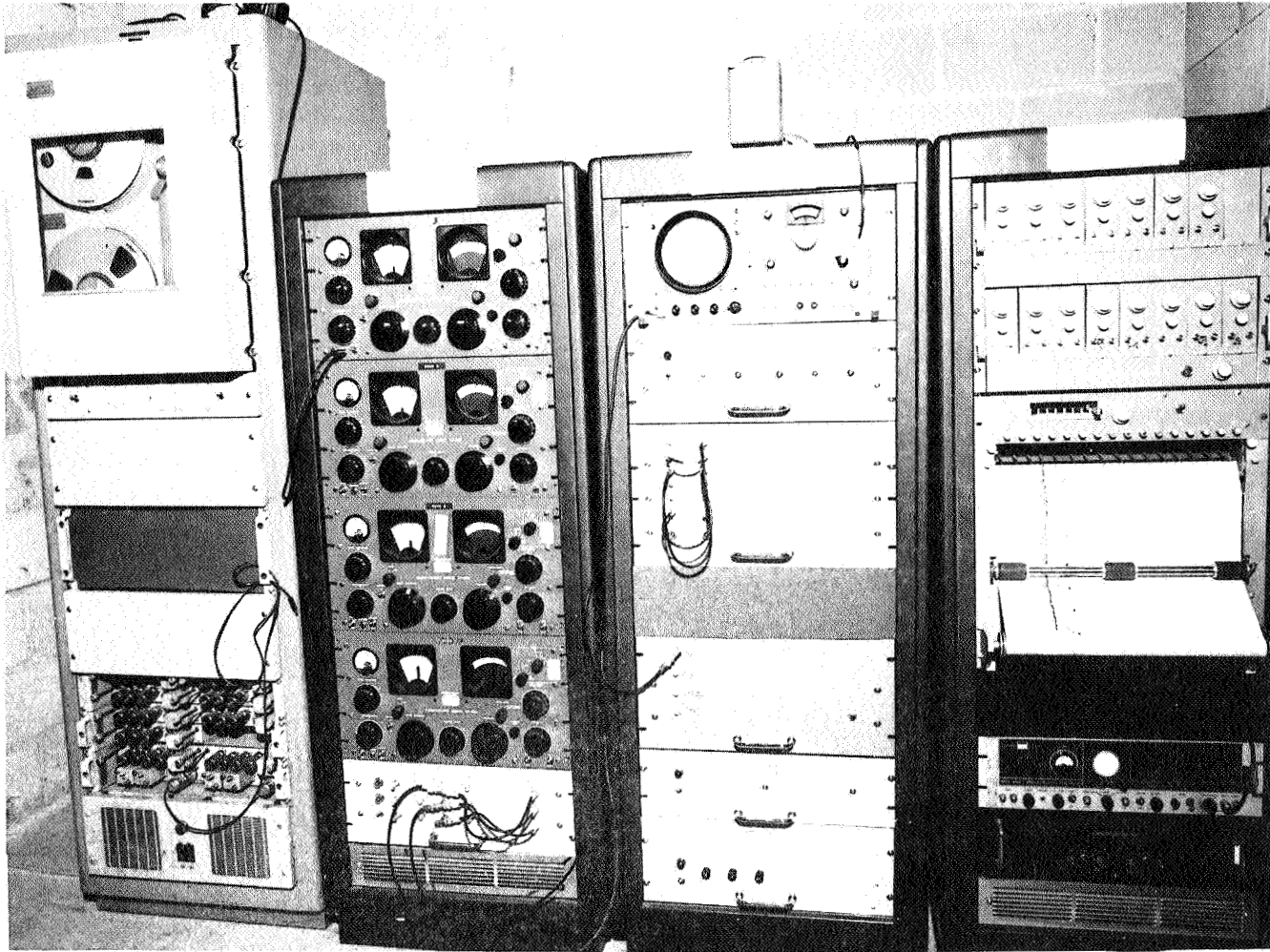


FIGURE 3. HUNTSVILLE RECEIVER SITE

is an Ampex FR-1107 operating at a speed of 2.38 cm/sec (15/16 in./sec). The later playback of the tape at 152 cm/sec (60 in./sec) when coupled with the 90 Hz output will place the recorded data in the frequency range of the Rayspan spectral analysis equipment. The 90 Hz reference signal will provide compensation for tape speed fluctuations or power source variations so that the phase variations observed may be assumed to be caused solely by ionospheric motions. The Rayspan spectral processing will filter any signal outside of ± 10 Hz of the center frequency. The center frequency for each oscillator is the frequency of the Somerville, Alabama, site and the other oscillators are cut to frequencies offset from ± 6 Hz to ± 8 Hz from this center frequency. As a result, one frequency from each site will fall within the ± 10 Hz bandwidth of the processed data.

Figure 4 is a diagram of a transmitter-receiver combination of the phase path sounder technique. Each site transmits three separate frequencies which reflect in the ionosphere at a point where

$$f = 9 \times 10^3 N^{1/2} . \quad (1)$$

In this equation, f is the transmitted frequency in Hertz and N is the electron density in electrons per cubic centimeter. Since three frequencies are being broadcast from each site, three points in the ionosphere are being monitored simultaneously, and if the reflection heights are known, the vertical velocity of wave passage may be determined.

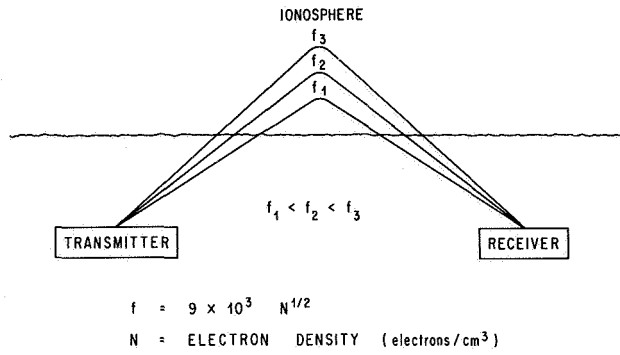


FIGURE 4. IONOSPHERIC REFLECTION OF TRANSMITTED WAVES

Figure 5 is a photograph of the MSFC model C-4 swept-frequency ionosonde. This equipment is operated in conjunction with the program to provide information on the height of signal reflections and for the detection of slow but large vertical ionospheric motions that might be beyond the resolution of the phase path sounders.

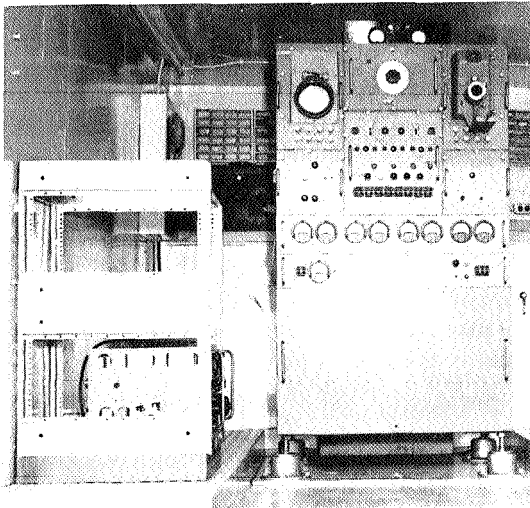


FIGURE 5. MSFC SWEPT-FREQUENCY IONOSONDE

The inclusion of the term "gravity" in acoustic gravity wave is somewhat unfortunate. An acoustic wave is simply a pressure wave which propagates outward when some resonant source becomes activated, and is normally damped out by the effects of atmospheric density. An acoustic gravity wave is this same type of wave traveling upward so that

gravity acts as a restoring force on the atmospheric particles in the pressure wave.

Figure 6 shows a record obtained following the S-IVB static test firing made on April 20, 1967. During this test only one site was operational so that only one frequency, 6.185 MHz, was recorded. The static test firing began at 1300 Central Standard Time and was 40 sec in duration. The slow, smooth, Doppler gradient observed from about 1300 to 1308 indicates the background motion of the ionosphere.

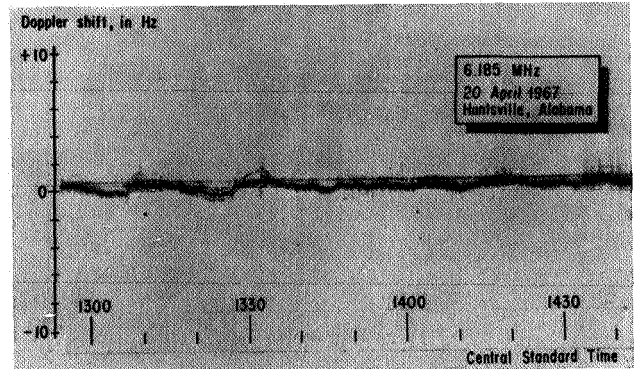


FIGURE 6. RECORD OF PASSAGE OF ACOUSTIC-GRAVITY WAVE

(Interestingly enough, this same motion has been subsequently observed at the time that ignition took place, and in one instance about 30 sec before.) Theoretically, the propagation time to the ionosphere should be on the order of 8 min, and at 1308 CST, a decisive change occurred in the record trend. There was a shift in the positive direction of about 1/2 cycle and a subsequent wave dispersion that may have been the reflection of the transmitted signal from the wavefront. The signal then stabilized, and subsequently, the ionosphere resumed a gradient similar to that observed before the wavefront passage. At about 22 min after the first wavefront passage, there was another rather large shift very similar to the first. It appeared that some resonant effect was taking place, although no satisfactory explanation for this currently exists, and the result is thus considered to be coincidental. This was the first recorded measurement in which the effects of static test firings on the ionosphere are shown.

Work is now underway on the theoretical mechanisms of propagation and coupling. To theoretically predict the magnitude of the wave at ionospheric height, its velocity, frequency range, etc., the effects of winds, temperature profiles and gradients, viscosity, and collision frequency must be considered.

Figure 7 depicts two effects that limit the frequency ranges that may propagate to ionospheric heights. The lower frequency range is limited by the acoustic cutoff frequency, w_a , where

$$w_a = \frac{a}{2H} = \frac{\gamma g}{2a} \quad (2)$$

Here a is the sound speed, H is the scale height, g is the acceleration due to gravity, and γ is the ratio of specific heats. The acoustic cutoff frequency results from atmospheric density stratification.

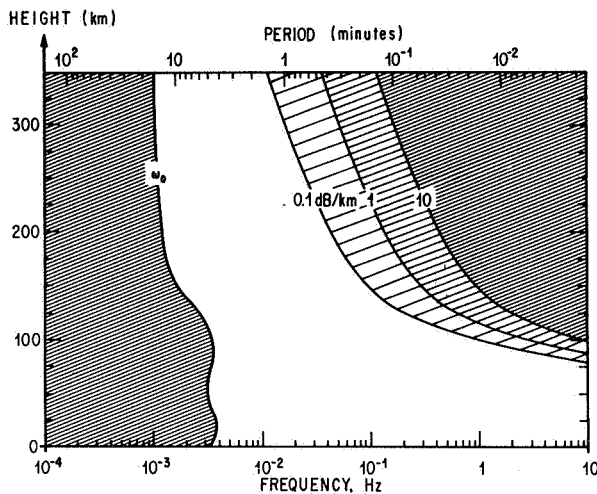


FIGURE 7. THE FREQUENCY RANGE OF ACOUSTIC WAVES THAT CAN EXIST IN THE ATMOSPHERE (LIGHT AREA) CONSIDERING THE LIMITATIONS IMPOSED BY ABSORPTION AND ACOUSTIC CUTOFF [6]

Based on the formulas used in atmospheric attenuation, and by calculating the "time constant" for the elasticity of air, the frequency can be calculated for which a given attenuation occurs.

By using the classical analogy of elasticity and inertia in the mass-spring system, a characteristic time constant, τ , may be calculated by

$$\tau = \frac{\mu}{\rho_0 a^2} \quad (3)$$

where μ is the coefficient of viscosity, ρ_0 is the gas density, and a is the speed of sound. According to Lord Rayleigh [4], the amplitude attenuation coefficient, α , for sound waves is

$$\alpha = \frac{8 \pi^2 N}{3 \lambda^2 a} \quad (4)$$

where N is the kinematic viscosity, $N = \mu/\rho_0$, and λ is the wavelength of the sound wave. Sears [5] put this in a more usable form,

$$\alpha = \frac{8 \pi^2 f^2}{3 a \gamma V} \quad (5)$$

where f is the sound wave frequency, γ is the ratio of specific heats (assumed to be constant at 1.4), and V is the molecular collision frequency. Thus,

$$f = 2.5 \times 10^{-3} (Va)^{1/2} \quad (6)$$

and since V and a may be derived from atmospheric models, f may likewise be determined as a function of altitude.

Figure 7 shows the rates of attenuation of 0.1 dB/km, 1 dB/km, and 10 dB/km. According to this graph, a wave whose period lies between 1.4 min and 4 min may freely propagate to a height of 350 km. Although they are neglected here, the effects of defocusing and reflection of the wave must be considered in the construction of a realistic model.

FUTURE PLANS

Data are now being taken to further identify ionospheric effects of ground-based acoustic energy sources. The problem of deriving a ray-tracing program for the propagation of these waves considering realistic model atmospheres is now being studied.

The coupling mechanisms are also being developed so that the experimental data may be thoroughly analyzed.

REFERENCES

1. Pierce, A. D.; and Coroniti, S. C.: A Suggested Mechanism for the Generation of Acoustic-Gravity Waves During Thunderstorm Formation. *Nature*, vol. 210, June 18, 1966, p. 1209.
2. Felker, J. K.; and Roberts, W. T.: Ionospheric Rarefaction Following Rocket Transit. *Journal of Geophysical Research*, vol. 71, no. 19, October 1, 1966, p. 4692.
3. Claerhart, J. F.; and Madden, T. R.: Initial Observations of 2-20 Minute Period Atmospheric Pressure Variations. 47th Annual Meeting of the AGU, *Transactions*, vol. 47, no. 1, March 1966.
4. Reyleigh, Lord (J. W. Strutt): *Theory of Sound*. McMillan and Co. Ltd., London, 1894.
5. Sears, F. W.: *Thermodynamics*. Addison-Wesley, Reading, Massachusetts, 1950.
6. Georges, T. M.: Private Communication, 1967.

THE MASSES OF METEORS AND THE SELECTION OF A REPRESENTATIVE DATA SAMPLE

By

Charles C. Dalton

SUMMARY

The mass of the particle of design interest for protection against meteoroid puncture of large vehicles with long missions in space is relatively nearly equal to that of a typical photographic meteor particle. But the usefulness of the photographic meteor data for this design interest has been beclouded by markedly different physical theory for the determination of the mass of the particle from the photographic data. A method is presented by which it is expected that a choice can be made when considering the relative plausibility of the alternative statistical results from an analysis of two samples of photographic meteor data selected according to the respective extrapolations of absolute photographic magnitude to low velocity.

LIST OF SYMBOLS

A total square meters of surface area of a space vehicle exposed to meteoroids

C_t target en-mass longitudinal sonic velocity, km/sec

e base of natural logarithms

I_{pm} maximum photographic luminous intensity

k_t target material parameter

log common logarithm, base ten

m meteoroid mass in grams

m_∞ "Harvard mass" elevation for m

M "Öpik mass" evaluation for meteoroid mass m

M_{pg} maximum absolute photographic magnitude

M_{pg0} value of M_{pg} extrapolated to correspond with 11 km/sec for V_∞

p target sheet thickness in centimeters

R probability of vehicle not encountering a meteoroid larger than m grams

t exposure duration in seconds

V_∞ meteor air-entry velocity in km/sec

Z_R zenith-to-radiant angular displacement

β meteor luminous efficiency; ratio of $\int_0^T I_{pm} dT$ and $\frac{1}{2} m V_\infty^2$

β_{11} value of β extrapolated to correspond with 11 km/sec for V_∞

Δ meteor magnitude-above-plate limit

Δ_0 value of Δ extrapolated for (V_∞, Z_R) = (11 km/sec, 60 degrees)

- ϵ_t target ductility, relative elongation
- ζ relative effective exposability of total surface area
- ρ_t target specific gravity

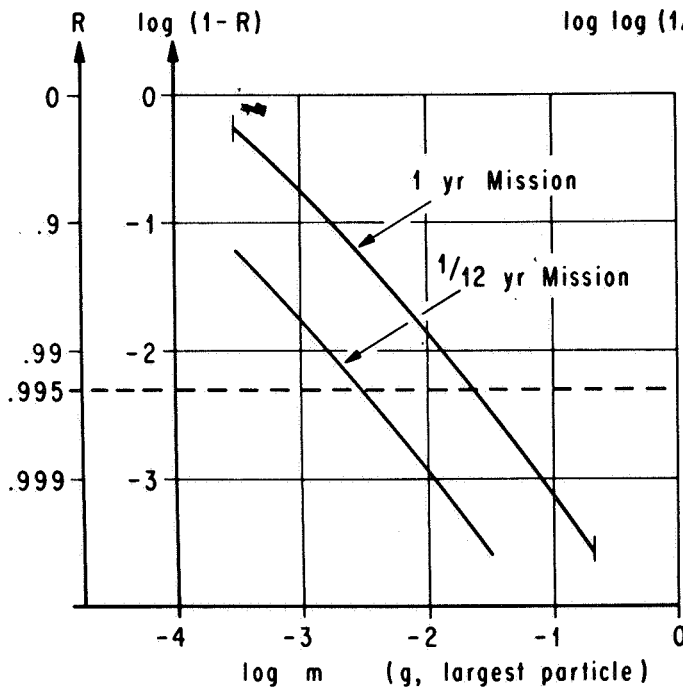
INTRODUCTION

Here at the NASA-Marshall Space Flight Center (MSFC) the interest in photographic meteors relates primarily to the puncture hazard of large vehicles exposed for long missions in space. An example of such interest is illustrated in Figure 1, which shows mission duration contours for the probability, R, that the S-IVB Orbital Workshop will not encounter a meteoroid with mass larger than m grams. Thus, when the probability of no meteoroid puncture during a 1-year mission of the Orbital Workshop must be as high as 0.995, then the vehicle must be protected against the impact of particles as large as about $10^{-1.6}$ grams. The formula (for the mission duration contours) in Figure 1, showing $\log \log (1/R)$ as a polynomial function of the independent variable $[0.24 + (19/54) \log m]$, is based on a model which

was first constructed by Dalton [1] in 1966 by extrapolation both of laboratory hypervelocity impact data from the NASA-Ames Research Center and of satellite puncture and photographic meteor data. Some refinements in the model were also presented by Dalton [2] in 1967. By this model, the independent variable $[0.24 + (19/54) \log m]$, mentioned above, is equal to the abscissa $(k_t + \log_p)$ of Figure 2. Thus, in Figure 2, the photographic meteor and thickest Pegasus target tie points correspond to just-sufficient-mass meteoroids of $10^{-0.66}$ and 10^{-6} grams, respectively. The particle mass of interest in the example from Figure 1, $10^{-1.6}$ grams, is then relatively closer to the mass of a typical photographic meteor particle. This example illustrates the primary practical basis for the interests in photographic meteors at MSFC.

DATA SAMPLES OF METEORS

In the puncture hazard model illustrated in Figures 1 and 2, the thickness of a sheet of a given material which can be punctured by a meteoroid is proportional to the product of the cube root of the



$$\log \log (1/R) = \log (\zeta A t \log e) - 13.03 - 3.81 [0.24 + (19/54) \log m] - 0.384 [0.24 + (19/54) \log m]^2 - 0.017 [0.24 + (19/54) \log m]^3$$

- ζ = Effective Exposability of Total Surface Area
= .663 at 482 km (260 n mi) Altitude
- A = Total Surface Area (m^2)
= 141.5 m^2 for Orbital Workshop
- t = Exposure time (sec)
= 3.15×10^7 sec for 1 year

FIGURE 1. PROBABILITY OF NOT ENCOUNTERING LARGER METEORIODS

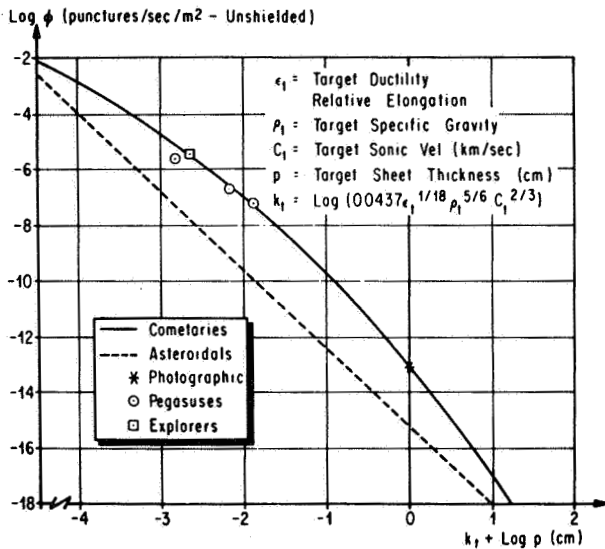


FIGURE 2. MEAN PUNCTURE FLUX FROM METEOROID INFLUX

kinetic energy and the $(1/54)$ -power of the mass of the particle. The velocities of the photographic meteor particles are known sufficiently accurately so that the uncertainty in the mass values is caused primarily by the uncertainty in the kinetic energy values. The kinetic energy is not directly ascertainable, but must be inferred from the integrated meteor trail intensity in consideration of a physical theory of meteors functionally relating the meteor luminous efficiency with initial mass and velocity. The luminous efficiency is the mean relative part of the rate of loss of kinetic energy of the particle which is accountable in the luminous intensity of the meteor.

To abbreviate notation in this discussion, one can refer to the "small sample" as the 285 sporadic meteors of known maximum absolute photographic magnitude in the random sample published by Hawkins and Southworth [3] in 1958. Some of the results which will be used for these meteors were published also by Hawkins and Southworth [4] in 1961. Also, let the "large sample" be the 2040 sporadic meteors of known maximum absolute photographic magnitude in the sample of 2529 meteors published by McCrosky and Posen [5] in 1961. In calculating the meteor mass values, which they published for the "large sample," McCrosky and Posen [5] used Whipple's [6] formulation for luminous efficiency as $10^{-4.07}$ times the air-entry velocity in kilometers per second, independently of mass, similarly as Hawkins and Southworth [4] did for the "small sample," and

stated that "the masses are therefore on the same scale as others published by the Harvard Meteor Project." This formulation or the corresponding mass values will be represented here by "Harvard luminous efficiency" or "Harvard mass" values. Although some of the earlier papers of E. J. Öpik, some of them dating as far back as 1922, were referenced by Whipple [6], who said that his luminous efficiency "has been taken from the calculations by Öpik," the "Öpik luminous efficiency" and "Öpik mass" will refer here to the more recent physical theory as given by Öpik [7] in 1958 and as further illustrated numerically by Öpik [8] in 1963. The "Öpik luminous efficiency," unlike the "Harvard luminous efficiency," is a nonlinear function of velocity and is not independent of mass.

Figure 3 shows, for the "small sample," the distribution of the most obvious parameters; i. e., velocity and absolute photographic magnitude, M_{pg} , which is a linear function of the logarithm of the maximum luminous flux adjusted for a 100-km height overhead. Actually the time integral of luminous intensity is of more interest in the determination of the mass because it is relative to the product of luminous efficiency and mass. Although it is considered a random sample of sporadic (i. e., non-stream) meteors, neither the "large sample" nor the "small sample" illustrated in Figure 3 constitutes a random sample of the sporadic meteoroids which enter the earth's atmosphere, because some of the entering particles with mass considerably above some lower value are not detected as meteors at low velocity and high zenith angle, whereas particles of intermediate mass may be detected as meteors if they have higher velocity or if their radiants are nearer the zenith. Thus, the sample of particles in a random sample of sporadic meteors is biased by physical selectivity. This bias can be counteracted in either the "large sample" or the "small sample" if an appropriate statistical weighting function can be found, but the choice is not obvious and may be difficult to justify.

The authors of the reports from which both the "small sample" and the "large sample" were taken tabulated values for Whipple's [9] statistical "cosmic weight" inversely proportional to the product of Öpik's [10] earth-encounter probability and the square of the air-entry velocity. In 1965 Dalton [11] reported an analysis of the "small sample" with statistical weighting inversely proportional to the product of the 1.5-power of the velocity and the square of the height at maximum brilliance, with some

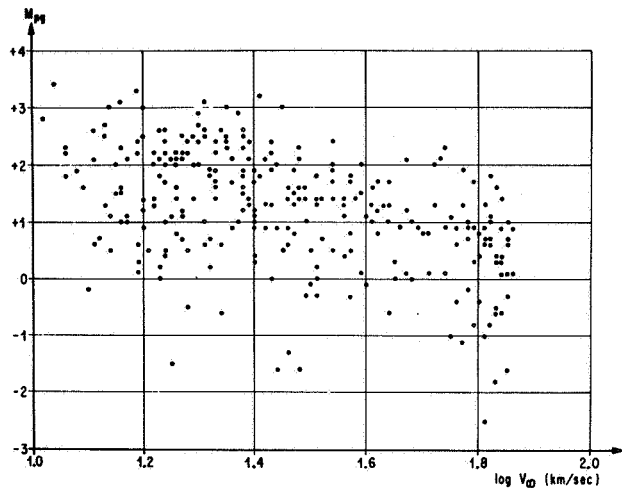


FIGURE 3. METEOR VELOCITY VERSUS ABSOLUTE PHOTOGRAPHIC MAGNITUDE

further weighting to restore symmetry with respect to the ecliptic plane. Whipple [9] had considered that weighting inversely with the square of the height should be nearly equivalent to weighting inversely with the 0.5-power of the velocity, which was the justification for Dalton's weighting [11]. But the weighted correlation between the logarithms of the air-entry velocity and the "Harvard mass" was computed as -0.69 , which is arithmetically much higher than one would expect. Suspecting the statistical weighting as a function of velocity, Dalton [12] later replaced it with Upton's and Hawkins' [13] weighting as a function of the meteor magnitude above the limit of the photographic plate [this function was intended to represent the relative detectability of the meteor]. The weighted correlation between the logarithms of velocity and "Harvard mass" was computed as -0.83 , which was arithmetically higher and less plausible than the corresponding result with the weighting as a function of velocity. These results are illustrated in Figure 4 by partitioning the sample with respect to "Harvard mass" into two subsamples of equal statistical weight and showing the velocity distribution for each superimposed. Suspecting the velocity dependence of the "Harvard luminous efficiency," Dalton [14] improvised a formula, involving velocity and maximum absolute photographic magnitude, for roughly approximating mass values proportional to "Öpik mass" values. Here this formula was applied to the "small sample," the correlation between the logarithms of mass and velocity was computed as 0.024 with uniform weighting

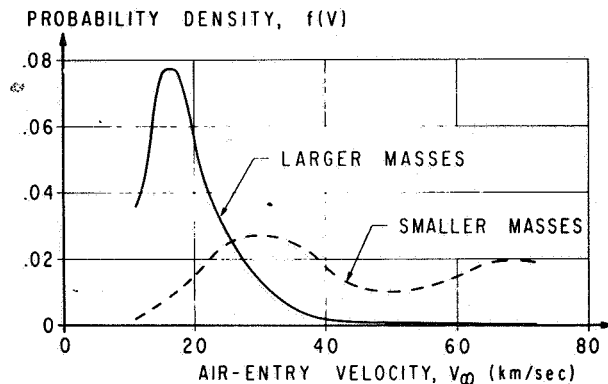


FIGURE 4. WEIGHTED DISTRIBUTION OF VELOCITY FOR HARVARD-MASS REGIMES

[14], and as 0.010 [14] and -0.11 [12] with the two respective weighting functions mentioned above. Either of these correlations is arithmetically small enough for physical plausibility, but they are accompanied by a complication. Dalton [11] showed that the slope of the logarithm of the weighted cumulative distribution plotted versus the logarithm of the parameter of interest should be invariant with respect to any parameter which is the product of mass and any power of velocity, provided that mass and velocity are statistically independent. But, with either of the weighting functions, Dalton [15] found that the recomputed mass values gave slopes of -1.34 , -1.09 , and -0.92 for mass, momentum, and kinetic energy, respectively. On the other hand, the "Harvard mass" values satisfy a -1.34 slope invariantly even though, with such a strong inverse correlation, it would not be expected.

It must be concluded, then, (1) that the "small sample" is too small for analysis with statistical weighting to remove the bias between mass and velocity resulting from physical selectivity, (2) that "Öpik mass" should be computed from the integrated meteor intensity instead of from the maximum absolute photographic magnitude, and (3) that the statistical weighting effort must be minimized by selecting a subsample of meteors from the "large sample" bright enough to have been detected even if they would have had only the 11 km/sec "escape" velocity. Some further analysis with the "small sample," shown in Figures 5 and 6, has been helpful in establishing criteria for selecting subsamples from the "large sample" which are compatible with the respective formulations for luminous efficiency presupposed.

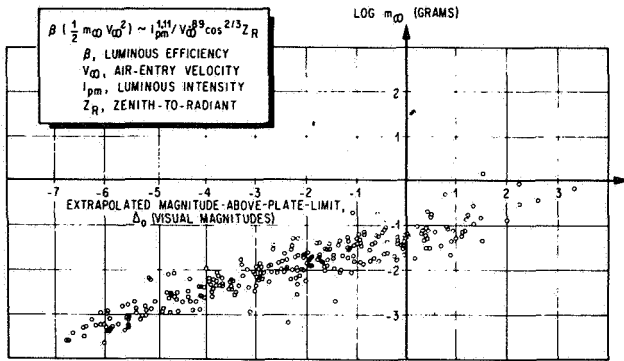


FIGURE 5. RELATION BETWEEN HARVARD METEOR MASS AND MAGNITUDE-ABOVE-PLATE-LIMIT EXTRAPOLATED FOR 60 DEGREES ZENITH-TO-RADIANT AND 11 km/sec PRESUPPOSING HARVARD LUMINOUS EFFICIENCY

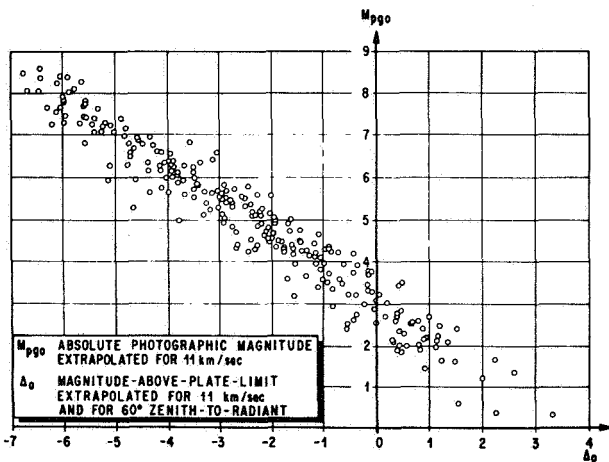


FIGURE 6. EXTRAPOLATED RELATIONS BETWEEN METEOR ABSOLUTE PHOTOGRAPHIC MAGNITUDE AND MAGNITUDE-ABOVE-PLATE-LIMIT PRESUPPOSING HARVARD LUMINOUS EFFICIENCY

An empirical relation for meteors by Jacchia, Verniani, and Briggs [16] indicates that the integrated photographic intensity, and therefore also the product of luminous efficiency and kinetic energy, should be proportional to

$$I_{pm}^{1.11} / V_{\infty}^{0.89} \cos^{2/3} Z_R,$$

where I_{pm} is the maximum photographic luminous intensity and Z_R is the zenith-to-radiant deviation.

If the same particle had entered at 11 km/sec and a 60 degree zenith-to-radiant, then the absolute photographic magnitude and magnitude-above-plate limit would have been, by designation, M_{pgo} instead of M_{pg} , and Δ_o instead of Δ , respectively. Then

$$M_{pgo} = M_{pg} + \frac{(5/2)}{1.11} \log (\beta/\beta_{11}) (V_{\infty}/11)^{2.89} \quad (1)$$

$$\Delta_o = \Delta - \frac{(5/2)}{1.11} \log (\beta/\beta_{11}) (V_{\infty}/11)^{2.89} \left(\frac{\cos Z_R}{\cos 60^\circ} \right)^{2/3}, \quad (2)$$

where the luminous efficiency, β , would have the value β_{11} at 11 km/sec.

Values for the magnitude-above-plate limit, Δ , are not available for the "large sample"; but the values of Δ_o computed for the "small sample" by eq. (2) are shown in Figures 5 and 6 versus "Harvard mass", m_o , in Figure 5 and the corresponding values of M_{pgo} in Figure 6, extrapolated for M_{pg} by substituting the "Harvard luminous efficiency" for β in eq. (1). The mean resultant linear fit for Figure 6 is not so shallow as in Figure 5 and gives a somewhat sharper relation (because mass values are computed from the time integral of intensity rather than from the maximum value); i. e.,

$$M_{pgo} = 3.0 - \Delta_o \quad (3)$$

Then by eqs. (1) and (3), the criterion for selecting the subsamples from the "large sample" is

$$M_{pg} + \Delta_o \leq 3.0 - (2.5/1.11) \log (\beta/\beta_{11}) (V_{\infty}/11)^{2.89}, \quad (4)$$

where the ratio of the luminous intensity values, β/β_{11} , depends upon the physical theory which is presupposed. This criterion, giving $V_{\infty}/11$ for β/β_{11} with the "Harvard luminous efficiency" for β , is illustrated in Figure 7.

In order to select a subsample as large as 333, from the "large sample" of 2040 sporadic meteors, it was necessary to choose Δ_o as low as 0.7 when

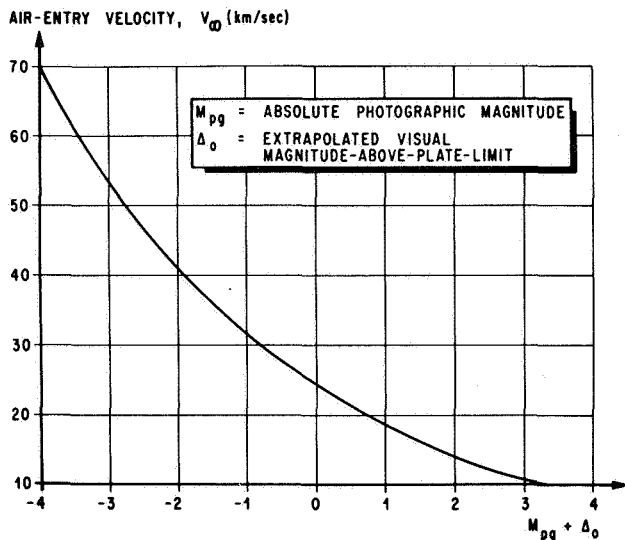


FIGURE 7. MEAN RELATION BETWEEN METEOR VELOCITY, ABSOLUTE PHOTOGRAPHIC MAGNITUDE, AND MAGNITUDE-ABOVE-PLATE-LIMIT EXTRAPOLATED FOR 60 DEGREES ZENITH-TO-RADIANT AND 11 km/sec PRESUPPOSING HARVARD LUMINOUS EFFICIENCY

the "Harvard luminous efficiency" was substituted for β in eq. (4). By Upton and Hawkin's [13] graphical relation for meteor relative visibility as a function of the magnitude-above-plate limit, Δ , meteors barely satisfying this criterion would have a probability of detection on the photographic plates increasing from about 0.20 at a 60 degree zenith-to-radiant, to about 0.60 at the zenith. It may be of some interest to note that only one of these 333 meteors, which could be selected with "Harvard luminous efficiency," β , had a velocity $V_\infty \cong 32$ km/sec; whereas the (uniformly weighted) average velocity for the (random) "small sample" is 34 km/sec (Dalton [2]). The median value of the "Harvard mass," m_∞ , for this subsample is 0.110 gram.

The physical theory of meteors given by Öpik [7] in 1958 seems most suitable for calculating the mean luminous efficiency, β , and consequent integrated intensity for a particle of given structure and mass entering the atmosphere at a given angle and velocity. The integrated intensity, which is equal to the product of the kinetic energy and mean luminous efficiency, was used in the computation for the "large sample" tabulated values for "Harvard mass," m_∞ , for dividing by the "Harvard luminous efficiency" $10^{-4.07} V_\infty$. Therefore, the problem at hand is to

compute the mean "Öpik luminous efficiency," β , for a known integrated intensity and unknown mass, instead of for a known mass and unknown integrated intensity. The air-entry "Öpik mass," M , is found subsequently by dividing the known product $M\beta$, by the mean "Öpik luminous efficiency" β . In 1963 Öpik [8] gave three tables of values for the application of his physical theory [7] to stone dustballs, compact iron meteoroids, and compact stony meteoroids. Some of these values are illustrated in Figure 8 to show fixed "Öpik mass" contours for the velocity dependence of the mean "Öpik luminous efficiency," β , for dustball meteors. It may be of interest to note that although at above average velocity, the "Öpik luminous efficiency," β , in Figure 8 is a decreasing function of velocity, V_∞ , the product of luminous efficiency and kinetic energy, $\beta \left(\frac{1}{2} M V_\infty^2 \right)$, and therefore also the integrated intensity, is an increasing function of velocity.

Concerning the structure of meteoroids, the current practice for design criteria purposes at MSFC is to consider that the distribution of compact meteoroids within the photographic meteor range corresponds to Parkinson's [17] extrapolation of Hawkins' [18] results for air-entry mass cumulative influx adjusted from stone and iron meteorite statistics. The results, as can be seen in Figure 2, are that about one percent of the photographic meteors may be compact particles of asteroidal origin, and the remaining 99 percent are stone dustballs with a mean body density only about ten percent as high as that for compact meteoritic stone. Jacchia, Verniani, and Briggs' [16] results are of interest on this point too. The 413 photographic meteors which they selected for study gave an average specific gravity of only 0.26, and only one of them was found to possess all the requisites to qualify as being of asteroidal origin. Therefore, in the absence of specific information which might suggest which of the meteors in the "large sample" belong to the three structural types in Öpik's [8] tables, they will all be presupposed as dustballs. Also the "Öpik luminous efficiency" will be approximated from a mathematical model which will now be constructed in consideration of Öpik's [8] 24 values for dustball meteoroids illustrated as specific points in Figure 9.

The mathematical model illustrated in Figure 9 has linear relations between the repeated logarithms of the reciprocals of β and $M\beta$ for the dependent and independent variables, respectively, with slope, intercept, and break-point depending on velocity, V_∞ , as an auxiliary independent variable as illustrated in Figures 10 through 12, respectively. The model

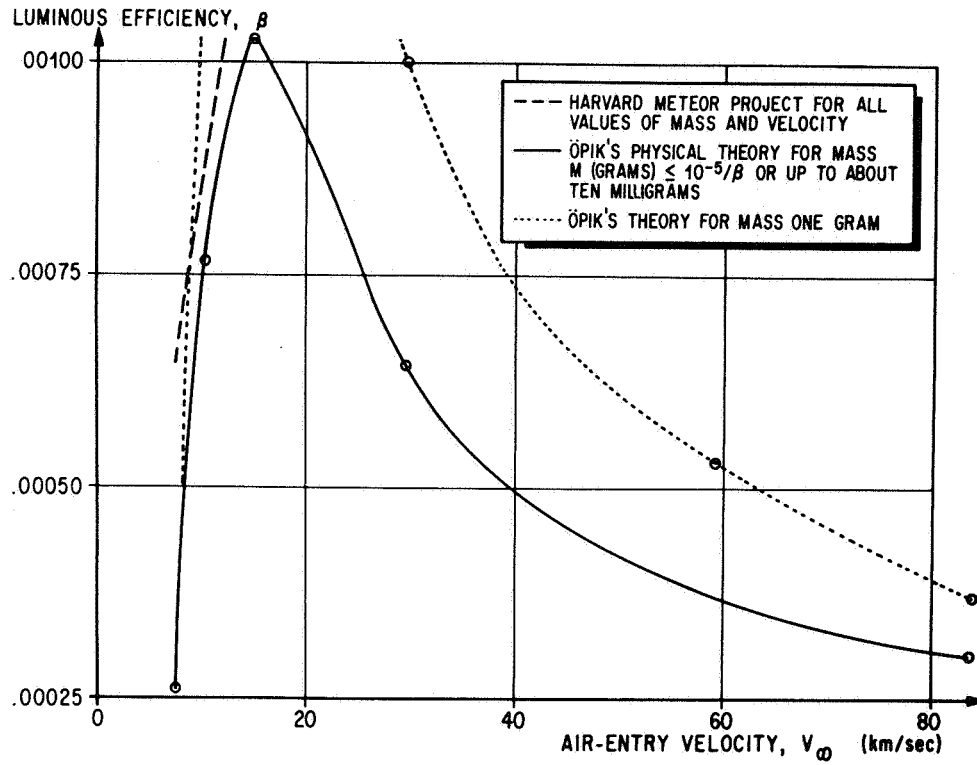


FIGURE 8. LUMINOUS EFFICIENCY VERSUS VELOCITY FOR DUSTBALL METEORS

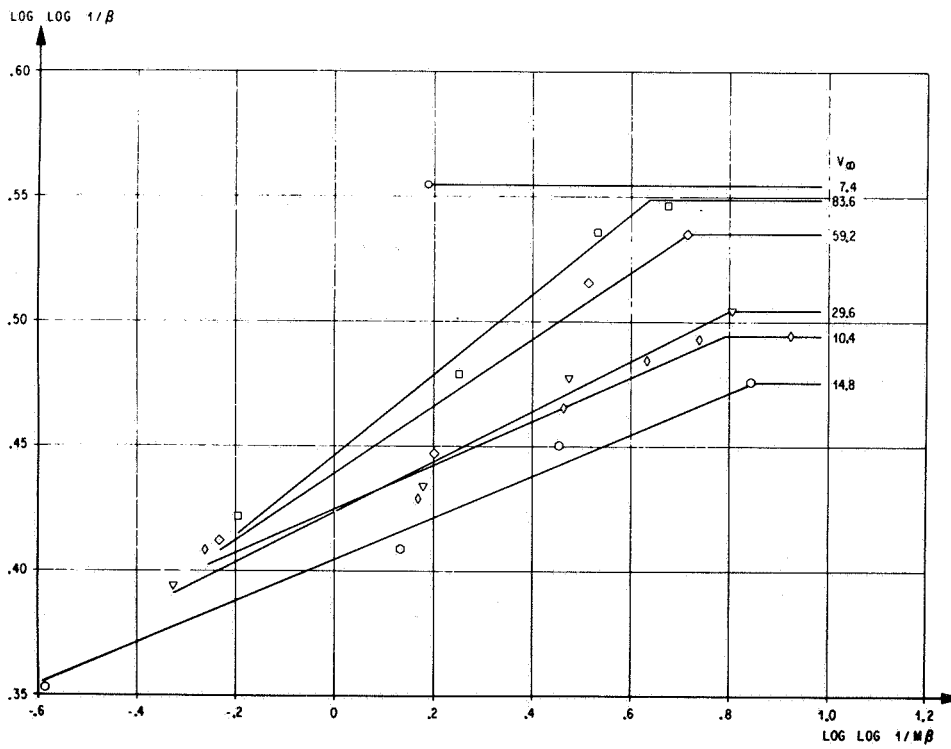


FIGURE 9. MODEL APPROXIMATING ÖPIK'S LUMINOUS EFFICIENCY FOR DUSTBALL METEOROIDS SMALLER THAN ONE HUNDRED GRAMS

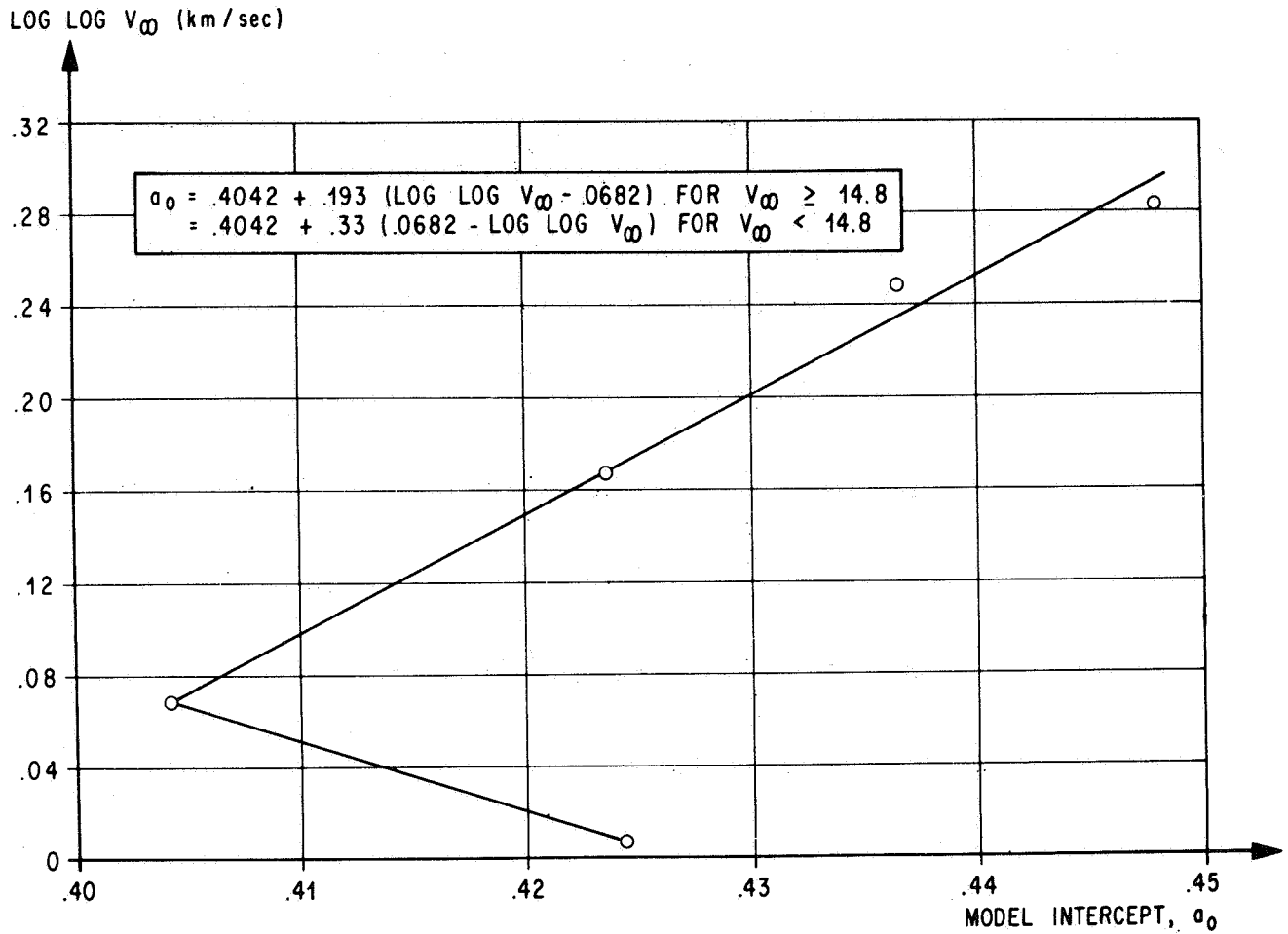


FIGURE 10. VELOCITY-DEPENDENCE OF THE INTERCEPT FOR THE MODEL IN FIGURE 9

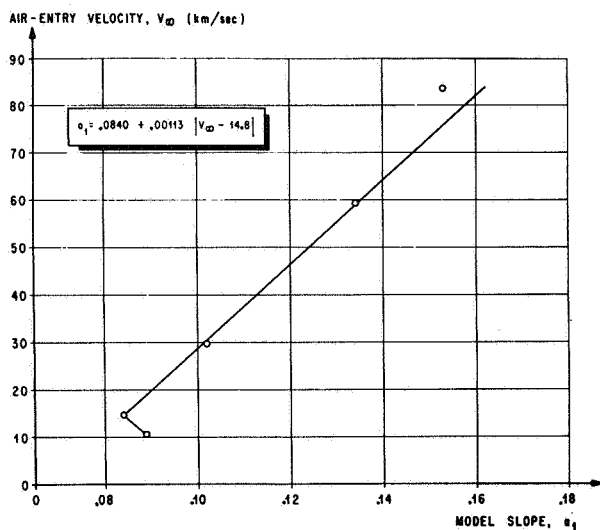


FIGURE 11. VELOCITY-DEPENDENCE OF THE SLOPE FOR THE MODEL IN FIGURE 9

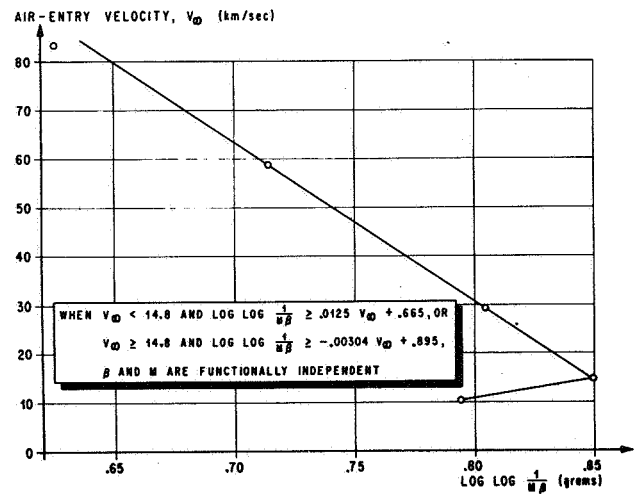


FIGURE 12. CRITERION FOR THE RIGHT-HAND DISCONTINUITY IN FIGURE 9: LUMINOUS EFFICIENCY INDEPENDENT OF MASS FOR SMALLER METEOROIDS

was constructed independently of the values given for velocity 7.4 km/sec. The highest specific points on each of the other five velocity contours were given as limiting values in the sense as indicated. Those limiting points were ignored in the least squares preliminary velocity contour fittings. The intercepts, slopes, and break-points for the respective least squares preliminary velocity contour fittings are shown as specific points in Figures 10 through 12, respectively. The plotted specific points in Figures 10 through 12 were used as visual aids for the construction of the indicated linear segments, the equations for which constitute the model represented by the line segments in Figure 9.

For computational purposes the model illustrated in Figure 9 is described as follows: β and M are functionally independent when either

$$V_{\infty} < 14.8 \text{ and } \log \log 1/M \beta \geq 0.0125 V_{\infty} + 0.665$$

or

$$V_{\infty} \geq 14.8 \text{ and } \log \log 1/M \beta \geq -0.00304 V_{\infty} + 0.895;$$

otherwise,

$$\log \log 1/\beta = a_0 + a_1 \log \log 1/M \beta$$

where

$$a_0 = 0.4042 + 0.193 (\log \log V_{\infty} - 0.0682) \text{ for } V_{\infty} \geq 14.8$$

$$= 0.4042 + 0.33 (0.0682 - \log \log V_{\infty}) \text{ for } V_{\infty} < 14.8$$

and

$$a_1 = 0.0840 + 0.00113 |V_{\infty} - 14.8|.$$

This model has a maximum deviation from the "Öpik values," as shown by the next to the lowest point for the 59.2 km/sec contour in Figure 9, of 33 percent too high for β or too low for M , which would result in a value of 12 instead of 16 grams for the value of M for that particular point.

The model approximation for the "Öpik mass" M is found by dividing $M\beta$ by the model approximation for the "Öpik luminous efficiency," β . The role of the product $M\beta$ in the model follows from the fact that the product of luminous efficiency and kinetic energy, and therefore also the product of luminous efficiency and mass, is invariant between different physical theories; i. e.,

$$M\beta = 10^{-4.07} m_{\infty} V_{\infty}, \quad (5)$$

where m_{∞} is the "Harvard mass" tabulated for the "large sample" and V_{∞} is the known velocity.

By eqs. (1) and (3) with the values for the "Öpik luminous efficiency," β , approximated by the model in the preceding paragraph, the values for the extrapolated magnitude-above-plate limit, Δ_0 , corresponding to 11 km/sec and 60 degree zenith-to-radiant, were calculated for the "large sample" of 2040 sporadic meteors and ranked. In order to select a subsample the same size as was selected with the "Harvard luminous efficiency," 333 meteors with the largest values of Δ_0 , the limiting criterion for Δ_0 was 1.04.

By Upton and Hawkins' [13] relative detectability function, this minimum value of Δ_0 would correspond

nominally at 11 km/sec to a probability of detection on the photographic plates varying from about 0.44 for 60 degree zenith-to-radiant to about 0.83 at the zenith. Of the 59 meteors in this subsample which were not selected by the other criterion, there were 25 meteors with velocity $V_{\infty} \geq 32$ km/sec; whereas, of the 274

meteors common to both subsets only one of them is that fast. The median value of the model-approximated "Öpik mass," M , for this subsample is 0.138 gram.

Statistical analysis and comparison of the results for the two subsamples, each of 333 meteors selected from the "large sample," are being pursued currently here at MSFC. No more significant results are available at this time (28 September 1967); and one does not presume to know which of the alternative physical theories may be more nearly correct. But the distributions of and correlations between various dynamic and orbital parameters should be of most important interest for comparison of results correspondingly developed with the alternative subsamples.

It is not yet possible to anticipate whether or not the results might be such that one could discount one of the alternative formulations of luminous efficiency on grounds of obvious physical implausibility.

CONCLUSIONS

Two alternative formulations for meteor luminous efficiency, the model used by the Harvard Meteor Project since 1943 (see Whipple [6] and McCrosky and Posen [5]) independent of mass but proportional to velocity, and the 1958 formulation by Öpik [7] depending nonlinearly on both mass and velocity, are used as bases for selecting corresponding subsamples for statistical analysis. Each subsample consists of the 333 meteors, from McCrosky and Posen's [5] 2040 sporadic meteors of known magnitude, which would have been most easily detected if both velocity had been as low as 11 km/sec and zenith-to-radiant had been as high as 60 degrees. With the various known parameters, and with the mass values consequent to each of the two formulations for luminous efficiency, the subsamples are thought to constitute a pertinent basis for comparative statistical analysis which might facilitate a resolution of alternatives on grounds of physical plausibility.

REFERENCES

1. Dalton, C. C.: Effects of Recent NASA-ARC Hypervelocity Impact Results on Meteoroid Flux and Puncture Models. NASA TM X-53512, September 7, 1966.
2. Dalton, C. C.: Near Earth and Interplanetary Meteoroid Flux and Puncture Models. Paper NO. EN-14, American Astronautical Society 1967 National Symposium "Saturn V/Apollo and Beyond," Huntsville, Alabama, 11-14 June, 1967, vol. I, pp. AAS 67-334 (EN-14-1) through AAS 67-334 (EN-14-21).
3. Hawkins, G. S.; and Southworth, R. B.: The Statistics of Meteors in the Earth's Atmosphere. Smithsonian Contributions to Astrophysics, vol. 2, no. 11, Smithsonian Institution, Washington, D. C., 1958, pp. 349-364.
4. Hawkins, G. S.; and Southworth, R. B.: Orbital Elements of Meteors. Smithsonian Contributions to Astrophysics, vol. 4, no. 3, Smithsonian Institution, Washington, D. C., 1961, pp. 85-95.
5. McCrosky, R. E.; and Posen, A.: Orbital Elements of Photographic Meteors. Smithsonian Contributions to Astrophysics, vol. 4, no. 2, Smithsonian Institution, Washington, D. C., 1961, pp. 15-84.
6. Whipple, F. L.: Meteors and the Earth's Upper Atmosphere. Reviews of Modern Physics, vol. 15, no. 4, October 1943, pp. 246-264.
7. Öpik, E. J.: Physics of Meteor Flight in the Atmosphere. Interscience Publishers, Inc., New York, 1958.
8. Öpik, E. J.: Tables of Meteor Luminosities. The Irish Astronomical Journal, vol. 6, no. 1, March 1963, pp. 3-11.
9. Whipple, F. L.: Photographic Meteor Orbits and their Distribution in Space. Astronomical Journal, vol. 59, number 6, No. 1218, July 1954, pp. 201-217.
10. Öpik, E. J.: Collision Probabilities with the Planets and the Distribution of Interplanetary Matter. Proceedings, Royal Irish Academy, vol. 54, Sec. A, 1951, pp. 165-199.
11. Dalton, C. C.: Statistical Analysis of Photographic Meteor Data, Part II; Verniani's Luminous Efficiency and Supplemented Whipple Weighting. NASA TM X-53360, November 18, 1965.
12. Dalton, C. C.: Velocity Dependence of Meteor Luminous Efficiency and Consequent Statistical Results. Appendix in "Effects of Recent NASA-ARC Hypervelocity Impact Results on Meteoroid Flux and Puncture Models." NASA TM X-53512, September 7, 1966, pp. 23-31.
13. Upton, E. K. L.; and Hawkins, G. S.: The Influx Rate of Meteors in the Earth's Atmosphere. Interim Report 24, Contract AF 19(122)-458, Sub-contract No. 57, October 1957.
14. Dalton, C. C.: Statistical Analysis of Photographic Meteor Data, Part I: "Öpik's Luminous Efficiency and Supplemented Whipple Weighting." NASA TM X-53325, September 2, 1965.
15. Dalton, C. C.: Inferences from Photographic Meteors. Proceedings of the Symposium "Meteor Orbits and Dust," Cambridge, 9-13 August 1965, Smithsonian Contributions to Astrophysics, vol. 11, pp. 81-90 (NASA Special Publication SP-135, SCA Vol. 11, 1967.)

16. Jacchia, L. G.; Verniani, F.; and Briggs, R. E.: An Analysis of the Atmospheric Trajectories of 413 Precisely Reduced Photographic Meteors. Special Report No. 175, Smithsonian Astrophysical Observatory, Cambridge, Mass., April 23, 1965.
17. Parkinson, J.: Space Environment Criteria. MSFC Contract NAS8-11285, Aerojet-General, presented 26 May 1965.
18. Hawkins, G. S.: Impacts on the Earth and Moon. Nature Magazine, vol. 197, no. 4869, 23 February 1963, pp. 781.



MARTIAN ATMOSPHERIC VARIABILITY

By

George S. West, Jr.

SUMMARY

This paper traces the background of Martian atmospheric model development and indicates why present MSFC models have been developed to overcome difficulties experienced with previous models and interpretations of available data. It also indicates future plans for acquiring observational data for improvement of the present models.

INTRODUCTION

Natural environmental criteria are essential to the design and mission planning of spacecraft used for planetary exploration, for example, the successful Mariner IV mission to Mars, and the planned Voyager missions to Mars in the 1970's [1].

Only the thermal aspects of the upper and lower atmosphere that affect orbital entry heating and orbital lifetime for vehicle design are discussed in this paper. These thermal aspects are determined from kinetic temperature, molecular temperature, atmospheric pressure, atmospheric density, molecular weight, density scale height, pressure scale height, number density, speed of sound, columnar mass, mean free path, and coefficient of viscosity. Surface and atmospheric winds are not treated in this paper.

For any planet, the establishment of environmental information must be considered an iterative process; the environmental parameters logically planned for measurement by a planetary probe are those required for the design and planning of a planetary mission in the first place. Mariner IV yielded

a wealth of new information on surface conditions, the atmosphere, the planetary magnetic field, and the planetary mass. From the data acquired, more realistic evaluations of the planetary environment of Mars have been extracted, thereby making possible the derivation of engineering and design parameters of a higher confidence level for use, for example, in orbital entry heating and orbital lifetime analyses for the Voyager missions to Mars contemplated for the 1970's.

In planning the Voyager program, for example, a very detailed estimate of the Martian atmosphere is required for the selection of an optimum orbit altitude for the science package that does not violate planetary quarantine restraints. In turn, each Voyager mission will provide data for more sophisticated and realistic criteria as each successive iteration narrows the range of values.

BASIS FOR DEVELOPMENT OF THE MSFC MODELS

In the initial development of the required environmental information, it was first necessary to consider what information was available. Prior to the Mariner IV occultation experiment in 1965, polarimetric and spectrophotometric observations of Mars were used to derive surface pressure and atmospheric composition; i. e., radiometric observations were used to obtain surface temperatures, while atmospheric temperature profiles were based primarily upon earth analogies. Figure 1 shows that the temperature profiles and surface pressure values derived by these techniques differed considerably. This was caused, in part, by differences in the observations, but was primarily caused by differing opinions and interpretations of the investigators.

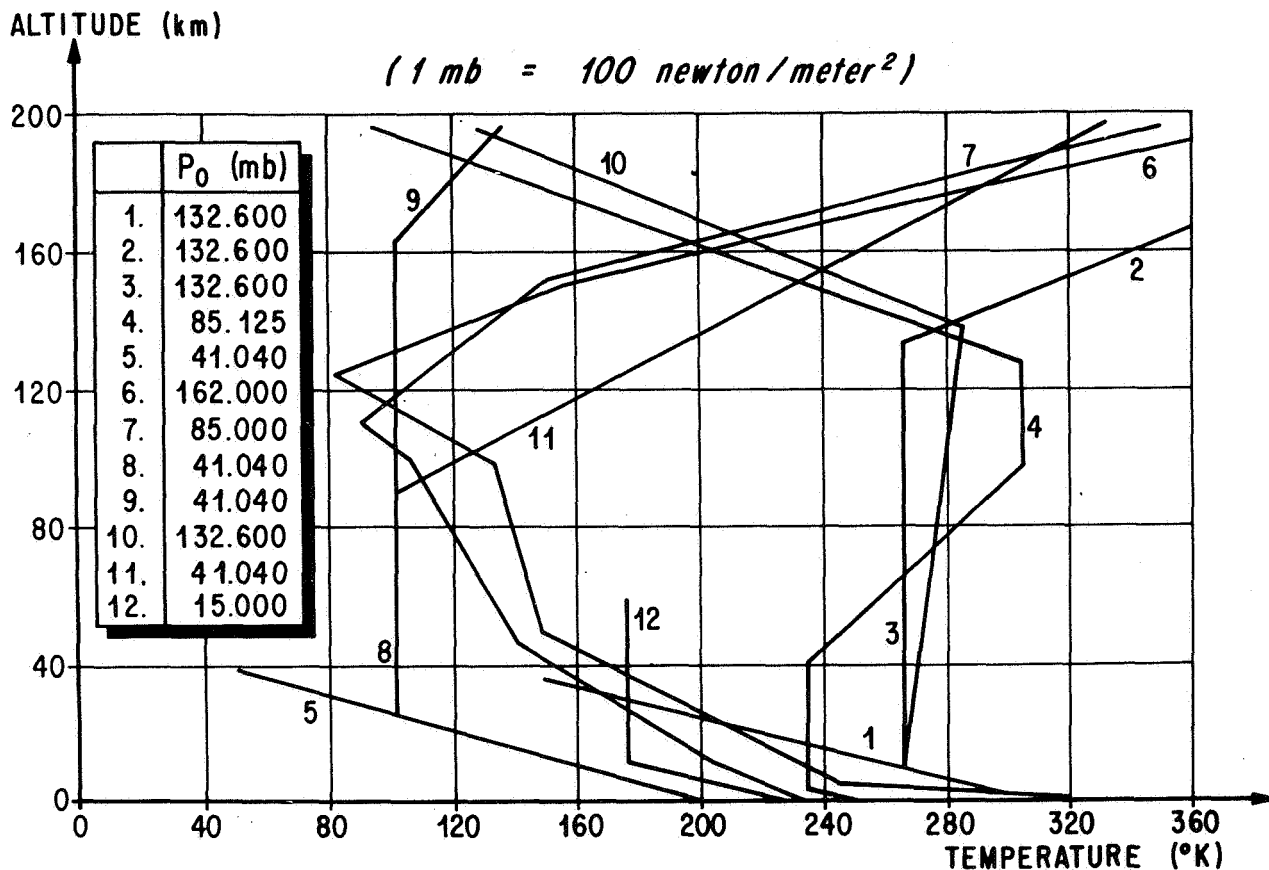


FIGURE 1. PREVIOUS MODELS OF THE MARS ATMOSPHERE

The Mariner IV occultation experiment was designed to measure two profiles of the electron density of the Martian atmosphere. From these two electron density profiles, parameters of interest such as pressure, temperature, and density may be derived. However, in transforming the electron density profiles to the desired parameters, it is necessary to establish the atmospheric constituent distribution at the ionospheric base and employ a theoretical concept of the Martian atmospheric chemical processes and related reaction rates, time constants, etc. This technique, of necessity, leads to many differing interpretations of the Mariner IV data. Some of the temperature profiles derived from these data are illustrated in Figure 2. Some investigators have taken the envelope formed by the different interpretations of data as representative of the variability of the Martian atmosphere. This is not a valid assumption. The differences in these profiles are caused solely by the different techniques,

applications, and opinions of the various investigators. Dr. F. S. Johnson [2] of the Graduate Research Center of the Southwest has postulated that the Martian ionosphere is similar to the F₂ layer of the earth's ionosphere, which implies that the main ion is O⁺. Chamberlain and McElroy [3] of Jet Propulsion Laboratory (JPL) have theorized that the Martian ionosphere is an E-type layer where the main ion is NO⁺ or O₂⁺. In studying the various interpretations of the Mariner IV data, the F-type layer interpretation was chosen for use in formulating the Mars atmospheric studies and models [4]. This choice was made because of the reasonable agreement of the temperature of F-type ionospheric models with temperature of theoretical heat budget computations, and from what appears to be unreasonable effective recombination coefficients and average ion mass assumptions in order to make an E-layer compatible with the ionization profile measured by Mariner IV [5].

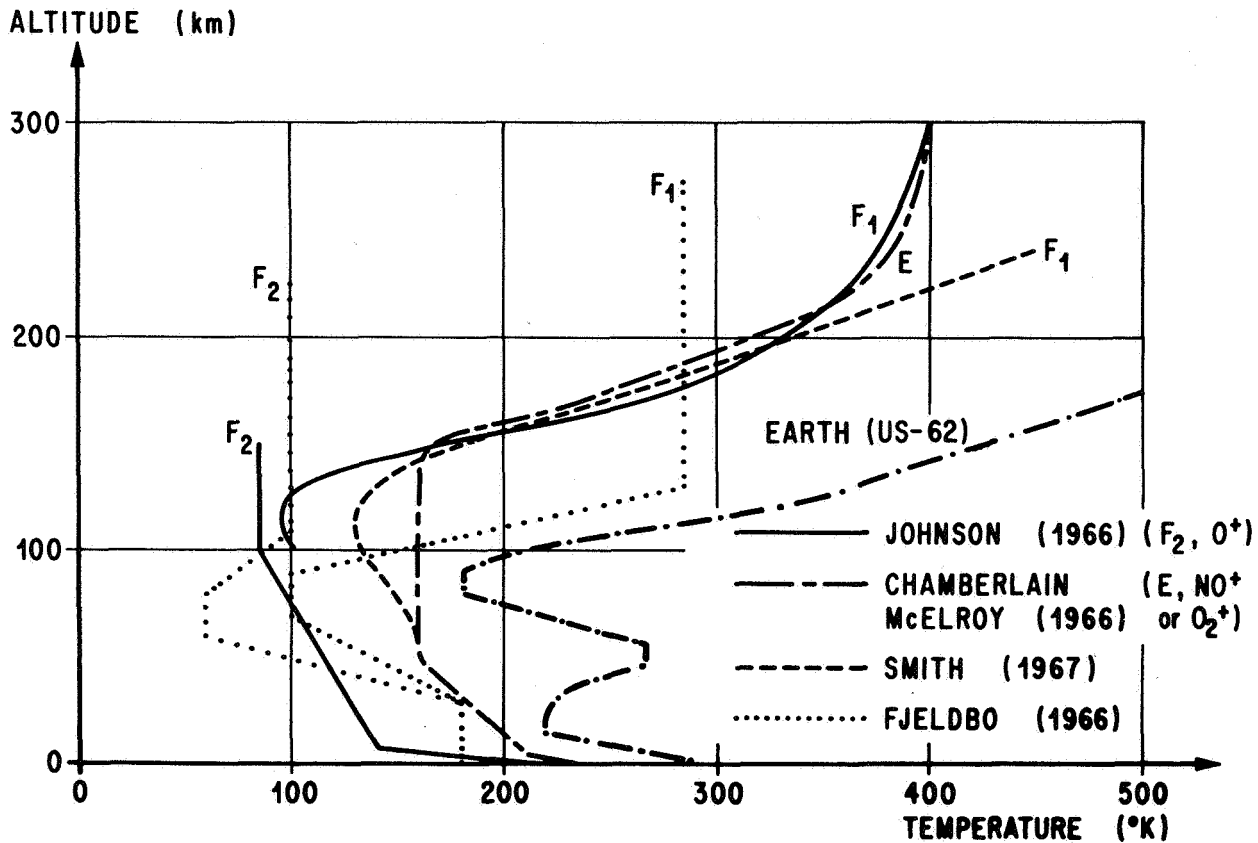


FIGURE 2. COMPARISON OF MARTIAN TEMPERATURE PROFILES DERIVED FROM MARINER IV

One other point that should be stressed is that the Mariner IV data do not represent the mean atmosphere as some investigators have indicated. These data represent two profiles for two points in space at the time of orbital entry and exit. The entry data, for example, concern the main ionization layer over electris \sim (50 degrees S, 177 degrees E) at 1300 hrs., local Martian time in late winter.

In developing the natural environmental criteria for Voyager, we have conducted detailed studies in these areas:

1. The various radiative models.
2. Various interpretations of Mariner IV data.
3. The diffusion and possible escape of Martian exospheric constituents.
4. The relationship of temperature and exospheric constituent distribution.

5. The probability of space plasma and Martian exospheric mixing.

6. The dependence of exospheric temperature on solar flux and sunspot cycle.

Temperature profiles generated by these studies are illustrated in Figure 3. The lower portion of these profiles is based upon the Mariner IV data. In establishing the upper portions, consideration was given to the relationships between temperature and atmospheric constituent distribution. These temperature profiles, in conjunction with derived molecular weight profiles and surface pressure values of 400, 800, and 1000 N/m^2 (4, 8, and 10 mb) that are based upon improved spectrophotometric observations and the Mariner IV data, were used to derive the density profiles illustrated in Figure 4. The extreme density envelopes pictured here, which include five orders of magnitude, represent our best estimate of the total variation to be expected in the Martian atmosphere. However, this five orders of magnitude variation might be reduced if more observational data were available.

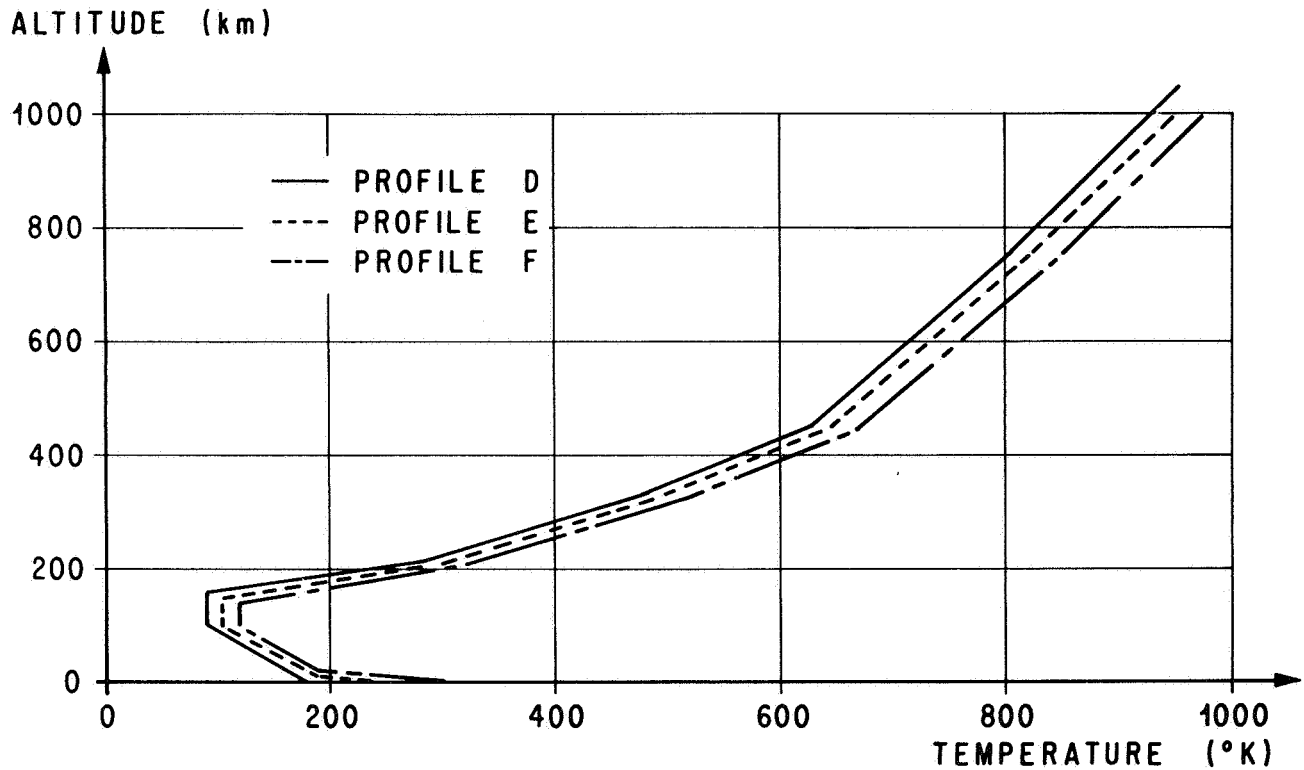


FIGURE 3. IDEALIZED MARTIAN TEMPERATURE PROFILES ASSUMING F_2 OR F_1 IONIZATION LAYER

PLANS FOR OBTAINING FUTURE DATA

In attempting to obtain required observational data, an electromagnetic probing experiment has been proposed for the Mars atmosphere, and studies have been conducted concerning the feasibility of obtaining Martian atmospheric information through vacuum simulation experiments. In the area of "on-the-spot" data acquisition (Fig. 5) a method of great promise for obtaining large amounts of data from occultating absorption and radiometric techniques for actual measurements of a planetary atmosphere are inherent in the orbiting satellite pair. Briefly, the orbiting pair would accomplish electromagnetic measurements of a planetary atmosphere and ionosphere, such as Mars, by essentially an occultation approach in which the source of radiation and the detector are both relatively near the planet to be probed. If two satellites are placed in similar orbits about the planet, refractivity measurements may be

made along the line of sight by methods derived from the Mariner IV radio occultation technique. Absorption spectroscopy measurements may be made by methods tested on the NRL-1965-16-D satellite at two points on each orbit where there is a direct line of sight relationship between the two satellites and the sun. Radiometric techniques for planetary surface temperature measurement are derived from standard techniques. The occultation measurements yield electron density, species, pressure, and temperatures, and from these data the atmospheric refractivity profile and scale height may be directly derived. The spectroscopic data yield identification of the species and determination of the mean molecular weight and number density. The radiometric measurements provide the surface temperature. Surface temperature and mean molecular weight allow an independent derivation of the atmospheric scale height, which can be cross checked with the atmospheric scale height obtained directly from the refractivity measurements.

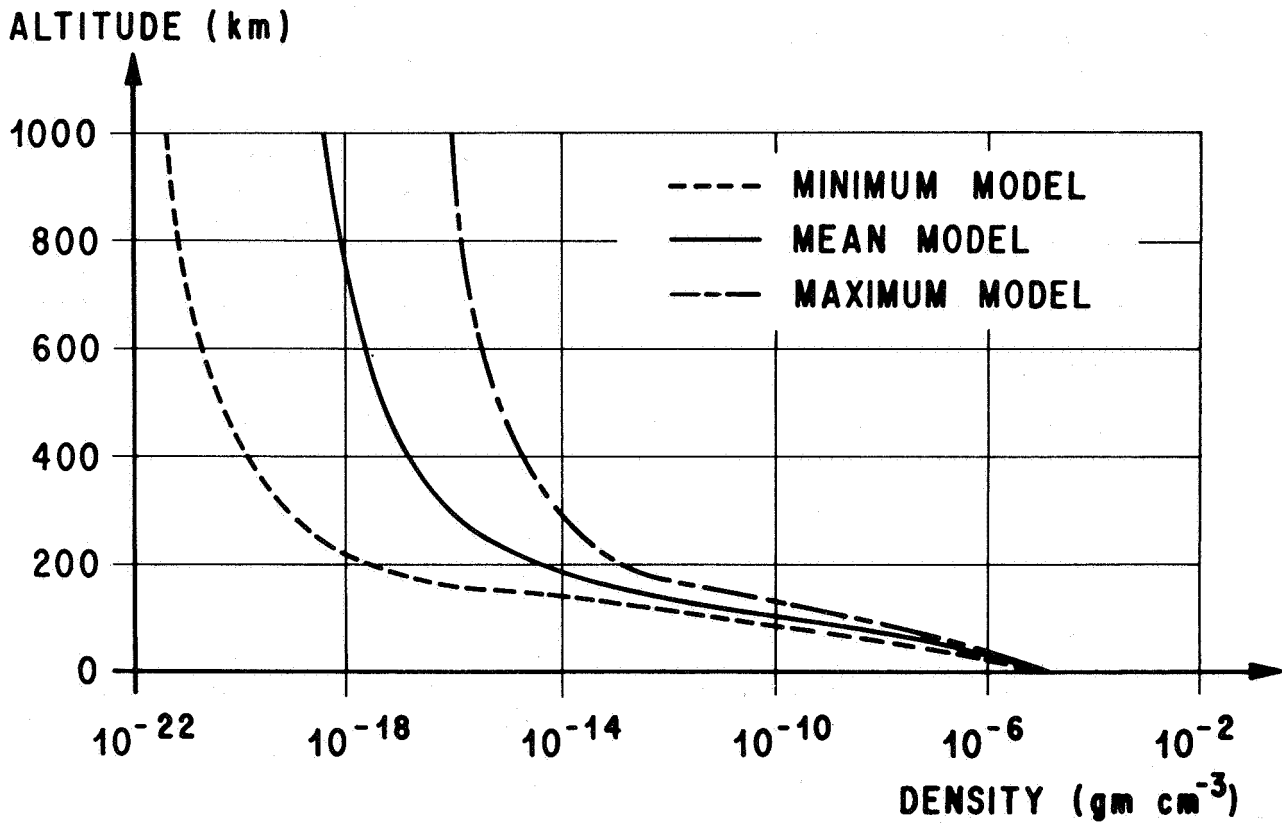


FIGURE 4. ATMOSPHERIC DENSITY

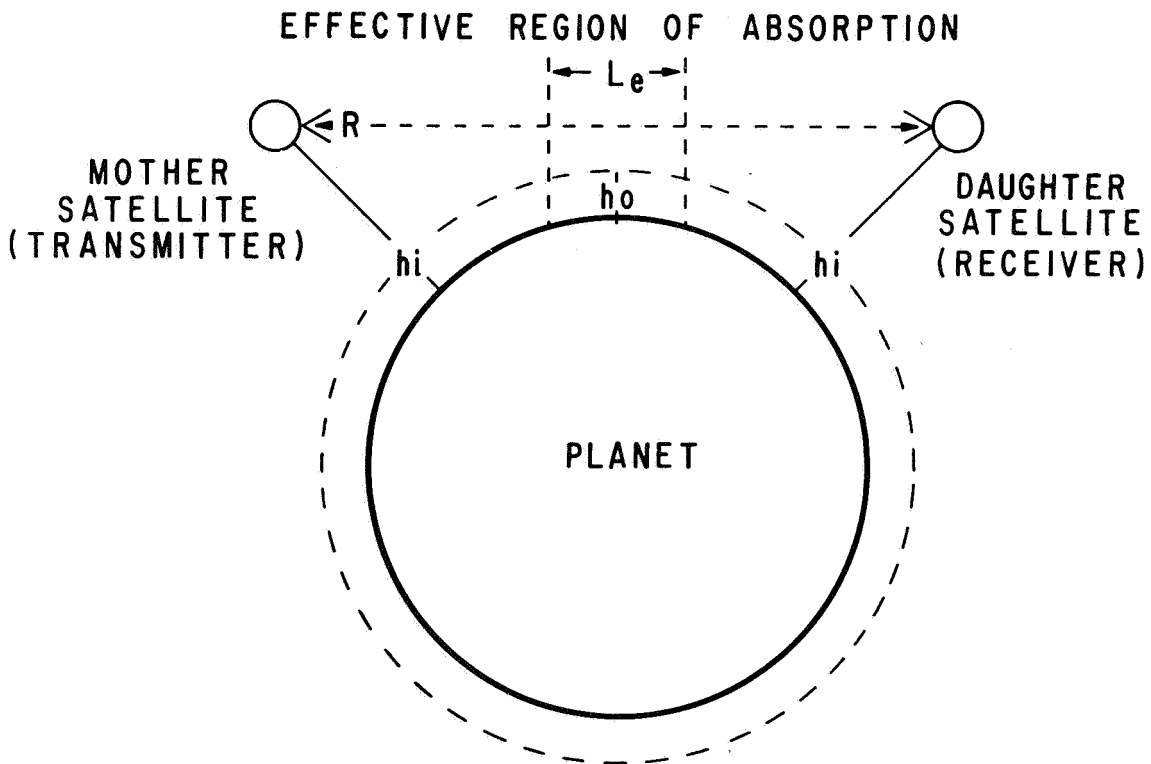


FIGURE 5. MICROWAVE SPECTROSCOPY EXPERIMENT CONFIGURATION

Current results are listed in Reference 1, and future studies and programs are as follows:

1. Mars atmospheric simulation.
2. Orbiting satellite pair.
3. Theoretical studies.
 - a. Seasonal-latitude studies.
 - b. Solar cycle.
 - c. Martian atmospheric processes.

REFERENCES

1. Weidner, D. K.; and Hasseltine, C. L.: Natural Environment Design Criteria Guidelines for MSFC Voyager Spacecraft for Mars 1973 Mission. TM X-53616, MSFC, Huntsville, Alabama, June 8, 1967.
2. Johnson, F. S.: The Atmosphere of Mars. Science, vol. 150, 1965, p. 1445.
3. Chamberlain, J. W.; and McElroy, M. B.: Martian Atmosphere: The Mariner Occultation

Experiment. Science, vol. 152, no. 2718, April 1, 1966, p. 21.

4. Smith, Newburn; and Beutler, Abigail E.: A Model Martian Atmosphere and Ionosphere. Space Physics Research Laboratory, The University of Michigan, Ann Arbor, Michigan.
5. Gross, S. H.; McGovern, W. E.; and Rasool, S. I.: Mars: Upper Atmosphere. Science vol. 151, March 1966.

BIBLIOGRAPHY

1. Smith, R.: Space Environment Criteria Guidelines for Use in Space Vehicle Development (1967 Revision). NASA TM X-53521, MSFC, Huntsville, Alabama, February 1, 1967.
2. Weidner, D. K.: A Preliminary Summary of the MSFC Planetary Atmosphere Computer Program. NASA R-AERO-IN-5-67, (Internal Note), MSFC, Huntsville, Alabama, June 30, 1967.
3. DeVaucoulers, G.: Physics of the Planet Mars. Faber and Faber Limited, 24 Russell Square, London, England.